SMITHSONIAN CONTRIBUTIONS TO THE EARTH SCIENCES • NUMBER 12

An Atlas of Volcanic Ash

Grant Heiken

SMITHSONIAN INSTITUTION PRESS
City of Washington
1974

ABSTRACT

Heiken, Grant. An Atlas of Volcanic Ash. *Smithsonian Contributions to the Earth Sciences,* number 12, 101 pages, 15 figures, 33 plates, 3 tables, 1974.—Volcanic ash samples collected from a variety of recent eruptions were studied, using petrography, chemical analyses, and scanning electron microscopy to characterize each ash type and to relate ash morphology to magma composition and eruption type.

The ashes are best placed into two broad genetic categories: magmatic and hydrovolcanic (phreatomagmatic). Ashes from magmatic eruptions are formed when expanding gases in the magma form a froth that loses its coherence as it approaches the ground surface. During hydrovolcanic eruptions, the magma is chilled on contact with ground or surface waters, resulting in violent steam eruptions. Within these two genetic categories, ashes from different magma types can be characterized. The "pigeon hole" classification used here is for convenience; there are eruptions which are driven by both phreatic and magmatic gases.

The morphology of ash particles from magmatic eruptions of high-viscosity magma is governed primarily by vesicle density and shape. The vitric ash particles are generally angular, vesicular pumiceous fragments, or thin vesicle wall fragments. The morphology of lithic fragments is dependent on the texture and mechanical properties of the rock units broken up during the eruption; most of the samples studied contain equant, angular to subrounded lithic fragments.

Ash particles from eruptions of low-viscosity magmas are mostly droplets; droplet shape is in part controlled by surface tension, acceleration of the droplets leaving the vent, and air friction. Shapes range from perfect spheres to a variety of twisted, elongate droplets, with smooth, fluidal surfaces.

The morphology of ash particles from hydrovolcanic eruptions is controlled by stresses within the chilled magma which result in fragmentation of the glass to form small blocky or pyramidal ash particles. Vesicle density and shape play only a minor role in determining the morphology of these ash particles.

OFFICIAL PUBLICATION DATE is handstamped in a limited number of initial copies and is recorded in the Institution's annual report, *Smithsonian Year.* SI PRESS NUMBER 4983. SERIES COVER DESIGN: Aerial view of Ulawun Volcano, New Britain.

Library of Congress Cataloging in Publication Data
Heiken, Grant
An atlas of volcanic ash.
(Smithsonian contributions to the earth sciences, no. 12)
1. Volcanic ash, tuff, etc. I. Title. II. Series: Smithsonian Institution. Smithsonian contributions to the earth sciences, no. 12.
QE1.227 no. 12 [QE461] 552'.2 73-13519

For sale by the Superintendent of Documents, U.S. Government Printing Office
Washington, D.C. 20402 - Price $2.00

Contents

An Atlas of Volcanic Ash

Grant Heiken

Introduction

Morphologic descriptions of volcanic ash particles are present in the literature, mostly as thin-section descriptions. Shard shapes are rarely described as three-dimensional forms; analyses of this sort are generally restricted to bombs and other coarse-grained volcanic ejecta (Wentworth, 1938). Furthermore, only recently, Walker and Croasdale (1972) and Heiken (1972) have related ash morphology to the composition of the magma or type of eruption.

The purpose of this study was to analyze a large variety of volcanic ash samples, using most standard laboratory techniques, to determine if there is a relation between the type of eruption, the magma composition, and the ash particle morphology.

The following items were determined for each ash sample studied: the locality, eruption type, type (s) of volcanic features associated with this ash, bulk chemistry (in most cases), and modal analysis (grain counts, rather than point counts, were made of each ash thin section). Petrographic and scanning electron photomicrographs (SEM) were taken to characterize the ash morphology. The chemical analyses and size analyses of ashes studied here are summarized in Appendices 1 and 2.

Ash names used here are based on the size classification of volcaniclastic fragments by Fisher (1961) (Plate 1A), used in conjunction with a compositional classification set up by Cook (1965) (Plate 1B).

For brevity, each petrographic mode is summarized in the text with percentages of glass, tachylite, crystal fraction, lithic fragments.

This is an expanded version of a paper by Heiken (1972) on the morphology and petrography of volcanic ash. For a review of the mechanisms of ash formation and introductory text for each section of this atlas, see the paper by Heiken; there is, however, some necessary duplication between the two papers.

It is hoped that the reader using this catalog as a reference can, on the basis of petrography and ash morphology, infer the genesis of an ash sample. This catalog is potentially useful when working with isolated ash beds found on land, in deep-sea cores, and perhaps in lunar soil. Most of the morphologic features studied here with scanning electron microscope can be identified with standard microscopes.

Ash Formation

There are two basic mechanisms of ash formation: (1) by exsolution and expansion of gases in a magma, resulting in the froth losing its coherence as it approaches the ground surface (magmatic eruptions), and (2) by chilling of a magma rising toward the ground surface on contact with ground or surface water (hydrovolcanic or phreatomagmatic eruptions).

Magmatic Eruptions

The basis for understanding the first type of ash formation was set forth in a paper by J. Verhoogen (1951):

Grant Heiken, Geology Branch, NASA, Johnson Space Center, Houston, Texas 77058.

> Ash formation is believed to depend especially on the kinetics of gas evolution, the crucial factor being the number of bubbles per unit volume which may be present at a certain time. Initial water content of the magma, degree of oversaturation developed, cause of oversaturation, viscosity, surface tension, temperature, depth, nature and amount of suspended crystals, are among the factors which determine the rate and mode of gas evolution, without much indication of any of these being more important than the others. . . . Differences in volcanic behavior, as between Pelean and Vulcanian explosions, formation of pahoehoe, quiet outflow and explosion of pumice, are not necessarily related to one or even two variables only. It is more probable that at least a half dozen variables should be required for an adequate analysis, and that such differences as are observed depend on a combination of a large number of apparently insignificant, or at least not very obvious, factors.

The shape of glassy ash particles is mostly dependent on bubble (vesicle) shape and density, which is, in turn, dependent on the variables outlined by Verhoogen.

Explosive eruptions of a magma with a low viscosity, caused by expanding, coalescing gas bubbles at the surface, throw out sprays of droplets or pasty clots. Droplet shapes are controlled mainly by the effect of surface tension and deformation of the droplet by acceleration and air resistance. In this case, the vesicle shapes within each droplet are partly controlled by the external forces listed.

Ash from magmas with slightly higher viscosities, such as basaltic magma with abundant phenocrysts or some andesitic magmas, is composed of scoria with few fluidal shapes (there is a small droplet component).

The morphology of ash eruptions of high-viscosity magma (rhyolitic, dacitic, and some andesitic magmas) is entirely dependent on the shape of vesicles in the rising magma before disintegration. The concavities, troughs, and tubes on grain surfaces are broken vesicle walls. Elongate grain shapes are controlled by elongate (pipe) vesicles and equant grain shapes by equant, undeformed vesicles. Flat or slightly curved platy shards are from broken vesicle walls. Only rarely are there scattered droplets of silicic ash from magmas with viscosities low enough to assume a fluidal shape.

The shape of lithic fragments in ash should be controlled by the mechanical properties of the wall rock, broken up by spalling or explosive expansion of gases in the magma as it approaches the surface. Generally, most lithic fragments of ash size are equant and slightly rounded, indicating some possible rounding by particles grinding against each other during the eruption.

Hydrovolcanic (Phreatomagmatic) Eruptions

Vesicle shape and density play only a minor role in the determination of grain shape in hydrovolcanic (phreatomagmatic) eruptions. In this sort of eruption, the rising magma is quickly cooled on contact with ground or surface water. Stresses within the "quenched" magma cause fragmentation into small blockly or pyramidal glass particles (Walker and Croasdale, 1972, and Heiken, 1971 and 1972). In many instances, it appears that the chilling occurs before much of the gas is released from the magma, explaining the low vesicularities characteristic of hyaloclastic ashes. (Hyaloclastic is a term coined by Rittman [1962] to describe ashes formed by the chilling-fracturing process described.)

This atlas is split into the two basic categories of magmatic and hydrovolcanic, with subdivisions based on magma type.

Acknowledgments

I want to thank the following people for providing very useful information and ash samples: W. I. Rose, Dartmouth University; Oliver Kola, Anchorage, Alaska; Arturo Alcarez, Phillippine Commission on Volcanology; K. R. Everett, Institute of Polar Studies, Ohio State University; D. Hadikusomo, Geological Survey of Indonesia; Gary Lofgren, Fred Hörz, and M. C. McEwen, NASA Manned Spacecraft Center; J. B. Dawson, University of St. Andrews, Scotland; Mike Sheridan, Arizona State University; S. Thorarinsson, Museum of Natural History of Iceland; the Portuguese Geological Survey; David Roddy, U.S. Geological Survey; J. Healy, and C. P. Wood, New Zealand Geological Survey; W. Melson, Smithsonian Institution; Roald Fryxell of Washington State University, R. Funiciello of the University of Rome, and Floyd McCoy, Woods Hole Oceanographic Institute. Special thanks go to R. V. Fisher, University of California, for providing abundant samples from Hawaii and for training in studies of pyroclastic rocks. Beverly Atkinson and Liz Alley efficiently typed the manuscript, David McKay, Tom Simkin, R. Fiske and W. Phinney criticized

the manuscript, and Sue Montgomery and Don Ryan edited it. Members of the Federacion Andismo, especially Arturo Veliz, helped greatly in supporting the sampling effort in Guatemala. Training for use of the scanning electron microscope was generously provided by David S. McKay and Garth Ladle of the NASA Manned Spacecraft Center.

Magmatic Eruptions

Ash of Basaltic Composition

Pacaya, Guatemala.—1968 eruption. The 1968 eruption occurred at one of two young cinder cones at the southwest peak, located 40 km south-southwest of Guatemala City (for a review of activity see Stoiber and Rose, 1970). There is mostly strombolian type of activity at this volcano. This sample is from the surface, 1 km west of the vent.

Petrography: This vitric ash sample consists of mostly light-brown, clear glass (sideromelane) droplets, or broken droplets with a thin dark-brown skin. There are phenocrysts of olivine, pyroxene, and feldspar ($\sim An_{70}$) in many of the droplets. (97:0:3:0)

Morphology: The ash (Plate 2) consists of mostly broken glass droplets. In contrast to the glass ovoids, spheres, and Pele's hair formed from melts of very low viscosity (such as those at Kilauea), the strombolian activity and lava fountains at Pacaya produced irregularly shaped droplets with botryoidal surfaces.

Most vitric ash grains from Pacaya are equant and contain ovoid or spherical vesicles. Present in minor proportions are slightly elongate grains that may be twisted about the long axis. The elongate grains contain irregular pipe vesicles, oriented parallel to the long axis of the grain.

The botryoidal glass droplet surfaces have a smooth skin that can be seen in thin section. The 10– to 50–micron-thick skin is formed rapidly after ejection of the droplet from the vent. It is broken or deformed by collapsed vesicles located near the outer edges of the droplet (Plate 2F). Droplets broken after cooling do not have a skin along the broken surface. The broken grain surfaces are irregular, with sharp, angular corners.

Fuego, Guatemala.—Fuego is a strato-volcano consisting of interbedded flows and pyroclastics of andesitic to basaltic composition. These samples are from the eruption of August 1966, when ash clouds reached elevations of approximately 12,000 m (Stoiber and Rose, 1970). The sample is from the surface, 3 km north of the active vent, on Acatenango, another volcano adjacent to Fuego.

Petrography: This vitric ash is of basaltic composition. The tachylite occurs as black opaque grains that are submicrocrystalline basalts. It is often associated with sideromelane, which is true basaltic glass. (72:9:19:0)

Morphology: The ash from Fuego (Plate 3) is similar to the Pacaya ash. It is composed mostly of broken sideromelane droplets, with lesser amounts of tachylite and mineral fragments. In contrast to the Pacaya ash, glass droplets produced in the violent ash eruption are all broken; none retain the fluidal grain shapes characteristic of droplets from Pacaya. Most of the particles are equant to slightly elongate, with hackly, irregular grain surfaces. Original droplet surfaces are only rarely preserved as patches of smooth skin (Plate 3A). Tachylite and basalt fragments have extremely hackly, irregular surfaces (Plate 3E).

Droplets were probably broken by grinding within the upper part of the vent or eruption cloud, or by continued expansion of vesicle gases. It is also possible that only a few droplets with perfect fluidal shapes were formed initially. Comminuted, irregularly shaped ash fragments are produced in large-scale ash eruptions of andesitic or basaltic magmas.

Cerro Negro, Nicaragua.—1968 eruption. Cerro Negro is the youngest of four clustered cinder cones along a north-south fault line in the Central Marabios Range, Nicaragua. The 1968 eruption ejected abundant blocks and ash, and an ash cloud rose to an altitude of several thousand meters. A flank eruption was characterized by lava fountaining and an ash flow. The lavas and ejecta are of olivine basalt. The exact sample location is not known by the author.

Petrography: The vitric ash consists of mostly irregularly shaped, broken droplets of sideromelane and tachylite that contain abundant phenocrysts of clinopyroxene (augite) and plagioclase. There are grains of sideromelane containing patches of submicrocrystalline tachylite. (55:30:15:0)

Morphology: The grain morphology is similar

to that of the ashes from Pacaya—consists of a mixture of broken sideromelane droplets and tachylite fragments (Plate 4). The droplets have smooth botryoidal or lumpy outer surfaces, broken by depressions over vesicles in outer droplet edges (Plates 4A, 4C). Depressions with smooth edges were formed when the outermost vesicles broke while the droplet was still partly fluid (Plate 4A). The sharp-rimmed depressions were formed when thin vesicle walls were broken after the droplet had cooled (Plate 4C). The irregular droplets and broken droplets are associated with strombolian eruptions (mixed ash eruptions and lava fountaining).

ETNA, ITALY.—Etna is a broad stratovolcano, with multiple vents and abundant cinder cones near the summit and on the slopes. This ash is from accelerated Strombolian activity at cinder cones near the observatory in April 1971. This ash sample is from the First Cable Car Station (2400 m).

Petrography: This is a lithic-vitric ash, consisting of mostly broken porphyritic, pale brown (sideromelane) droplets, with very low vesicularities (Plate 5E, F). Only a small percentage of the droplets have a few spherical vesicles. There are dark reddish-brown glass fragments, which are probably an oxidized form of the sideromelane. Some of the glass grains are partly devitrified, with small brown bundles of spherulites.

The tachylite grains are porphyritic, equant to elongate grains with low vesicularity. Included in the crystal fraction are euhedral plagioclase crystals (length 0.15 mm), many of which exhibit oscillatory zoning. In lesser amounts is pale green augite, olivine, and porphyritic basalt fragments exhibiting an equigranular groundmass. (59:28:9.5:3.5)

Morphology: The following forms are evident from the SEM Photomicrographs:

1. Equant, blocky, nonvesicular fragments with hackly grain surfaces, which are the tachylite grains. Some of these grains have been rounded. At higher magnification, many of these grains exhibit diktytaxitic texture, with an open, meshlike network of feldspar (?) grains, 1μ–2μ long and 0.3μ wide. Voids between the crystals occupy 30 to 50 percent of the rock by volume (Plate 5B, C).

2. Angular, broken droplets exhibiting low vesicularity. The shards are mostly blocky fragments, with scalloped edges where the grain surface consists of broken vesicle walls (30– to 150–micron-diameter vesicles). Fracture surfaces are smooth and sometimes conchoidal (Plate 5D).

3. There are a few agglutinates in the sample (droplets welded together as irregular, botryoidal grains) (Plate 5A).

4. Clinopyroxene and feldspar grains.

DECEPTION ISLAND, ANTARCTICA.—1969 eruption. Deception Island, a volcanic island composed of tuff rings and cinder cones, is located off Graham Land, Antarctica, near the South Shetland Islands. This sample of cinders and ash is from the eruption that began on 21 February 1969. The eruption was characterized by the ejection of ash, scoria, and bombs. The exact location of the sample is not known. Both magmatic and hydrovolcanic activity occurred on the island during this eruption.

Petrography: The vitric ash consists of mostly irregular, broken droplets of sideromelane or tachylite, each containing feldspar microlites and some olivine phenocrysts. (64.5:35:0:0.5)

Morphology: The ash consists of equant to moderately elongate sideromelane and tachylite grains and is similar to the ashes from Fuego, Guatemala. Most of the ash fragments have rough, irregular surfaces (Plate 6). Smooth droplet surfaces characteristic of ashes from lava fountains are rare.

A few ash grains exhibit a diktytaxitic texture, which consists of an open network of feldspar microlites coated with a thin layer of glass. This texture may have been formed by fluid draining from between feldspar microlites or by the growth of irregular vesicles between the crystals in the melt.

KILAUEA IKI, HAWAII.—Kilauea Iki is a pit crater adjacent to the eastern edge of the Kilauea Caldera. The vitric ash is from lava fountaining that occurred in 1959. The samples were collected 2100 m southwest of the vent.

Petrography: The sideromelane droplets contain few or no phenocrysts or microlites. The mode is 100 percent sideromelane droplets. (100:0:0:0)

Morphology: Lava fountaining produced an abundance of unbroken glass droplets and Pele's hair (long, thin strands of glass) in the ash-size fraction (Plates 7, 8). Glass spheres and ovoids were droplets of melt in which surface tension had a greater effect than either air resistance or accelera-

tion of the droplets from the vent. Vesicles within the spheres are nearly always spherical. Nearly all the droplets have a 10– to 50–micron-thick skin. The skin is broken by small-scale contraction joints oriented perpendicular to the droplet surface. In places where the joints separated during expansion of the droplet, the cracks were penetrated by fluid from the droplet interior (Plate 7F). Droplet surfaces were generally broken over some of the outermost vesicles (Plates 7B, 7C, 8D). Some are smooth, lacking these surface depressions.

Long, thin strands of glass (Pele's hair) are formed by the acceleration of droplets from the vent, possibly aided by gas streaming by a droplet or fluid clot. The initial stages in the formation of Pele's hair begin with the development of tapering tails on droplets (Plate 7C). Vesicles within the glass strands are drawn into long, pipelike shapes (7G–L).

The abundance of spherical and ovoid droplets in the Kilauea ashes is a characteristic of ashes from Hawaiian eruptions of low-viscosity magmas. This is in contrast with ashes from the strombolian eruptions of Central American volcanoes (Pacaya, Fuego, Cerro Negro), where spherical and ovoid droplets are rare.

KILAUEA, HAWAII (reticulite).—This sample of reticulite ash (also known as limu or thread-lace scoria) was taken from the reticulite pumice layer near the Hawaii Volcano Observatory; the first volcaniclastic unit above flows on the rim of the crater. It is a light-brown glass of basaltic composition that was blown downwind from the lava fountaining of a low-viscosity, high-temperature melt.

Petrography: This vitric ash is composed of a sideromelane froth, lacking phenocrysts or microlites of any kind. The mode is 100 percent sideromelane. (100:0:0:0)

Morphology: The continued growth of vesicles in a basaltic magma with very low viscosity (Kilauea) produces an open network or froth. The froth, called reticulite, consists of a lattice-shaped network of triangular glass rods (Plate 9). The low density of this ejecta allows the bits of froth to drift for some distance in the wind.

ALOI-ALAE VENT AREA, HAWAII.—The ash is from lava fountaining in the Aloi-Alae craters area, on the Chain of Craters Road (Puna Rift Zone), in December 1969. These are pit craters on the flank of a large shield volcano. The sample was collected approximately 1 km west of Alae Crater.

Petrography: The vitric ash consists of Pele's hair, spheres, and ovoids. The mode is 100 percent sideromelane droplets and broken droplets. (100:0:0:0)

Morphology: The ash, from large-scale lava fountaining, is nearly identical to the Kilauea ashes (Plate 10).

OSHIMA, JAPAN.—Oshima is a polygenetic shield volcano consisting of basaltic ash and tholeiitic basalt flows. There is a central main vent with caldera and 40 parasitic cones on the shield.

This sample is from the "S_1" layer (midslope on the main cone, a unit approximately 0–5 m thick), which is an accretionary lapilli tuff. The age is 650 ± 150 years B.P. (Nakamura, 1964). The ash is possibly from a strombolian-type eruption.

Petrography: This lithic-vitric ash consists of mostly broken sideromelane and tachylite droplets or agglutinates (several droplets welded together). The lithic component consists of equant fragments of aphanitic basalt. There is a trace of pyroxene phenocrysts, not in vitric or lithic fragments. (55:21:Tr:24)

Morphology: The ash consists of irregular, equant sideromelane and tachylite fragments (Plate 11). Most are broken fragments. Botryoidal grain surfaces are characteristic of the sideromelane droplets. Included in the ash are basalt fragments, exhibiting irregular, hackly surfaces. This sample contains a number of agglutinates, that is, sideromelane and tachylite droplets welded to each other or to lithic and mineral fragments.

The type of eruption was not observed. Because of the similarity of the ash to the Central American basaltic ashes, it is possible that it was ejected during a strombolian eruption.

TAAL, PHILIPPINES.—1968. Volcano Island, in Lake Taal, Philippines, consists of overlapping tuff rings and cinder cones. An eruption beginning in 1965 was hydrovolcanic (phreatomagmatic), caused by lake water coming into contact with rising magma. In the later eruptive phases, as the tuff ring was built, water no longer had access to the craters. After this, a cinder cone was formed by ash eruptions and lava fountaining. This basaltic ash sample is from the cinder cone.

Petrography: The vitric ash consists of mostly sideromelane droplets that contain 10 to 30 percent

microlites of feldspar and some small olivine phenocrysts. There are a few equant basalt fragments and feldspar crystals in the ash. (96.6:0:2.5:0.8)

Morphology: The ash, produced during intermittent ash eruptions and lava fountaining (strombolian), consists of mostly sideromelane droplets, broken droplets, and glass-coated phenocrysts (Plate 12). There are a few imperfect spheres and ovoids in the ash (Plate 12E). Most of the broken droplets are tabular or flattened, with long axes of flattened vesicles oriented parallel to long axes of the grains. Droplet surfaces are lumpy or botryoidal (Plates 12D, 12F, 12I). The more elongate droplets are sometimes twisted about the long axis. The ends may taper to a point but are generally broken (Plates 12A, 12B). Tachylite grains are similar in shape to the tabular, broken sideromelane droplets but have rough, pitted surfaces.

Ashlike Particles of Basaltic Composition

Makaopuhi Pele's Hair.—Lava flowing from Alae Crater, Hawaii, into the Makaopuhi pit crater forms lava falls. As the lava falls hit irregularities in the crater wall, irregular streams of lava arc out from the falls. Strong whirlwinds generated at the crater edge pick up strands of glass and carry them out of the crater, along with thin glass sheets. This sample was collected on the north rim of Makaopuhi Crater, within 30 m of the lava falls.

Petrography: This is a vitric "ash," consisting of thin strands of clear, pale brown glass. The glass is homogeneous, with 2 to 5 percent clots of 0.02–0.6 mm diameter, olivine crystals; there are lumps in the glass strands over the phenocryst clots (Plates 13C, E, F). Some of the olivine crystals have ovoid bubbles. There is a trace of 0.2–0.3 mm long plagioclase laths.

In contrast with other forms of Pele's hair, the skin is very thin and poorly developed. Hair diameters range from 15μ–500μ; 81 percent of the hairs are vesicular and 19 percent are nonvesicular; the vesicular hairs have about 10 percent vesicularity. Most of the <50μ diameter hairs are nonvesicular, with few exceptions.

Morphology: Two types of pele's hair are present in this sample: (1) Ribbed strands of glass (ribs parallel the long axis of the strand); one example characteristic of this form is a 250–micron-diameter strand which has one 165–micron-wide rib flanked by ribs 11μ–25μ wide (Plate 13C, F). The grain surface is extremely smooth. In a few places on the strand, where the surface is broken, the ribs overlie elongate vesicles. In one case, the outer vesicle walls of an elongate vesicle under a strand are 1μ–3μ thick. There are some 1– to 2–micron-diameter glass strands welded to the surface of the larger grains. (2) Cylindrical or nearly cylindrical strands with very smooth surfaces (Plate 13A, B).

These pele's hairs are nearly impossible to separate from those formed during lava fountaining on the basis of petrography and morphology.

Flow Top Glass–Kilauea Crater, Hawaii.—These glass fragments were formed by the mechanical disintegration of the glassy crust of the September 1971 pahoehoe flow into the north end of Kilauea Crater. On fresh pahoehoe flows, the highly vesicular skin breaks off only minutes after cooling, to form vesicular platelets with flattened vesicles. The platelets, which are from 1–20 cm long, are broken up during movement by wind and water. The small fragments are carried off by the wind. This is not an ash, but I have included it because the windblown fragments could be easily mixed into ash deposits around a volcano.

Petrography: This sample consists of pale brown homogeneous glass (sideromelane), with about 5 percent phenocrysts and 5 to 10 percent spherulites in early growth stages (Plate 14B). The olivine phenocrysts are 0.4–0.2 mm long. Many contain abundant ovoid to elongate bubbles; long axes of the bubbles are parallel to the long axis of each crystal. Feldspar phenocrysts, 0.12–0.13 mm long, have thin "haloes" of spherulites. Smaller feldspar crystals have spherulitic prongs at both ends. Other sheaf spherulites are present singly or in clusters throughout the glass. Each cluster has a brown "halo."

Morphology: The larger plates, when viewed from the top, have a rough, ropy, flattened surface, with superimposed, collapsed vesicles. From the bottom, the surface consists of smooth, curved vesicle walls, with vesicles 2 mm–2 cm in diameter (Plate 14A).

Ash-size particles formed by the disintegration of the glassy crust consist of |- or T-shaped vesicle-wall fragments. Vesicle walls are smooth except for some shallow depressions and lumps (possibly over phenocrysts). The fracture surfaces are hackly

to conchoidal. Vesicle-wall fragments are 0.1–1 mm thick; no smaller vesicles are visible in the walls (Plate 14A).

These could be confused with a component of littoral cone ash deposits, which are formed also by the disintegration of presolidified pahoehoe crusts.

Ash of Andesitic to Rhyolitic Composition

Ruapehu, New Zealand.—June 1969 eruption. The ash was erupted in an initial burst that may have spread ash-flow ash in several directions on the steeper slopes of the volcano, with subsequent airfall material drifting farther northwest. Later came the explosive eruption that threw out large masses of crateral material, including boulders and mud, as well as some of the crater-lake water. This, combined with snow melted by the hot blast, formed a number of lahars which carried ash down into several of the outward-draining streams (Healy, written communication, 1970). It is possible that there might not have been an ashflow at all, but only mudflows as the eruption emptied the crater lake and the lake sediments. Wood (written communication, 1972) has examined the "ash-flow" material and has evidence that most of this tephra is from detritus and lake-derived minerals. Gypsum is abundant in these samples.

The sample was collected at the south margin of Whangaehu Glacier, approximately 350 m northeast from the center of the crater lake. The sample may have been part of a nuée ardente or partly deposited by lahar (Healy, 1970, personal communication).

Petrography: The lithic-vitric ash consists of fragments of porphyritic andesite; mudstone; medium-crystalline pyroxene-hypersthene andesite; tachylite; feldspar-rich andesite; crystals of andesine, hypersthene, and augite; and fine-grained colorless glass shards and pumice. Some of the pumice grains have brownish, oxidized rims. (12:0:4.3:83.7)

Morphology: Most of the ash consists of equant, elongate, and pyramidal lithic fragments of andesitic composition (Plate 15). The lithic fragments generally have rough, pitted surfaces; they may range from the freshly comminuted rock, with planar fracture surfaces, to grain surfaces rounded by grinding of particles within the vent or eruption column.

The vitric component of the ash consists of equant grains with low vesicularity and spheroidal ovoid shapes and pumice fragments with elongate vesicles. Pumice surfaces are very rough, with bladed edges of closely spaced vesicles exposed at the surface of each grain. No droplets are present; the vitric ash grains left the vent as solid pumice fragments. Most grains are coated with irregular patches or layers of sublimates, mainly sulfur compounds. Many grains are weathered rock fragments that may have been from an ash deposit in the crater from previous eruptions.

This eruption may have been partly hydrovolcanic and is a mixture of magmatic and hyaloclastic ashes.

Merapi, Indonesia.—The eruption began 10 October 1967, with formation of a lava dome and nuées ardentes. In January 1969, eruptive activity included nuées ardentes, airfall, and secondary lahars (associated with heavy rains). This is an airfall sample of andesitic composition. The exact sample location is not known but is suspected to be some distance from the vent because of the well-sorted nature and very fine grain size of the ash.

Petrography: The sample is a crystal ash, consisting of mostly very small feldspar, orthopyroxene, and clinopyroxene crystals and angular, colorless glass shards. The ash is very well sorted. (35:0:64:1.0)

Morphology: The ash may not be completely characteristic of ejecta from this eruption. The exact location is not known, but the extremely fine grain size indicates that it was probably collected far enough from the vent to have been sorted by wind and gravity.

Most of the ash consists of broken, anhedral feldspar crystals (Plate 16). The remaining portion consists of very fine-grained, angular, and pointed glass shards. A few of the shards contain small, irregularly shaped vesicles. The fine-grained vitric fragments are probably pieces of thin vesicle walls.

Mayon, Philippines.—29 May 1968. Mayon is a symmetrical stratovolcano composed of dominantly andesitic flows and pyroclastic rocks. This ash is from an eruption of porphyritic augite-hypersthene andesite ash in airfall and nuées ardentes clouds (Moore and Melson, 1969). There are some accre-

tionary lapilli in the ejecta. The exact distance of the sample from the vent is unknown.

Petrography: The crystal-lithic ash consists of broken crystals of augite, hypersthene, and plagioclase; equant andesite fragments; and colorless glass shards and pumice. Most of the pumice and some shards have a thin, brown oxidized rim. (59:0:27.7:13.3)

Morphology: The ash is similar to, but coarser grained than, the Merapi ash sample and may have been collected closer to the vent. The vitric component is dominant in this sample. As in the Merapi ash, there is an abundance of thin, elongate, pointed glass shards (Plate 17), the product of finely comminuted pumice. Larger glassy particles are curved, being the more complete remnants of vesicle walls.

Surfaces of grains that are bits of vesicle wall are smooth and curved. Fractured grain surfaces are more irregular, exhibiting conchoidal fracture surfaces. Pumice fragments, with a wide range of vesicle shapes (generally elongate), are equant to slightly elongate. The grain shape reflects the vesicle shapes within it. The ash is probably the product of disintegration of a plug of viscous, gas-rich pumice rising in the vent.

KRAKATAU, SUNDA STRAITS, INDONESIA.—I have included this study as an early example of the relation of ash type to eruption type and as an example of a particularly violent eruption. Krakatau was a 200–meter (?)-high volcano that was destroyed in 1883, leaving a submerged caldera and three islands (Van Padang, 1951). Activity began on 21 May 1883, with ash clouds rising to 11 km. The most violent eruptions occurred during the period of 26–28 August. It is believed that ash clouds reached heights of 70–80 km (Van Padang, 1951).

Sample Description: I have abstracted this description from a report on the eruption of Krakatau by J. W. Judd (1888). The ejecta consists of colorless to dirty grayish-white ash and pumice; the pumice has irregular vesicles with little knots of feldspar, pyroxene, and magnetite crystals. Some of the pumice grains are rounded. Lithic fragments present in the ejecta were andesitic, believed to be from the old crater ring.

Judd correctly assumed that the pumice was formed by the escape of volatiles while the magma was still viscous. Vitric ash fragments, which make up most of the ejecta, consist of curved plates and angular threads which were assumed to have formed by the explosion or grinding of pumice fragments against each other. Judd found that the ash could be simulated by grinding Krakatau pumice (Plate 18).

SANTIAGUITO, GUATEMALA.—Santiaguito is a multiple dacite dome, active since 1922. The bulk of the ash eruptions and nuées ardentes originate at the Caliente dome. This ash was airfall from ash emission occurring on 28 July 1970, and was collected approximately 1.5 km west of the vent.

Petrography: This lithic ash consists of equant hyalocrystalline dacite fragments (these could possibly be classified as vitric, with abundant microlites and phenocrysts), plagioclase (An_{43}), and quartz crystals. Most vesicles are irregular, flattened ovoids. (0:0:25:75)

Morphology: The most abundant components in the ash are equant, slightly vesicular, irregularly shaped, hyalocrystalline dacite fragments (Plate 19). Most grain surfaces are hackly to conchoidal. The more glassy fragments are slightly more vesicular and have smooth grain surfaces (Plates 19D, 19E). Plagioclase is the most common mineral component in the ash. Individual phenocrysts are highly fractured, often breaking along twin planes. The ash formed during the vesiculation and disintegration of the upper part of a growing dacite dome and flow.

KATMAI, ALASKA.—The sample is from the ash flows in the Valley of Ten Thousand Smokes, which were deposited in 1912 by nuées ardentes from a center at what is now the Novarupta dome (G. Lofgren, oral communication). The sample was collected 20 cm from the bottom of the ash-flow tuff unit, approximately 17.5 km from Novarupta.

Petrography: The vitric ash is composed of colorless and brown pumice and shards from a "mixed" magma (andesitic and rhyolitic compositions). Most of the fragments are elongate, with the long axis parallel to the thin pipe-shaped vesicles. Vesicle walls broke up to form flat or slightly curved, very thin glass shards. (92.4:0:1.8:6.1)

Morphology: The ash from this eruption consists of small, elongate pumice fragments (Plate 20). The highly vesicular fragments contain elongate, flattened pipe vesicles, separated by very thin glass walls. Present in lesser amounts are fragments

with flattened spheroidal or ellipsoidal vesicles (Plates 20G, 20H), which grade into the more common pipe vesicles within the same fragment.

The fine-grained portion of the ash consists of mostly shards broken from thin vesicle walls. It consists of flat, curved, and Y-shaped fragments. The ash was formed by the disintegration of a plug of rhyolitic magma at or near the surface.

MAZAMA (CRATER LAKE) ASH.—This sample was collected in Steptoe Canyon, 0.8 km from Stewart Canyon, Whitman County, Washington. The eruption of Mt. Mazama (Crater Lake), located in south-central Oregon, consisted of large Plinian eruptions, with extensive ash fall and ash flows. The age, determined by C_{14} methods is 6600 years B.P. This eruption was not observed, but is included here because of the numerous studies of it (Fryxell, 1963; Williams, 1942; Wilcox, 1965) and its importance as a stratigraphic marker in the Pacific Northwest.

Petrography: This is a vitric ash, consisting of colorless, flat, and curved shards and small pumice fragments. Pumice fragments are up to 50 micrometers long with very angular shapes. Shards 1μ–100μ long, in cross section, have a variety of shapes including Y-shaped, curved, platelike and flat, tapered platelets. (100:0:0:0)

Morphology: The 1- to 30-micron-long particles include the following shapes (Plate 21):

1. Stubby, channeled fragments. These were probably thin-walled, elongate vesicles, which are now broken into short sections.
2. Curved, platelike shards.
3. Needle-shaped, pointed shards.
4. Flat, equant to slightly elongate particles, with 4- to 8-micron-diameter vesicles.
5. Triangular (in cross section) to Y-shaped particles, slightly curved along the long axis. These are vesicle walls from the junction of three adjacent vesicles.
6. 20μ–100μ long, elongate pumice fragments. These are rare in this particular sample.

ASH OF CARBONATITE COMPOSITION

OLDOINYO LENGAI, TANZANIA.—1966 eruption. Oldoinyo Lengai is the youngest of the volcanoes in the Neogene volcanic province of northern Tanzania, 19 km south of Lake Natron. According to Dawson and others (1968), "the volcano is a steep 6,500 foot cone, with two summit craters. The volcano is a dominantly pyroclastic cone with interbedded lavas in which the general trend is from phonolite-nephelinite-melanephelinite. The ejecta are unique, containing a substantial portion of sodium carbonate." Violent ash eruptions occurred in August 1966, varying from minor emissions of ash to major Plinian- and Vulcanian-type eruptions. A new ash cone built up and ash was widely distributed on the slopes of the volcano. The sample is from the surface, at the southern rim of the Southern Crater.

Petrography: The ash consists of sodium carbonate (trona) with crystals of nepheline, pyroxene, wollastonite, apatite, melanite, and pyrite. The ash was black originally and turned white. Lapilli are cemented by crystals of trona (Dawson and others, 1968).

Morphology: The ash consists of nearly all mineral fragments (Plates 22), including perfect euhedral (Plates 22A, 22F) and broken anhedral nepheline crystals. All the ash particles are coated with clumps of blade-shaped trona crystals. The trona is secondary, having precipitated onto grain surfaces after saturation of the ash with rainwater.

Hydrovolcanic (Phreatomagmatic) Eruptions

ASH OF BASALTIC COMPOSITION

CAPELINHOS, AZORE ISLANDS.—The sample is hyaloclastic ash from the 1965 eruption. The basaltic ash was deposited by hydrovolcanic (phreatomagmatic) eruptions in a shallow marine environment (Servico Geologicos de Portugal, 1959, 1962). Deposition was by airfall and base-surge flows. The exact location of the ash sample is not known.

Petrography: The vitric ash consists of primarily reddish-brown, transparent sideromelane fragments, with a trace of feldspar phenocrysts and feldspar microlites in some of the large fragments. Olivene and pyroxene are present as separate crystal components of the ash. (86.3:0:5:8.7)

Morphology: The vitric ash consists of mostly equant, block-shaped particles (Plate 23). The grain surfaces are mostly planar faces, meeting at nearly right angles. These surfaces are generally flat and smooth, or conchoidal. The flat fracture surfaces are characteristic of hyaloclastic ashes.

Vesicularity is very low; the vesicles are spherical and only rarely are stretched into elongate shapes. The skin characteristic of sideromelane droplets from magmatic eruptions is absent on sideromelane fragments of hyaloclastic origin.

SURTSEY, VESTMANN ISLANDS, ICELAND.—Surtsey is a tuff ring formed in the ocean off the Icelandic coast. The early stages of eruption were characterized by violent phreatomagmatic eruptions. Steam was generated when the seawater rushed into the vent, resulting in vertical and base-surge eruption clouds. Steam generation occurred at great depths and near the surface (Thorarinsson, 1967). The sample was collected from the deck of a Coast Guard vessel, 3 km from the vent, on 1 December 1963.

Petrography: The vitric ash consists of sideromelane fragments, with phenocrysts of olivine (Fo_{80}) and plagioclase (An_{60}) and no microlites. There is a trace of tachylite. (98.5:Tr:1.2:0)

Morphology: The ash consists of blocky sideromelane fragments (Plate 24) similar to the ash particles from Capelinhos. Most of the fragments are blocky and nearly equant. As in the Capelinhos ash, the vesicles are all spherical. The smooth, planar grain surfaces are broken by depressions where the fractures cut through vesicles.

TAAL, PHILIPPINES.—This sample is hyaloclastic ash from the hydrovolcanic (phreatomagmatic) eruptions of Taal in 1965 and was taken from the backset beds of a base-surge dune, 1 km west of the crater. The base-surge clouds, an important mode of deposition of ash in hydrovolcanic eruptions (Fisher and Waters, 1969, 1970), consist of clouds of steam, ejecta, and water that move radially away from the vent, across the ground surface, at hurricane velocities. These are associated with tuff rings and explosion pits.

Petrography: The moderately well-sorted vitric ash consists of equant, blocky sideromelane fragments, equant tachylite fragments (these may be from underlying, older ash deposits), augite crystals, and feldspar crystals ($\approx An_{45}$). (68.5:22.5:9.0:0)

Morphology: The vitric ejecta (Plate 25) is similar, but not identical, to the ashes from Surtsey and Capelinhos. The main ash component consists of a mixture of blocky and irregularly shaped sideromelane fragments. None are vesicular; the chilling of magma rising in the conduit must have taken place at a depth where vesiculation had not yet begun. Exotic (?) subrounded tachylite fragments with rough grain surfaces make up a minor component of the ash (Plate 25D). The tachylite fragments, atypical of hyaloclastic ejecta, may have come from older pyroclastic units underlying the vent area, mixed in during the phreatomagmatic eruptions.

TABLE ROCK, OREGON.—The Table Rock tuff-ring complex in the Fort Rock–Christmas Lake Valley Basin consists of a series of eight overlapping tuff rings and a tuff cone. The tuff rings were formed in a lake that existed during Pleistocene time. The ash was deposited by base-surge flows and by airfall during hydrovolcanic (phreatomagmatic) eruptions. The ash forms very well-bedded tuff rings around the crater. The sample was collected 1 km from the vent of ring 2 of the complex.

Petrography: The sample is composed of light-brown sideromelane, with thin rims of orange-brown palagonite. There are only a few phenocrysts and sparse microlites in the glassy fragments. (94.4:0:3.7:0.6)

Morphology: The least altered sideromelane fragments in this ash have grain surfaces pitted by weathering, but are morphologically and petrographically very similar to the ash from Surtsey. The ash particles (Plate 26) are blocky, with planar or slightly curved grain surfaces. The vesicularity is low.

This older (Pleistocene) ash has been altered, at least in part, to palagonite, a mixture of clays, iron oxides, and zeolites. The fragments completely altered to palagonite have scalelike grain surfaces with thin spalls of the alteration product (Plate 26A). The original grain shapes can be determined if the alteration is not complete and some glass remains in the core of the particle.

KILAUEA, HAWAII.—1924 phreatic eruption. The sample is of ejecta from the phreatic eruption in Kilauea, which occurred when rising magma came into contact with ground water in highly permeable aquifers. Ground water penetrated the vent at Kilauea and, on contact with incandescent materials, an enormous phreatic eruption was caused. The eruption lasted 17 days, resulting in the collapse of over 2×10^8 m^3 of rock into the empty vent. The exact location of this sample is not known.

Petrography: The lithic-crystal ash contains weathered, equant basalt fragments, hyalocrystal-

line basalt, olivine-rich basalt, tachylite, olivine crystals, orthopyroxene crystals, opaque minerals, and blocky sideromelane fragments. (33.3:0:35.2:32.3)

Morphology: This ash is similar to the Taal hyaloclastic ash; that is, it consists of a mixture of juvenile hyaloclastic ash and comminuted rock fragments from rock units below the vent area (Plate 27). The lithic fragments are the main constituent of this ash and consist of equant to elongate basalt fragments, with rough or hackly grain surfaces. Most have been pitted by weathering as well. The smaller sideromelane fraction is similar to the ashes from Capelinhos and Surtsey. The fragments are characterized by smooth, planar grain surfaces and low vesicularity.

Ash of Rhyolitic Composition

Panum Crater, California.—Panum Crater is a dome surrounded by a low-rimmed crater in the Mono Craters chain. It is possible that it is a maar of rhyolitic composition that erupted into Mono Lake. The sample was collected from the flank of the tuff ring.

Petrography: This is a crystal tuff, consisting of crystalline components and colorless pumice and shard fragments. The vitric and crystal components are nearly equal. Crystal components include sanidine, plagioclase, orthopyroxene, hornblende, and biotite. (49.9:0:50.1:0)

Morphology: Although this ash (Plate 28) was apparently thrown out during a hydrovolcanic (phreatomagmatic) eruption, it is quite similar to ashes from magmatic eruptions of rhyolitic and andesitic magmas. The main difference between this and rhyolitic ash from magmatic eruptions is the presence of a significant proportion of small, equant, blocky to bladelike shards (Plates 28E, 28F).

The pumice fraction consists of thin, elongate fragments, with flattened pipe vesicles parallel to the long axes of the grains. Some of the pumice fragments (Plate 28D) have smooth outer surfaces. These may have been parts of pumiceous fragments enclosed by an outer skin.

Sugarloaf, San Francisco Mountains, Arizona.—The vitric ash of rhyolitic composition is from a Pleistocene (?) tuff ring at the base of the eastern slopes of the San Francisco Mountains near Flagstaff, Arizona. The ejecta consists of extremely well-bedded ash in beds less than 1 mm to several centimeters thick. Cross-bedded dunes within the deposit indicate that part of the ejecta may have been deposited by base-surge flows during the eruption (Sheridan and Updike, 1971). The crater of the ring is filled with a large dome extruded during or after deposition.

It is probable that the ash is hyaloclastic; the magma chilled on contact with ground water. The blocky shard shapes, typical of hyaloclastic ash, the presence of base-surge dunes, and the plastic nature of the ash deformed by blocks thrown out during the eruption favor a phreatomagmatic type of eruption. The sample was collected on the northeast flank of the tuff ring.

Petrography: This sample of rhyolitic lithic-crystal ash consists of mostly colorless shards and pumice fragments containing 5 to 30 percent subparallel phenocrysts of K-feldspar, quartz, and plagioclase. The shards are generally equant or pyramidal and are subangular to rounded. Pumice fragments have straight to slightly curved vesicles, with average diameters of 0.01 mm and lengths of approximately 0.3 mm. The rounded lithic fragments consist of hyalocrystalline to equigranular rhyolite. The matrix material of the ash, with an approximate mean grain size of 0.01 mm, consists of mostly angular, pointed glass shards and lesser amounts of K-feldspar, quartz, and plagioclase. (47:0:34.5:18.5)

Morphology: The ash is similar to that from Panum Crater. The bulk of it consists of small, equant, blocky to pyramidal vitric fragments (Plate 29). The vitric fragments have both smooth and conchoidal grain surfaces. Most exhibit low vesicularity.

Pumice fragments, most of which are less than 400 microns across, contain poorly developed ellipsoidal to lensoidal vesicles. Blocky, rhyolitic lithic fragments are quite often rounded, possibly by grinding within the vent and ash cloud.

Ash from Littoral Steam Eruptions

Ash similar to that of tuff rings is characteristic of littoral cones, which are built by steam explosions generated when lava flows into a body of water (Moore and Ault, 1965; Fisher, 1968). At Puu Hou, Hawaii (Fisher, 1968), the production of

hyaloclastic sediments resulted from the rapid conversion of water into steam by a high-temperature lava flow. Evidence suggests that the explosions occurred when steam was trapped beneath lava crusts. The resulting varied mixture consists of: (1) crystalline basalt fragments and olivine phenocrysts, (2) sideromelane fragments with a few small vesicles, and (3) irregular, equant fragments with no vesicles.

Fisher has distinguished three basic particle types within the ashes from the Puu Hou littoral cones.

Type a—Vesicles are elongate or are spherical. Those with stretched vesicles have fluidal edges. Those with spherical vesicles are from presolidified pahoehoe crusts.

Type b—Frozen droplets—some are tear-shaped, or bizarre, bent shapes. No pele's hair or spheres.

Type c—Irregular to equant with few or no vesicles from broken portions of quickly chilled degassed lava.

Most of the basalt liquid was comminuted by the force of steam explosions and cooled in air; less was cooled by immersion in water. Pumice fragments with stretched vesicles, many of which are irregular droplets indicates that vesiculation occurred prior to cooling, but was not the cause of comminution. Vesiculation halted and bubbles frozen before fracturing in most of the pumice fragments, as shown by the general absence of corners rounded by surface tension (Fisher, 1968).

Basaltic Composition

Puu Hou Littoral Cones, Hawaii.—The littoral cones were formed by steam explosions when the 1868 lava flow reached the sea. Water entering the interior of the flow caused the steam explosions. The cones were built on both sides of the lava flow, at the shoreline. The sample is from one of the littoral cones.

Petrography: The vitric ash consists of (1) scalloped sideromelane fragments with abundant vesicles; (2) drawn sideromelane glass with small vesicles, elongate shapes, and fluidal edges (frozen droplets); and (3) irregular or equant sideromelane fragments with few or no vesicles (Fisher, 1968). (95.1:0:4.9:0)

Morphology: This ash is the most easily characterized of all the ash samples in this study. The ash consists of a mixture of blocky and pyramidal sideromelane fragments (hyaloclastic), broken and unbroken sideromelane droplets, and rough-surfaced fragments of tachylite and sideromelane flow crust (Plate 30).

The well-developed vesicularity near the flow top accounts for the oddly shaped hyaloclastic component of this ash. When the lava was chilled and the resulting quench shattered by thermal stresses, irregular pyramidal and crescent-shaped fragments were formed. In contrast, hyaloclastics produced in phreatomagmatic eruptions generally are blocky and have low vesicularities or are nonvesicular. The steam explosion resulting from the contact of lava and water also carries out droplets of unquenched lava and bits of old flow crust in addition to the hyaloclastic ejecta.

Sand Hills Littoral Cone, Hawaii (historic).—The Sand Hills cone is a recent (1848) littoral cone formed when a flow from the northeast rift, Kilauea, reached the sea. The sample is from the cone.

Petrography: The ash consists of mostly sideromelane fragments and droplets, containing olivine phenocrysts and 5 to 20 percent feldspar and opaque microlites. The droplets have a thin, dark-brown skin that is not found on the hyaloclastic fragments. (97.7:0:2.3:0)

Morphology: The morphology of the ash fragments (Plate 31) is identical to that of the Puu Hou ash.

Ash-Size Particles of Meteorite Impact and High-Energy Explosive Origin

Ries Basin, Germany.—The Ries Basin, Germany, is an impact crater, with ejecta consisting of molten crystalline basement rocks and Mesozoic sediments (Preuss and Schmidt-Kahler, 1969). The fragments studied here were picked out of the matrix of a suevite breccia. The photomicrographs (Plate 32) are from papers by Hörz (1965) and von Engelhardt and Stöffler (1968).

Petrography: According to von Engelhardt and Stöffler, "All fläden contain many vesicles; they are mixtures of molten glasses and fine mineral fragments. Phases contained in the fläden include diaplectic quartz glass, molten quartz glass, unaltered feldspar, diaplectic feldspars, normal feldspar glass, and diaplectic feldspar glass." Fläden consist of multiple thin layers of glass that are alternately poor and rich in angular mineral grains. Glass within the fläden is heterogeneous and consists of fine schlieren that differ in refractive index and

in color. "The structure reflects the heterogeneous nature of the parent rock, the intense movement of the melt, and the short duration of the molten state" (von Engelhardt and Stöffler, 1968).

DIAL-PACK EXPLOSION, ALBERTA, CANADA.—An explosion of 4.5 × 10^5 kg of TNT at the ground surface simulated a meteorite impact. The blast produced a crater 72 m in diameter and 4.5 m deep. Ejecta were thrown out in small rays. Small glass spheres that formed in the fireball rained down within and for at least 3.2 km from the crater in the prevailing wind direction. The underlying rock at the blast site consisted of lake sediments. The inhomogeneous glass spheres formed by quick melting in the fireball, followed by rapid quenching (Heiken and Lofgren, 1971). This sample was collected in the crater area immediately after the explosion.

Petrography: The ejecta consist of blocks of sediment underlying the blast center, fused soil, and spherules. Only the fine-grained fragments were studied here. These consisted of light-gray to light-brown, inhomogeneous glass, exhibiting light and slightly darker bands. Some of the bands have slightly different refractive indices than the bulk of the glass. There are a few anhedral, partly melted feldspar crystals. A dark-brown skin, 10 to 20 microns thick, encloses the spheres. The spheres are hollow; some contain only one large central vesicle and others have several.

Morphology: Most of the fine-grained ejecta involved in the fireball consist of glassy spheres (Plate 33). Most of the lunar spheres are studded with smaller spheres imbedded or splashed onto the surface. The debris-laden outer skin is rarely broken by outer vesicles. The population of spheres imbedded in or splashed onto larger spheres is generally high, and smooth spheres are rare.

Conclusions and Summary

The ashes are best placed into two broad genetic categories: magmatic and hydrovolcanic (phreatomagmatic). Ashes from magmatic eruptions are formed when expanding gases in the magma form a froth that loses its coherence as it approaches the ground surface. During hydrovolcanic eruptions, the magma is chilled on contact with ground or surface waters, resulting in violent steam eruptions. Within these two genetic categories, ashes from different magma types can be characterized (Table 1).

In low-viscosity magmas, droplet shape is, in part, controlled by surface tension, by acceleration of the droplets as they leave the vent, and by air friction. The ash particles consist of mostly sideromelane or tachylite; the sideromelane particles exhibit smooth, fluidal surfaces and a thin skin.

In magmas of higher viscosity, the morphology of ash particles is controlled primarily by vesicle density and shape, the vitric fraction generally consisting of very angular pumice fragments and thin vesicle walls, broken from pumice fragments during or after the eruption. The morphology of the lithic fragments is dependent on the texture and fracture pattern of the rock type broken up during the eruption.

The morphology of ash particles from hydrovolcanic eruptions is controlled by thermal stresses within the chilled magma, which result in fragmentation of the glass to form small blocky or pyramidal glass particles. Vesicle density and shape play a minor role in determining the morphology of these ash particles. Table 1 is a summary of the ash morphology of the ash samples collected.

It is hoped that this study will enable a worker to infer the genesis and possibly the source of isolated volcanic ash samples from stratigraphic sections or deep-sea cores.

Literature Cited

Cook, E. F.
1965. Stratigraphy of Tertiary Volcanic Rocks in Eastern Nevada. *Nevada Bureau of Mines Report,* 11: 66 pages.

Dawson, J. B., P. Bowden, and G. C. Clark
1968. Activity of the Carbonatite Volcano Oldoinyo Lengai, 1966. *Geologische Rundschau,* 57:865–879.

von Engelhardt, W., and D. Stöffler
1968. Stages of Shock Metamorphism in the Crystalline Rocks of the Ries Basin, Germany. Pages 159–168 *in* Bevan M. French and Nicholas M. Short, editors, *Shock Metamorphism of Natural Materials.* Baltimore: Mono Book Corporation.

Fisher, R. V.
1961. Proposed Classification of Volcaniclastic Sediments and Rocks. *Geological Society of America Bulletin,* 72:1409–1414.

1966. Rocks Composed of Volcanic Fragments and Their Classification. *Earth Science Reviews,* 1:287–298.
1968. Puu Hou Littoral Cones, Hawaii. *Geologische Rundschau,* 57:837–864.

Fisher, R. V., and A. C. Waters
1969. Bed Forms in Base Surge Deposits: Lunar Implications. *Science,* 165:1349–1352.
1970. Base Surge Bed Forms in Maar Volcanoes. *American Journal of Science,* 268:147–180.

Fryxell, Roald
1963. Mazama and Glacier Peak Volcanic Ash Layers: Relative Ages. *Science,* 147:1288–1290.

Heiken, Grant H.
1971. Tuff Rings: Examples from the Fort Rock-Christmas Lake Valley, South-Central Oregon. *Journal of Geophysical Research,* 76:5615–5626.
1972. Morphology and Petrography of Volcanic Ashes. *Geological Society of America Bulletin,* 83:1961–1988.

Heiken. Grant H., and Gary Lofgren
1971. Terrestrial Glass Spheres. *Geological Society of America Bulletin,* 82:1045–1050.

Hörz, Friedrich
1965. Untersuchungen an Riesglasern. *Beitrage zur Mineralogie und Petrographie,* 11:621–661.

Judd, J. W.
1888. On the Volcanic Phenomenon of the Eruption, and on the Nature and Distribution of the Ejected Materials. Pages 1–56 *in* G. J. Symens, editor, *The Eruption of Krakatoa and Subsequent Phenomena.* London: Trubner and Company.

Loney, Robert A.
1968. Flow Structure and Composition of the Southern Coulee, Mono Craters, California—A Pumiceous Rhyolite Flow. *Geological Society of America Memoir,* 116:415–440.

McBirney, Alexander R.
1968. Compositional Variations of the Climactic Eruption of Mount Mazama. *Oregon Department of Geological and Mineral Industries Bulletin,* 62:53–57.

Moore, J. G., and W. V. Ault
1965. Historic Littoral Cones in Hawaii. *Pacific Science,* 19:3–11.

Moore, J. G., and W. G. Melson
1969. Nuées Ardentes of the 1968 Eruption of Mayon Volcano, Philippines. *Bulletin Volcanologique,* 33:600–620.

Nakamura, Kazuaki
1964. Volcano-Stratigraphic Study of Oshima Volcano: Izu. *Bulletin of the Earthquake Research Institute of Japan,* 42:649–728.

Norrish, K., and J. T. Hutton
1969. An Accurate X-Ray Spectrographic Method for the Analysis of a Wide Range of Geological Samples. *Geochimica et Cosmochimica Acta,* 33:431–453.

Rittman, Alfred
1962. *Volcanoes and Their Activity.* 305 pages. New York: John Wiley and Sons.

Servico Geologicos de Portugal
1959. Le Volcanisme de L'Isle de Faial et l'eruption de Volcan de Capelinhos. *Memoir (Nova Serie),* 4: 100 pages.
1962. Le Volcanisme de L'Isle de Faial et l'eruption de Volcan de Capelinhos. *Memoir (Nova Serie),* 9: 54 pages.

Sheridan, M. F., and R. G. Updike
1971. Sugarloaf Tephra–A Rhyolitic Deposit of Base Surge Origin in Northern Arizona [abstract]. *Geological Society of America Proceedings,* 3:191–192.

Stoiber, Richard E., and William E. Rose
1970. The Geochemistry of Central American Volcanic Gas Condensates. *Geological Society of America Bulletin,* 81:2891–2912.

Tanguy, J. C.
1971. Mount Etna Volcanic Eruption. *Smithsonian Center for Short-Lived Phenomena Bulletin,* December 15, 1971.

Thorarinsson, Sigurdur
1967. *Surtsey–The New Island in the North Atlantic.* 47 pages. New York: Viking Press.

Van Padang, M. Hermann
1951. Indonesia. Part I in *Catalogue of the Active Volcanoes of the World.* 271 pages. Naples: International Volcanological Association.

Verhoogan, J.
1951. Mechanisms of Ash Formation. *American Journal of Science,* 249:729–739.

Walker, G. P. L., and R. Croasdale
1972. Characteristics of Some Basaltic Pyroclastics. *Bulletin Volcanologique,* 35:303–317.

Wentworth, C. K.
1938. Ash Formation of the Island of Hawaii. *Special Report of the Hawaiian Volcano Observatory,* 3: 183 pages.

Wilcox, Ray E.
1965. Volcanic Ash Chronology. Pages 807–816 *in* H. E. Wright and D. G. Frey, editors, *The Quaternary of the United States.* Princeton, N.J.: Princeton University Press.

Williams, Howel
1942. The Geology of Crater Lake National Park, Oregon. *Carnegie Institution Publications,* 540: 162 pages.

Appendices

Appendix 1: Chemistry of the Volcanic Ashes Studied for this Report

Unless otherwise specified, the X-ray fluorescence analyses were made by Mike Rhodes, Kay Parker, and John Evans, Lockheed Electronics Company, NASA-Manned Spacecraft Center.

Most of the major elements (Si, Ti, Al, Fe, Mn, Ca, K, P, and S) were determined by X-ray fluorescence analysis, using a glass disk prepared by fusing 280 mg of powdered sample with a lanthanum-bearing lithium borate fusion mixture. Preliminary concentrations obtained for these samples were used to calculate matrix corrections, which in turn were applied to the preliminary data to obtain final corrected concentrations. This technique has been described and evaluated fully by Norrish and Hutton (1969).

The other elements were measured on separate aliquots of the sample; sodium by atomic absorption spectroscopy and ferrous iron and water by conventional chemical techniques. (Rhodes, 1971, personal communication.)

1. Pacaya: Rhodes, analyst.
2. Fuego: Baird, analyst, in Stoiber and Rose (1970).
3. Cerro Negro: Rhodes, analyst.
4. Etna: sample is of lava flow from the South Vent, May 7, 1971. Lenable, analyst, in Tanguy, J. C., (1971).
5. Kilauea Iki, 1959: Rhodes, analyst.
6. Kilauea Crater–Reticulite: Rhodes, analyst.
7. Ash from Aloi-Alae Craters area–Hawaii: Rhodes, analyst.
8. Taal, Philippines: Rhodes, analyst.
9. Ruapehu, New Zealand: Rhodes, analyst.
10. Merapi, Indonesia: Rhodes, analyst.
11. Mayon, Philippines: Rhodes, analyst.
12. Krakatau, Indonesia: collected on Perbuwatan. R. G. Reiber, analyst; *in* Van Padang (1951).
13. Santiaguito, Guatemala: Rhodes, analyst.
14. Katmai, Alaska: Rhodes, analyst.
15. Analysis of white pumice, 15 feet above the creek bed at the Pinnacles, Crater Lake, Oregon. Ken-ichiro Aoki, analyst, *in* McBirney (1968).
16. Ash from Oldoinyo Lengai, Tanzania: from Dawson et al. (1968).
17. Capelinhos, Azores: Guimares and Viera, analysts (Servico Geologicos de Portugal, 1959).
18. Surtsey, Iceland: from Thorarinsson (1967).
19. Table Rock, Oregon: Heiken, analyst.
20. Panum Crater, California: analysis is of rhyolite from the Southern Coulee, Mono Craters (Loney, 1968).
21. Puu Hou, Hawaii: Rhodes, analyst.
22. Sand Hills, Hawaii: Rhodes, analyst.
23. Ries Basin, Germany: from von Engelhardt and Stöffler (1968). An average of nine unrecrystallized glass bombs collected at nine different localities around the Ries Basin.

Appendix 2: Gas Release Study of Selected Volcanic Ashes

Everett K. Gibson, Jr.

Selected volcanic ash samples have been analyzed for their gas contents and weight loss during heating under vacuum. The analytical technique employed was a combined thermal analysis-mass spectrometric procedure described previously (Gibson and Johnson, 1971, 1972; Gibson, 1972; Gibson and Moore, 1972). A Mettler recording vacuum thermoanalyzer interfaced to a Finnigan 1015 quadrupole mass spectrometer was used for the analysis. The mass spectrometer source was placed directly in the reaction chamber. With this arrangement the evolved gaseous species could be analyzed rapidly and without requiring gas transfer procedures.

Sample sizes ranged from 20 mg for volatile rich ashes to 200 mg for ash samples which were depleted in volatiles. Samples were heated at 6°C/minute from room temperature to temperatures up to 1400°C under a vacuum of 10^{-6} torr. The sample's weight loss along with released gaseous species, abundances, temperature ranges, and sequences of release were determined simultaneously on the sample during the heating cycle. The sensitivity of the analytical balance used for weight-loss studies was ± 0.05 mg. Sample temperatures were measured with calibrated platinum/platinum–10 percent rhodium thermocouples located at the base of the platinum sample crucibles. Spectra were obtained every 5°C during the heating cycle. Reproducible background spectra were obtained during the bakeout procedures before sample analysis began and were later subtracted from the obtained spectra.

Everett K. Gibson, Jr., Geochemistry Branch, TN7, NASA, Johnson Space Center, Houston, Texas 77058.

The ash samples were neither crushed nor homogenized before analyses, under the assumption that gas-filled vesicles or inclusions might be ruptured. The petrographic descriptions of the ash samples analyzed have been given previously by Heiken (1972 and this atlas), with the exception of the basaltic ashes from Hekla. The Hekla ashes were collected during the summer of 1970 by Carleton B. Moore of Arizona State University, Tempe, Arizona.

A summary of the weight-loss data on the ash samples analyzed is given in Table 3. The weight-loss data has been calculated from the thermograms obtained from the thermal analysis-gas release measurements.

The gas release profiles for the ash samples analyzed are given in Figures 1 to 16. The system background has been subtracted from each spectra taken at a given temperature. The gases which are in low concentrations have been multiplied by factors of 10 and 100, to allow plotting on the same release profile. For example: if H_2O is plotted as $\times$ 1 and CO_2 is plotted as $\times$ 10, the H_2O concentration is 10 times that of the CO_2 or stated another way, the CO_2 concentration is one-tenth that of the water concentration. In selected samples containing large quantities of volatiles, the numbers given at the top of the release peaks represent how much higher the peak goes before it decreases. The same scaling factor is used as that given below 100 percent relative abundance.

Literature Cited

Gibson, Jr., E. K.

1973. Thermal Analysis–Mass Spectrometer–Computer System and Its Application to the Evolved Gas Analysis of Green River Shale and Lunar Soil Samples. *Thermochimica Acta,* 5:243–255.

Gibson, Jr., E. K., and S. M. Johnson

1971. Thermal Analysis-Inorganic Gas Release Studies of Lunar Samples. *Proceedings of the Second Lunar Science Conference,* 2:1351–1366. Cambridge: Massachusetts Institute of Technology Press.

1972. Thermogravimetric-Quadrupole Mass-Spectrometric Analysis of Geochemical Samples. *Thermochimica Acta,* 4:49–56.

Gibson, Jr., E. K., and G. W. Moore

1972. Inorganic Gas Release and Thermal Analysis Study of *Apollo 14* and *15* Soils. *Proceedings of the Third Lunar Science Conference,* 2:2029–2040. Cambridge: Massachusetts Institute of Technology Press.

Heiken, Grant H.

1972. Morphology and Petrography of Volcanic Ashes. *Geological Society of America Bulletin,* 83:1961–1988.

TABLE 1.—*Volcanic ash summary*

A. Magmatic eruptions*

Magma type	Basaltic	Andesitic	Rhyolitic and dacitic	Carbonatite (one sample)
Volcanic features associated with the ash	Cinder cones, lava lakes, basalt flows, and ash interbeds in strato-volcanoes.	Strato-volcanoes, domes, thick short lava flows, and ash-flow tuff units.	Domes and flows, some strato-volcanoes, calderas, and hypothetical fissure vents which are sources for ash flows; ash-flow tuff sheets.	Strato-volcanoes, ash cones.
Petrography	Mostly droplets and broken droplets of sideromelane (clear, brown basaltic glass) and tachylite (black, submicrocrystalline basalt); phenocryst population is variable.	The main components (vitric, crystal, lithic) vary, but all are generally present; the vitric component includes colorless glass shards and pumice fragments; generally containing oriented microlites; lithic fragments include andesite of varying textures and stages of alteration and igneous and sedimentary xenoliths; broken crystals of plagioclase, pyroxene, and opaque minerals are common.	Generally, there is a great amount of colorless glass with variable amounts of microlites and phenocrysts; phenocrysts of quartz, sanidine, biotite, and small amounts of other ferro magnesian minerals; small amount of lithic (rhyolitic or xenolithic) fragments.	Ash and lapilli consisting of crystals of sodium carbonate, nepheline, pyroxene, wollastonite, apatite, melanite, and pyrite are cemented by blade-like sodium carbonate crystals.
Chemistry of samples studied	SiO_2, 48 to 52 percent Total Fe as Fe_2O_3, 10 to 13 percent Al_2O_3, 12 to 19 percent	SiO_2, 56 to 59 percent Total Fe as Fe_2O_3, 6 to 8 percent Al_2O_3, 16 to 19.5 percent	SiO_2, 63 to 74 percent Total Fe as Fe_2O_3, 1.9 to 5.3 percent Al_2O_3, 13 to 17 percent	SiO_2, 25.23 percent Fe as Fe_2O_3, 8.71 percent Al_2O_3, 5.72 percent
Morphology	1. Irregular droplets with fluidal shapes (spheres, ovoids, dumbbell and teardrop shapes). 2. Broken droplets; some with original droplet surface present. 3. Long, thin strands of glass (Pele's hair). 4. Polygonal, lattice-like network of glass rods; highly vesiculated froth. The grain shapes vary from a dominance of spheres and droplets in lavas of very low viscosity to irregular elongate, often broken droplets from lavas of slightly higher viscosities; some droplets have been twisted around a central axis; all are highly vesicular. Smooth, fluidal surfaces broken by smooth-lipped vesicle cavities (these broke while the surface was still fluid) and cavities with angular rims (these near-surface vesicle walls broke after the surface of the grain was chilled). In detail, the surface skin, formed soon after ejection from the vent, is broken by parallel joints through which some later liquid may protrude (and is chilled). Some particles have warty surfaces.	1. Vitric component: equant to elongate pumice fragments; dependent on the shape of the vesicles in the fragment; elongate pumice fragments contain elongate, ovoid to tubular vesicles; fragments are irregular; only the exposed vesicle walls are smooth. Flat, pointed shards with smooth or conchoidal fracture surfaces are probably broken vesicle walls. 2. Lithic fragments: These are generally equant; the surface is entirely dependent on the texture and fracture of the rock type; some of the fragments are rounded. 3. Crystal fragments: Shape is governed by the fracture of the mineral; most appear to have been broken during the eruption.	1. Vitric fragments: elongate to equant pumice fragments (grain shape is dependent on vesicle shape) with thin vesicle walls; curved, Y-shaped, or flat thin shards are vesicle walls; these are very smooth and rarely chipped except by later reworking of the ash. 2. Lithic fragments are generally equant in these ash samples. The surfaces of pumice fragments are very rough, broken vesicles; no smooth surfaces other than vesicle walls; there are no smooth fluidal surfaces similar to those of droplets in low-viscosity lavas.	*Perfect crystals of nepheline and* broken (irregular but equant) crystals of the other components listed under petrography. Surfaces of nearly all the grains are coated with bundles of thin, bladed sodium carbonate crystals; the bundles are 5 to 50 microns thick; the bundles of sodium carbonate are generally concentrated in depressions in the grain surfaces.

B. Hydrovolcanic [Phreatomagmatic] eruptions† — C. Ash-size vitric particles of meteorite impact origin

Magma type	Basaltic	Rhyolitic	Basaltic (littoral)§	
Volcanic features associated with the ash	Maar-type volcanoes: tuff rings, tuff cones, and explosion pits.	Tuff ring with a central dome.	Littoral cones.	Impact craters: wide shallow craters with low ejecta rims.
Petrography	Vitric ash. Angular fragments of sideromelane; generally free of all crystals except phenocrysts; the lithic component of some ashes is dependent on the stratigraphy of rocks underlying the maars and the amount of magma reaching the surface.	Most ash particles consist of equant or elongate colorless glass fragments; traces of rhyolitic lithic fragments; the glass is generally free of microlites or contains very few microlites.	Vitric to vitric-lithic ash: the sample consists of mostly sideromelane droplets, tachylite, and fragments of aphanitic basalt.	Nonvesicular to highly vesicular; generally very inhomogeneous glass with abundant schlieren of different refractive indices and mineral detritus; shocked minerals are present in the detritus.
Chemistry of Samples Studied	SiO_2, 45 to 47 percent Total Fe as Fe_2O_3, 10 to 13 percent Al_2O_3, 16 to 17 percent	SiO_2, 75.4 percent Fe as Fe_2O_3, 0.9 percent Al_2O_3, 13.5 percent	SiO_2, 50 to 51 percent Total Fe as Fe_2O_3, 11.5 percent Al_2O_3, 12 to 13 percent	Dependent on the target surface and partly on composition of the meteorite.
Morphology	Equant blocky glass fragments with low vesicularity. Smooth flat fracture surfaces are formed when the glasses contract and fracture after chilling; these fracture faces cut across vesicles if the particles are vesicular.	Sharply pointed elongate shards and flat elongate pumice fragments. Conchoidal to irregular fracture surfaces of each grain; the vesicle walls are smooth.	1. Crystalline basalt fragments; equant lithic fragments. 2. Sideromelane glass fragments with few vesicles; these may be blocky or crescent shaped; the shape may be controlled mainly by vesicle shapes. 3. Nonvesicular pyramidal glass fragments formed by thermal strain leading to shattering of highly vesicular lava. 4. Broken and unbroken elongate to equant droplets; no Pele's hair. The droplets and broken droplets have round fluidal surfaces with sharp angular lips around depressions caused by the breaking of the vesicle wall of a vesicle located near the grain surface. The exposed vesicle walls have smooth curved surfaces. Fracture surfaces of hyaloclastic grains have flat and curved smooth surfaces.	Glass droplets (complete and broken) a few microns to several centimeters in diameter; abundant smaller spheres, droplets, and rock fragments are welded to the surface of larger spheres. The glass is generally smooth where there are no other fragments welded to the surface or no collapsed vesicles.

* The eruptions are caused by rapid release of gases or frothing in the magma as it reaches the surface, resulting in (1) large-scale ash eruption (Plinian, Vulcanian, or Pelean) with resulting ash falls and ash flows; high-viscosity lavas; associated lahars or volcanic mudflows if the eruption is into a crater lake or is accompanied by rainstorms; and (2) lava fountaining and ash eruptions (Hawaiian and strombolian types) of low-viscosity lavas.

† The eruptions are caused primarily by the steam generated when rising magma comes into contact with shallow bodies of surface water, ice, or ground water; magmatic gases add to the energy of the eruptions.

§ The ash is formed when lava flows into the sea and water penetrates into cracks in the flow surface.

TABLE 2.—*Chemistry of the ashes studied*

Chemistry	(1)	(2)	(3)	(4)	(5)	(6)	(7)	(8)	(9)	(10)	(11)	(12)
SiO_2	51.8	49.42	49.2	47.38	48.17	49.29	48.57	52.71	58.58	55.99	56.32	65.14
TiO_2	1.15	0.87	1.28	1.68	2.44	2.51	2.12	0.86	0.63	0.69	0.68	0.48
Al_2O_3	17.73	19.09	19.38	17.44	11.65	14.12	10.78	16.10	15.68	19.4	19.13	15.28
Fe_2O_3	2.96	–	4.42	6.00	1.87	–	1.48	10.99	2.49	7.04	7.81	2.57
FeO	6.49	–	5.55	5.16	9.66	–*	10.19	–*	3.15	–*	–*	1.79
MnO	0.22	–	0.14	–	0.22	0.23	0.23	0.25	0.10	0.22	0.20	0.14
MgO	4.03	6.75	5.41	5.52	10.84	7.33	14.04	5.52	3.18	1.91	3.71	1.38
CaO	9.52	10.07	11.89	10.77	10.25	10.44	9.41	9.99	5.58	7.69	8.54	3.17
Na_2O	4.05	3.09	1.76	3.42	3.08	–	2.75	3.37	3.17	4.23	4.15	3.77
K_2O	0.83	0.60	0.85	1.71	0.49	0.35	0.38	0.03	1.52	2.40	1.16	2.89
P_2O_5	0.26	0.41	0.05	–	0.25	0.23	0.22	0.18	0.12	0.29	0.28	0.06
S	0.06	–	–	–	0.11	0.09	0.08	0.06	2.17	0.06	0.12	0.42
H_2O+	–	–	–	0.50	–	–	–	–	–	–	–	2.24
H_2O-	–	–	–	0.06	–	–	–	–	–	–	–	0.74
Cl	–	–	–	–	–	–	–	–	–	–	–	0.13
Total	99.10	100.83	99.93	99.79	99.03	97.38	100.25	100.06	96.39	99.92	102.1	100.2
Total Fe as Fe_2O_3	10.35	10.61	9.97	11.16	12.61	12.79	12.81	10.99	5.99	7.04	7.81	4.36

	(13)	(14)	(15)	(16)	(17)	(18)	(19)	(20)	(21)	(22)	(23)	
SiO_2	62.44	73.52	71.82	25.23	47.59	46.5	44.45	75.4	51.53	50.46	63.54	
TiO_2	0.48	0.22	0.49	0.46	2.65	2.28	1.27	0.04	2.02	2.29	0.81	
Al_2O_3	16.69	12.15	15.07	5.72	17.05	16.8	9.73	13.5	13.15	12.22	15.10	
Fe_2O_3	2.98	0.49	1.33	8.71	2.97	1.65	9.97	0.42	11.34	11.58	0.99	
FeO	2.08	1.28	0.89	–*	7.44	10.8	–*	0.50	–*	–*	3.75	
MnO	0.21	0.07	0.06	0.38	0.20	0.20	0.17	0.05	0.21	0.21	0.10	
MgO	2.48	0.52	0.44	1.62	5.47	7.62	7.98	0.10	8.13	11.75	2.71	
CaO	5.02	1.29	1.91	14.10	9.09	9.45	10.51	0.42	9.87	9.98	3.45	
Na_2O	4.56	4.10	5.02	18.65	4.57	3.32	3.34	3.8	3.17	2.84	2.86	
K_2O	1.54	2.90	2.89	4.89	1.85	–	1.36	4.8	0.42	0.41	3.71	
P_2O_5	0.20	0.04	0.07	1.49	0.50	0.33	–	–	0.24	0.24	0.36	
S	0.07	0.02	–	0.31	–	–	–	–	0.08	0.11	–	
H_2O+	–	–	–	1.15	0.07	0.03	4.2	0.71	–	–	2.73	
H_2O-	–	–	–	4.89	0.37	0.02	6.0	0.17	–	–	–	
Cl	–	–	–	1.13	–	–	–	–	–	–	–	
Total	98.75	96.60	99.99	100.33	99.82	99.00	98.98	100.00	100.16	102.09	100.48	
Total Fe as Fe_2O_3	5.29	1.91	2.22	8.71	10.41	12.45	9.97	–	11.34	11.58	4.74	
			CO_2—8.75								CO_2—0.37	
			BaO—1.00									
			SO_3 —1.23									
			F —0.62									

* Insufficient material for FeO determination.

TABLE 3.—*Weight losses for volcanic ash*

Sample	*Sample wt. (mg)*	*Percent weight loss*														
		100°C	200°C	300°C	400°C	500°C	600°C	700°C	800°C	900°C	1000°C	1100°C	1200°C	1300°C	1400°C	1450°C
Santiaguito Dacitic	127.66	0.063	0.094	0.12	0.14	0.16	0.17	0.20	0.21	0.24	0.27	0.31	0.38	0.48	0.60	1.33
Oldoinyo Lengai	21.42	3.78	3.97	4.30	5.00	8.50	14.15	18.58	20.26	21.62	24.42	32.31 1050°C				
Hekla-Tephra	161.45	0.0	0.012	0.031	0.056	0.074	0.11	0.17	0.22	0.27	0.33	0.55 1080°C				
Mayon Volcano-Philippines 1968 andesitic airfall	42.32	0.047	0.095	0.14	0.19	0.21	0.26	0.31	0.33	0.38	0.45	0.57	0.66	0.97	1.61	
Cerro Negro-Nicaraugua Basaltic ash	51.85	0.019	0.058	0.077	0.096	0.14	0.15	0.17	0.21	0.25	0.33	0.41	0.48	0.75	1.31	
Taal-Philippines-1968	62.30	0.0	0.016	0.032	0.048	0.064	0.080	0.096	0.11	0.14	0.18	0.32	0.51	1.17	2.42	
Ruapehu-no sublimates	150.82	0.34	0.56	0.66	0.83	1.19	1.29	1.52	1.62	1.72	1.79	1.89	1.96	2.12	3.12	
Ruapehu-with sublimates	153.03	0.22	1.29	1.63	2.12	3.27	3.59	4.05	4.41	4.80	5.16	5.42	5.69			
Surtsey-1963	47.62	0.021	0.042	0.063	0.13	0.29	0.40	0.57	0.67	0.71	0.84	1.15	1.43	2.110	4.018	
Mt. Spurr, Alaska 1963, andesitic ash	46.0	0.48	0.98	1.83	3.37	5.57	7.22	7.76	8.30	8.67	8.83	9.022	9.20 1150°C			
Sugar Loaf, Arizona	197.67	0.025	0.28	0.68	1.11	1.37	1.51	1.59	1.64	1.68	1.76	1.86	1.92	1.99 1350°C		
Pacaya, Guatemala Basaltic	156.22	0.006	0.019	0.064	0.083	0.10	0.13	0.16	0.19	0.22	0.29	0.42	0.58	0.98	1.90	
Katmai, Alaska-1912	22.43	0.18	1.20	1.74	2.14	2.32	2.41	2.50	2.59	2.67	2.81	2.90	2.99	3.076	3.17	
Hekla	85.17	0.012	0.035	0.059	0.11	0.12	0.14	0.16	0.20	0.22	0.27	0.45	0.79	1.36		
Merapi, Indonesia	38.12	0.11	0.24	0.34	0.50	0.66	0.68	0.71	0.74	0.79	0.84	0.97	1.10	1.50		
Panum Crater, California Pleistocene	40.31	0.20	0.55	1.067	1.41	1.64	1.71	1.79	1.86	1.89	1.98	2.009	2.059	2.11 1250°C		

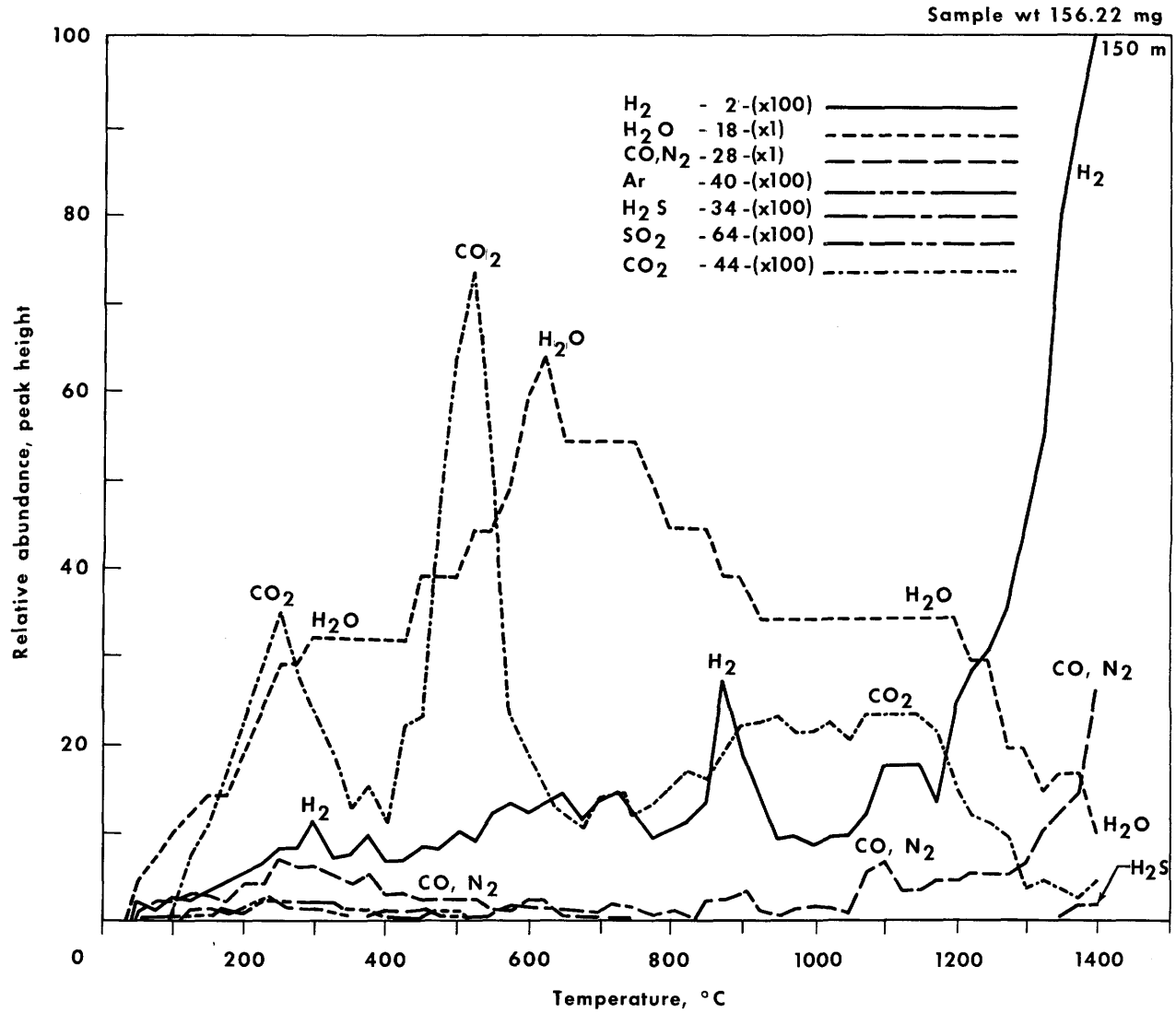

FIGURE 1.—Pacaya, Guatemala: Basaltic. The Pacaya basaltic ash is depleted in volatiles. The sample lost only 0.29 percent by weight after heating to 1000°C. The ash sample did not contain any absorbed gases. Water was released slowly over the complete heating range, with the maximum release occurring near 500°–600°C. Carbon dioxide was released in three regions. Below 350°C, a small amount of CO_2 was released. Between 400° and 550°C, CO_2 is suddenly released from the decomposition of carbonate phases such as calcite or a similar carbonate. At temperatures above 700°C, carbon dioxide is slowly evolved. This CO_2 results from residual carbon reacting with the silicate matrix to evolve CO_2. Upon heating to 1400°C, the Pacaya basaltic ash lost only 1.90 weight percent. The low abundance of volatiles in the Pacaya ash is characteristic of its high temperature history.

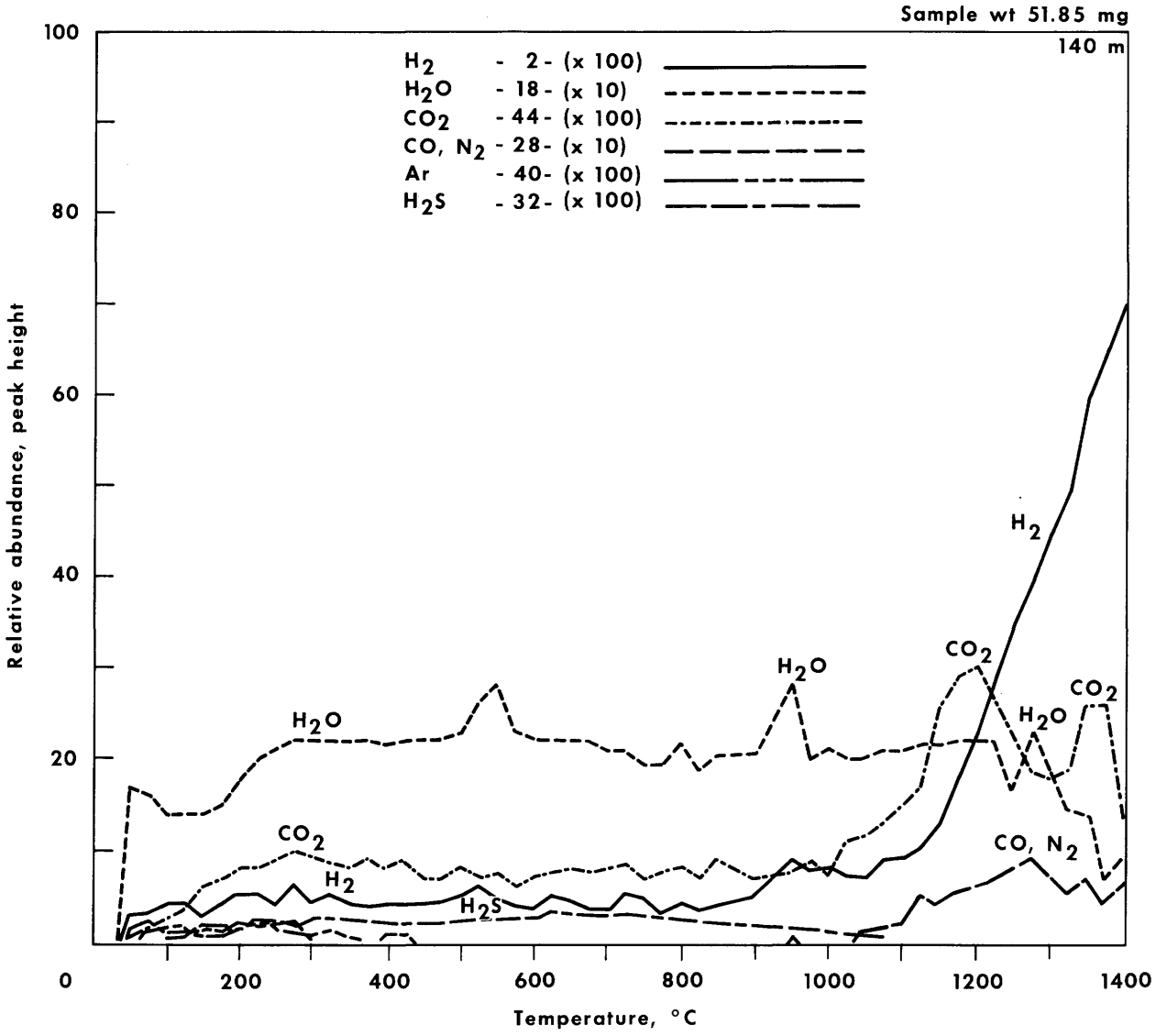

FIGURE 2.—Cerro Negro: Basaltic. The basaltic ash from Cerro Negro is extremely depleted in its volatile gases and low temperature mineral phases. The gas release pattern shows only trace amounts of H_2O released over the complete temperature range. Trace amounts of CO_2 are released above 1000°C, and the $C\Theta_2$ is undoubtedly a reaction product produced at the elevated temperatures. The Cerro Negro ash sample lost only 1.31 weight percent (total) during the heating to 1400°C. The Cerro Negro basaltic ash is typical of basaltic ashes which are depleted in their inorganic gases and are characteristic of their past high temperature histories.

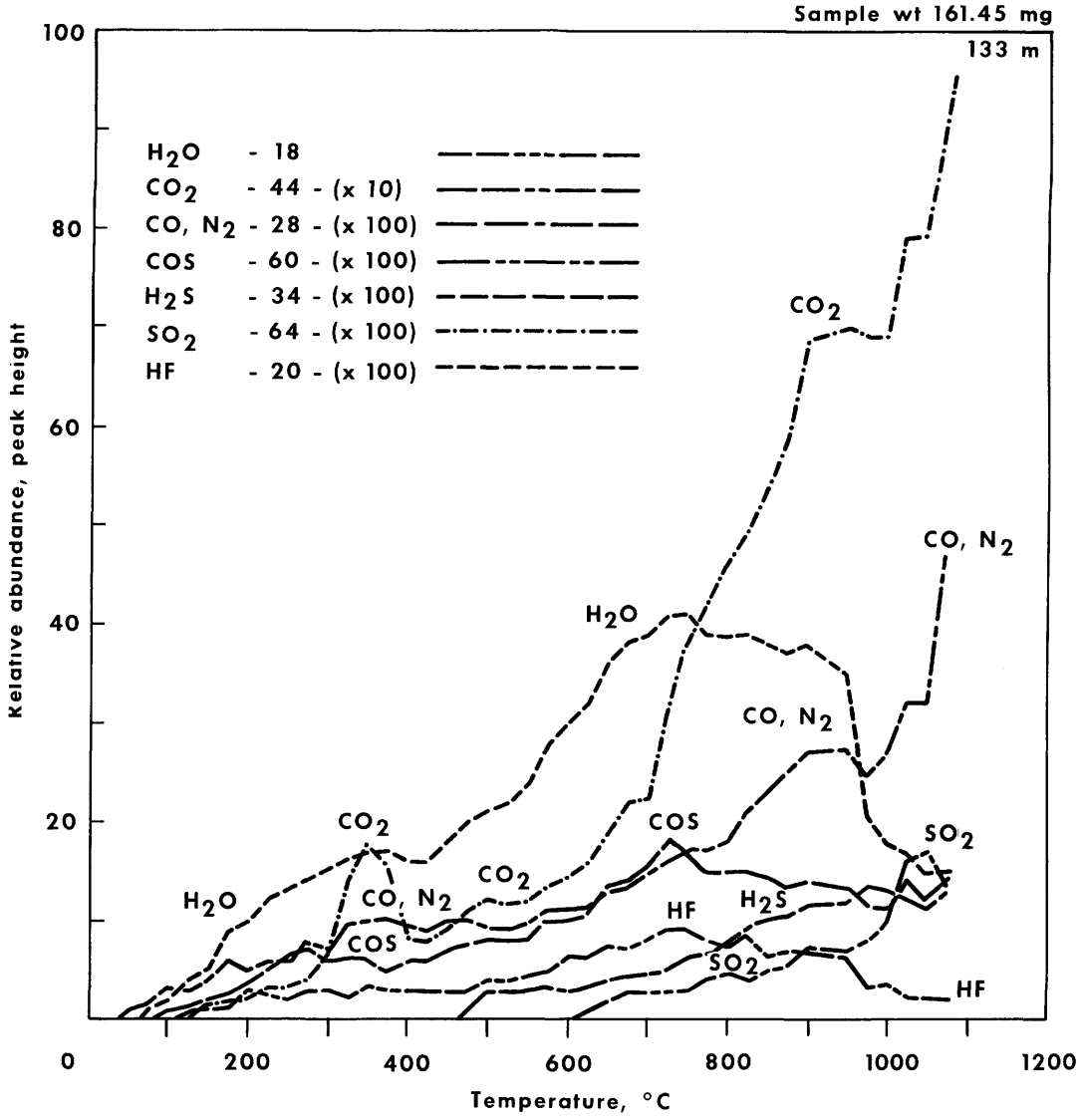

FIGURE 3.—Hekla: Basaltic. The Hekla tephra is extremely depleted in volatiles. The sample does not contain any terrestrially absorbed gases such as H_2O, CO_2 and/or CO, N_2 which are normally released below 150°C. The sample lost less than 0.01 percent total weight during heating below 200°C. The released CO_2 shows evidence of a possible carbonate decomposition between 300° and 400°C. The carbonate is probably secondary because of the high temperature history of this tephra sample. Trace amounts of the unusual gases HF and COS are seen in the gas release profile of the ash sample. The gases released above 700°C are reaction products of components found within the basaltic ash. Upon heating under vacuum to 1050°C, the sample lost only 0.55 percent total weight loss, further evidence of the high temperature history of the sample.

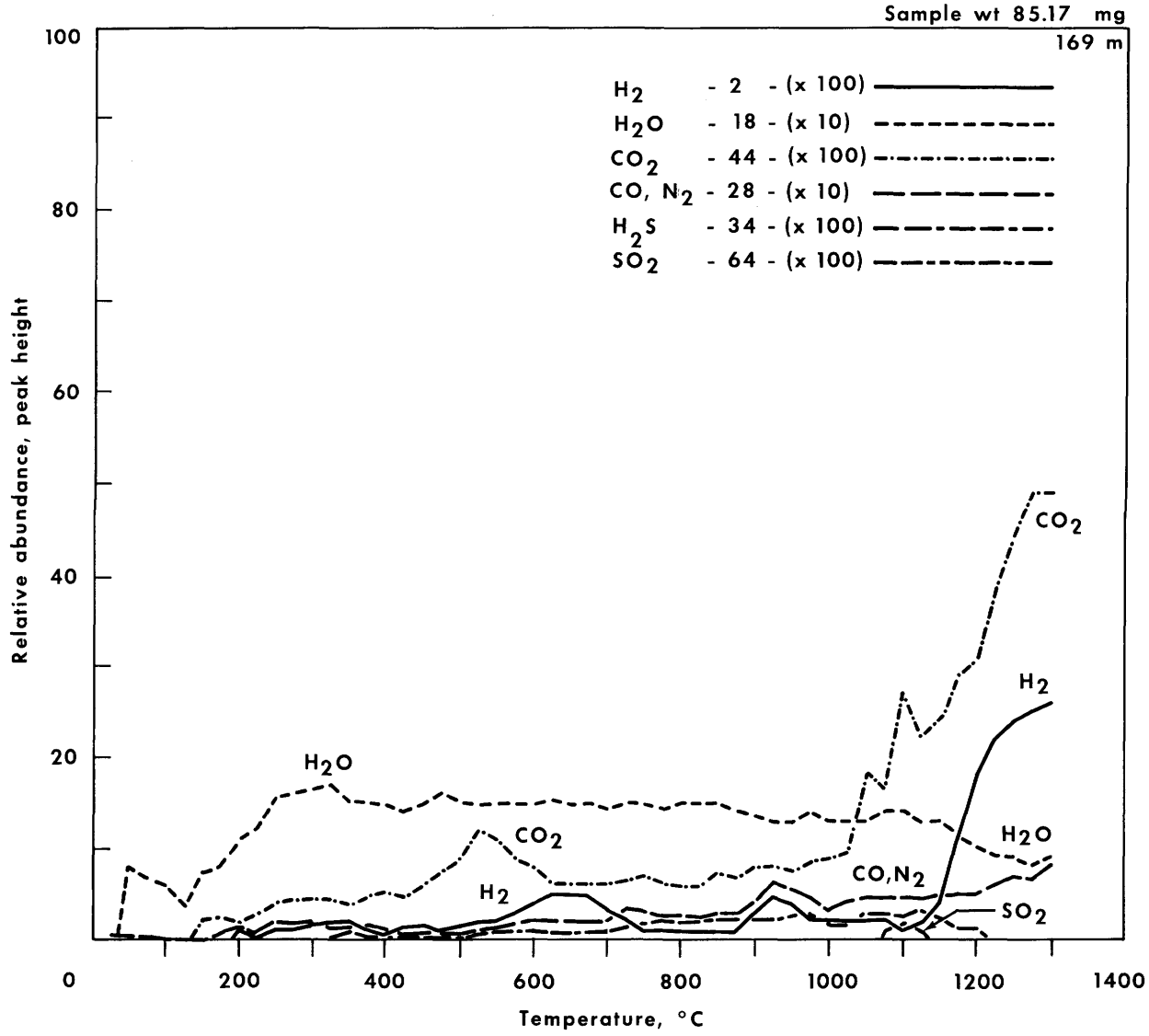
Sample wt 85.17 mg
169 m
H2 - 2 - (x 100)
H2O - 18 - (x 10)
CO2 - 44 - (x 100)
CO, N2 - 28 - (x 10)
H2S - 34 - (x 100)
SO2 - 64 - (x 100)
Relative abundance, peak height
Temperature, °C
0
20
40
60
80
100
200
400
600
800
1000
1200
1400
H2O
CO2
H2
CO2
H2
H2O
CO,N2
SO2

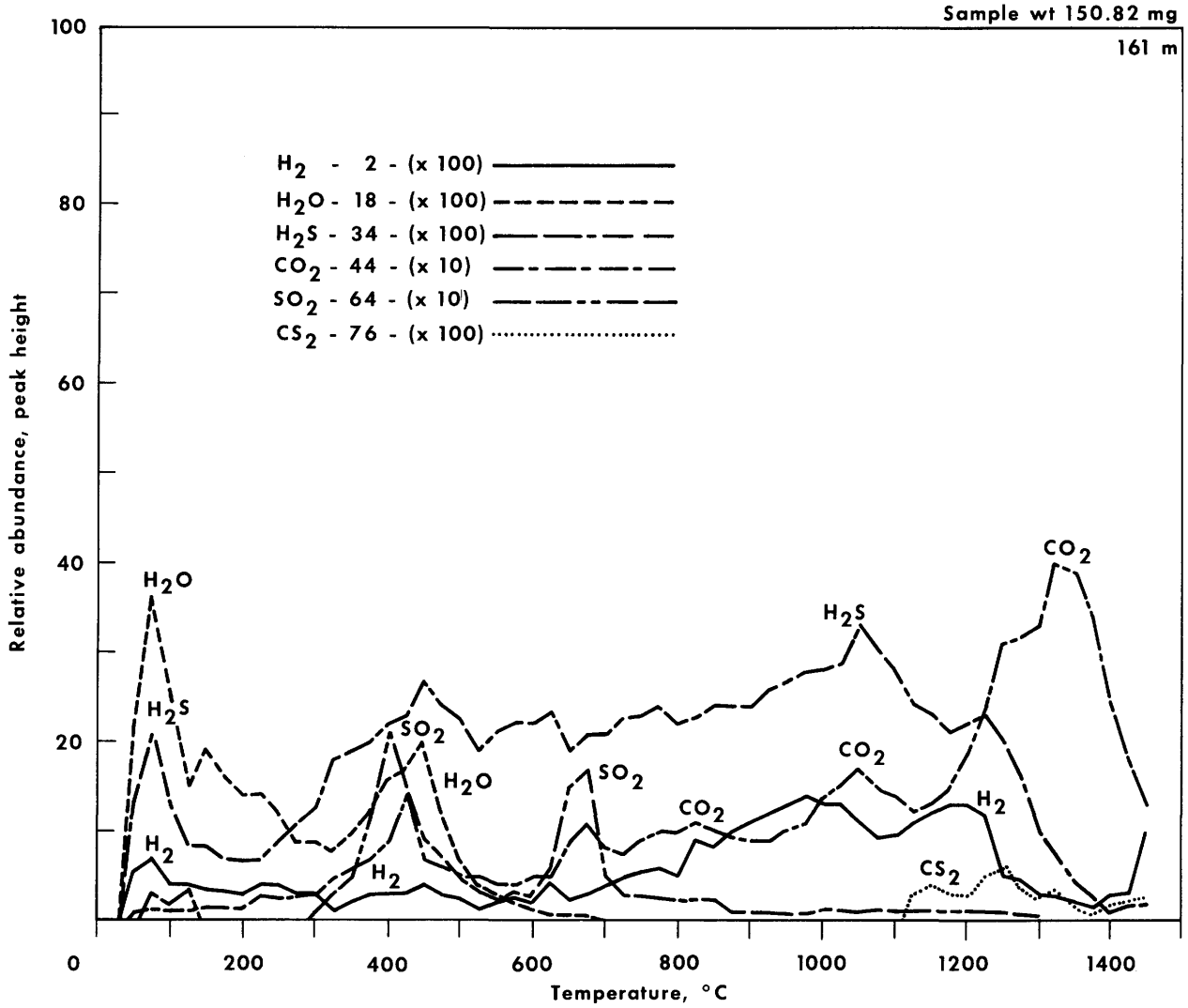

FIGURE 4.—Ruapehu airfall: Andesitic (no sublimates). The Ruapehu airfall ashes contain moderate amounts of volatiles. The sample contains adsorbed water which is released around 100°C. Water is the most abundant gas released from the Ruapehu ash. Carbon dioxide is the second most abundant gas phase released, and is released in two regions. Between 350° and 500°C, a small amount of CO_2 is evolved, which is probably from a secondary carbonate. Additional CO_2 is released above 1000°C and is a reaction product. Sulfur dioxide is released in two distinct temperature regions. SO_2 is released between 300°–500°C and 600°–700°C. The SO_2 evolved is from the decomposition products of secondary sulfate minerals. H_2S is released gradually over the complete temperature range and is probably a reaction product. At temperatures above 1100°C, CS_2 is released, which results from the reaction of carbon and sulfur-bearing phases. The Ruapehu airfall ash lost 3.12 weight percent upon heating to 1400°C.

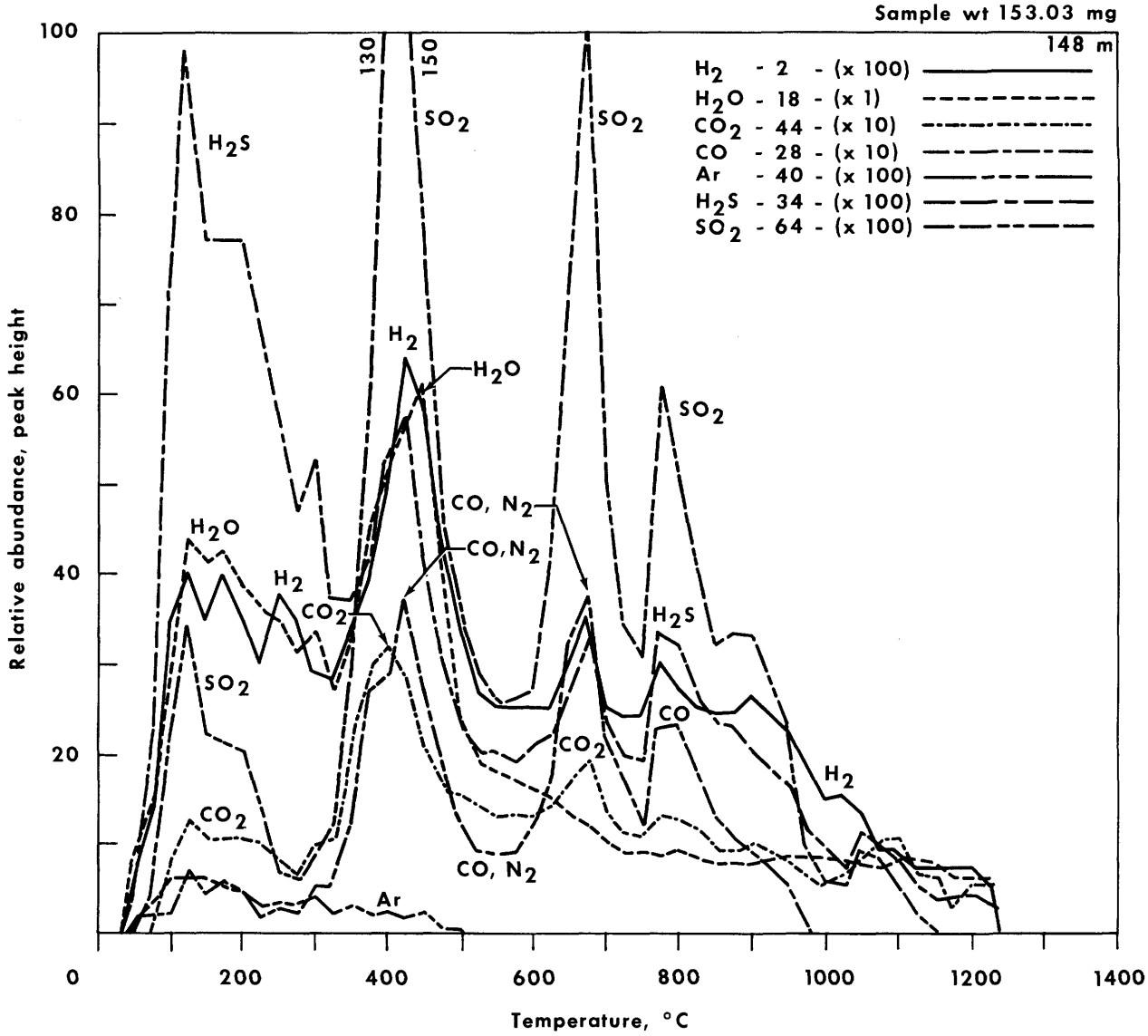

FIGURE 5.—Ruapehu airfall: Altered airfall. The altered Ruapehu ash contains the second largest quantity of volatile phases that we have observed during gas release studies of volcanic ashes. The volatiles observed undoubtedly arise from the secondary sublimates which are found on the surfaces of the ash particles (Heiken, 1972). During heating of the sample to 1200°C, the total weight loss was 5.69 percent. Most of the weight loss (4.80 percent) occurred below 900°C. Large quantities of water were released in two distinct temperature intervals. Adsorbed water and structural water from mineral phases, which are not thermally stable at temperatures above 300°C, were first released, followed by release of structurally bound water (between 350° and 550°C) associated with the sulfates (gypsum, etc.). During the second water release, sulfur dioxide was released in large quantities from the sulfate mineral phases. Sulfur dioxide and hydrogen sulfide were also released below 250°C. These gaseous species were either dissolved in the adsorbed water or strongly adsorbed to the ash particles. Carbon-bearing gases, CO_2 and CO, were released between 300° and 500°C and probably result from decomposition of carbonate phases such as calcite, siderite, and magnesite. Carbon dioxide and carbon monoxide were released in small quantities between 600° and 800°C and could arise from dolomite decomposition. At temperatures above 900°C, only small quantities of volatile phases are released. The large quantity of volatiles released from the Ruapehu ash are derived from secondary alteration of the ash samples by either ground water or vapor-bearing gas or fluid phases, which have since modified the ash samples.

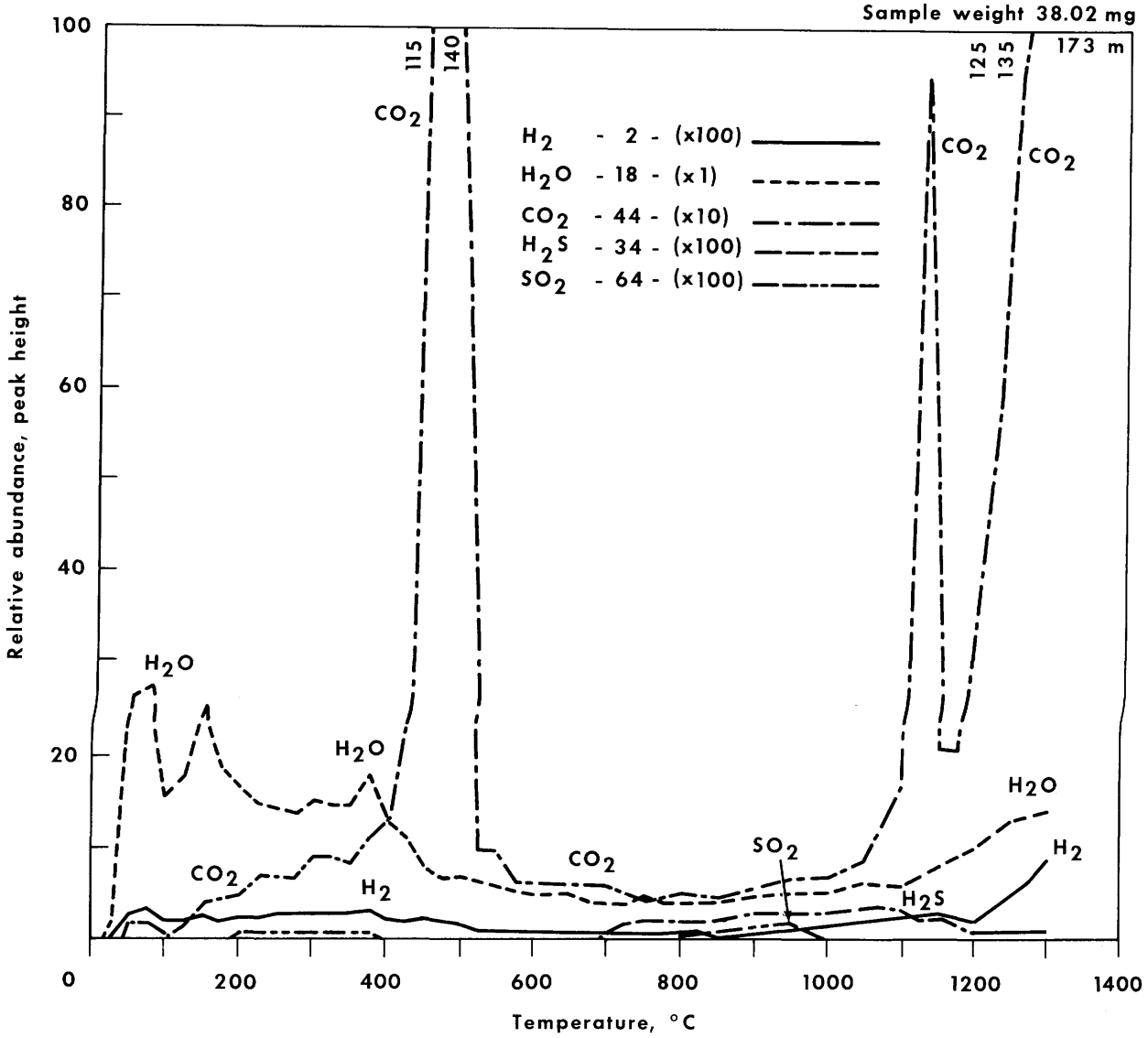

FIGURE 6.—Merapi, Indonesia: Andesitic. The Merapi andesitic ash has undergone secondary alteration as evidenced by the low temperature release of water and carbon dioxide. Below 400°C, loss of water accounts for almost all of the weight loss (0.50 weight percent). The water released results from both adsorbed water and decomposition of hydrate phases. Carbon dioxide is suddenly evolved between 400° and 525°C. The CO_2 release is from decomposition of carbonate phases, primary calcite. At temperatures above 1000°C, carbon dioxide is evolved a second time. The high temperature CO_2 release is from a reaction product of residual carbon phase, with the silicate melt. During heating under vacuum to 1300°C, the Merapi ash lost a total of 1.50 weight percent.

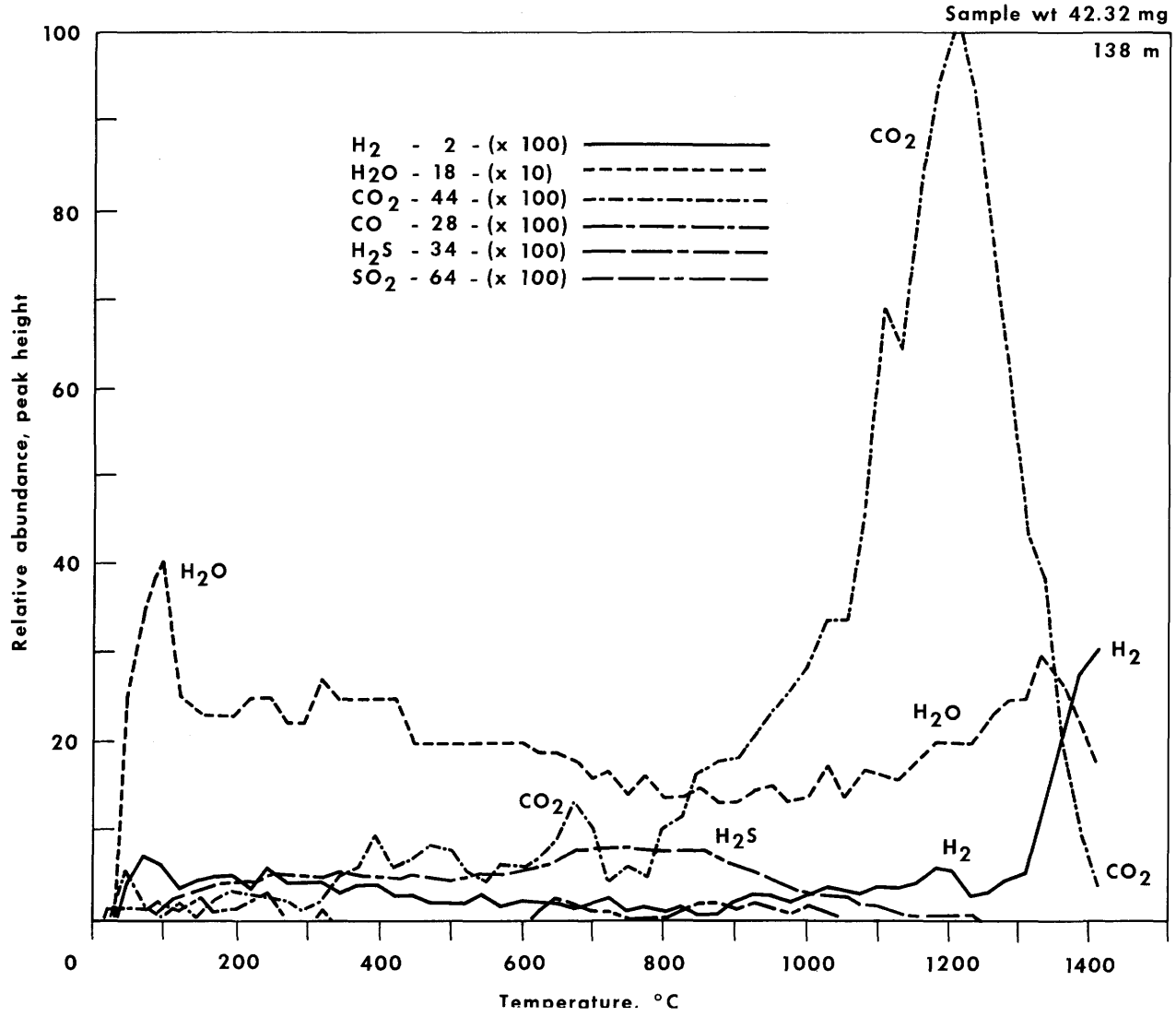

FIGURE 7.—Mayon, Philippines: Andesitic airfall. Mayon ash is a volatile depleted andesitic ash. The airfall sample analyzed shows evidence of terrestrially adsorbed H_2O which is released below 150°C. Carbon dioxide release near 400°C is characteristic of trace amounts of carbonates such as calcite. The CO_2 evolved between 600° and 700°C is similar to the release pattern of dolomites (??) or higher temperature carbonates. The andesite ash contains only trace amounts of sulfur-bearing phases which release SO_2 at temperatures above 700°C. The large CO_2 release profile between 1000° and 1300°C results from reaction products of carbon-bearing phases and the silicate melt. The Mayon volatile depleted airfall andesitic ash is characteristic of similar ashes which have had a high temperature history and retained very few volatiles. The weight loss for the Mayon ash was 1.61 percent (total) after heating to 1400°C.

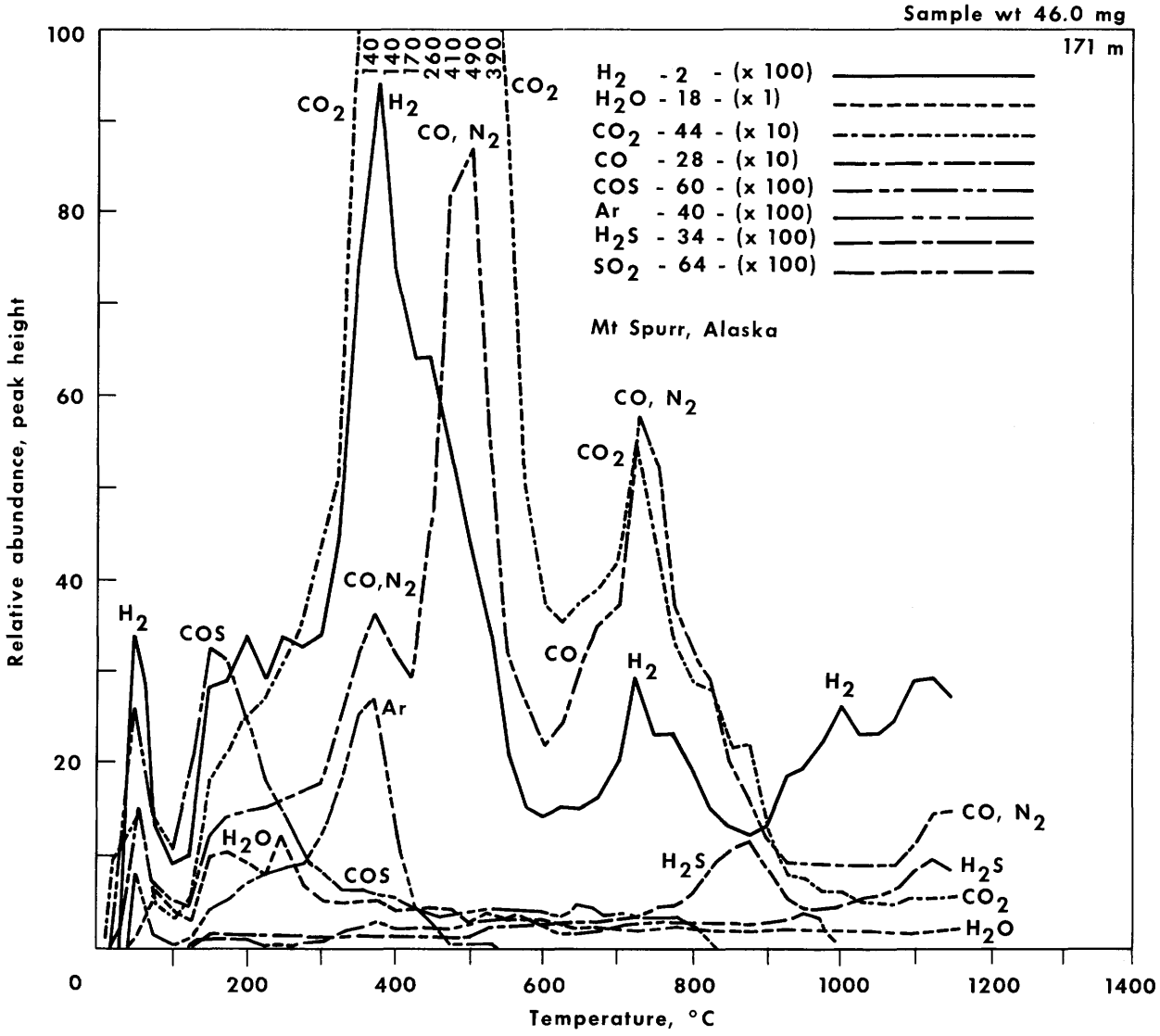

FIGURE 8.—Mt. Spurr, Alaska: Andesitic. The Mt. Spurr andesitic ash contains an unusually large quantity of volatile species which are released during heating to 1100°C. The major gas phase released is CO_2, which is associated with the decomposition of carbonate phases such as calcite, Na_2CO_3, magnesite, siderite. Trace amounts of H_2, H_2O, COS, H_2S, and Ar are also released. The sample lost 7.76 percent by weight below 700°C and 9.20 weight percent after heating to 1150°C. The low temperature (< 500°C) appearance of COS during the heating of the Mt. Spurr ash is very unusual. This phase normally is evolved at temperatures above 600°C in the presence of carbon and sulfur-bearing phases under reducing conditions.

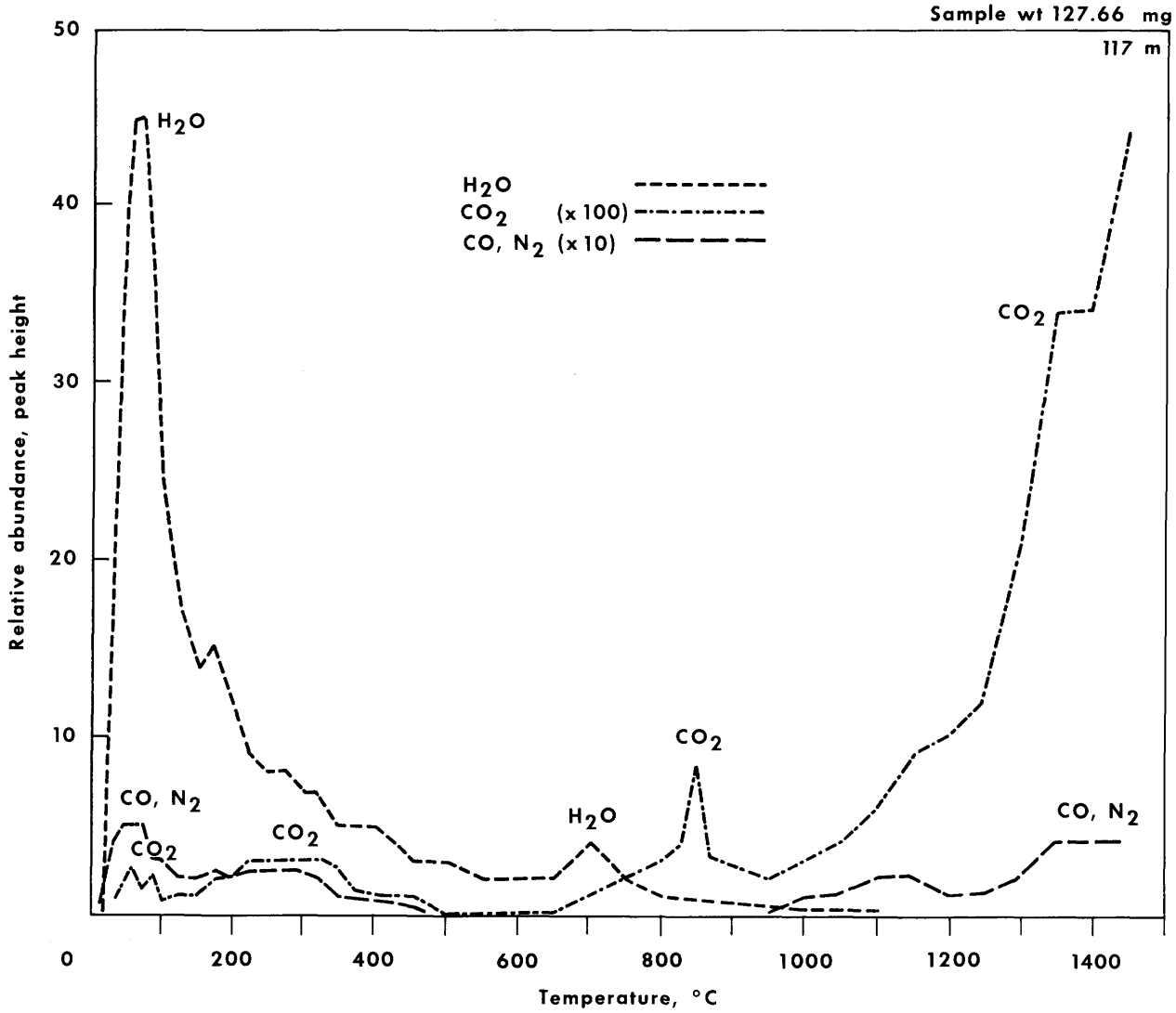

FIGURE 9.—Santiaguito, Guatemala: Dacitic. The gas release curve indicates the depletion of volatiles from the airfall-collected ash. The water released below 150°C accounts for 0.085 percent of the total weight loss of the sample. The water is mostly adsorbed as indicated by the low temperature release (< 150°C). Trace amounts (< 5 ppm) of CO_2 and N_2 are also released below 150°C. The CO_2 is apparently dissolved within the adsorbed H_2O. Between 200° and 500°C, a small release of CO_2 occurs and is apparently from trace amounts of secondary carbonates. At 850°C a sudden release of CO_2 is noted. The CO_2 is believed to result from rupturing of tiny gas-filled vesicles or tightly bound CO_2 trapped within microcavities of the ashes. The increase in CO_2 release above 1100°C results from reaction products of residual carbon phases with the silicate melt. The depletion of gases from the Santiaguito dacite ash is typical of airfall-collected dacite ashes. The sample lost 1.33 weight percent during heating under vacuum to 1450°C.

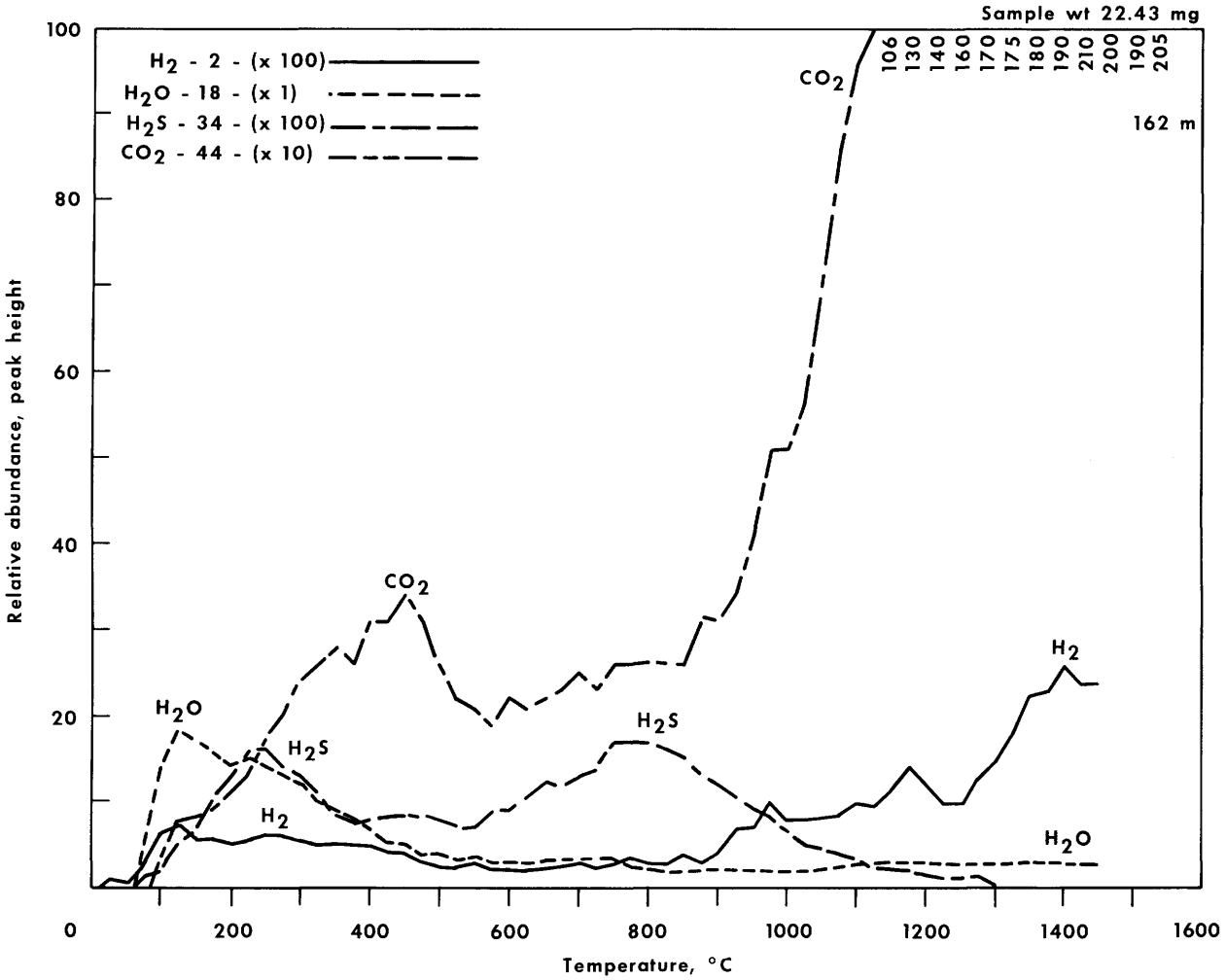

FIGURE 10.—Katmai, 1912: Rhyolitic. The Katmai ash has undergone secondary alteration. The sample contains large amounts of water-bearing phases. The ash sample lost 1.74 weight percent below 300°C, with CO_2 contributing to only a few percent of the weight loss below 300°C. Water is the major volatile phase released (below 800°C). Minor amounts of CO_2 and H_2S are also evolved from the sample. Above 800°C, carbon dioxide is the major gas phase evolved. The CO_2 evolution is from a reaction product of residual carbon with the silicate melt. After heating to 1450°C, the sample lost only 3.17 weight percent. The largest region of weight loss is below 400°C and occurs with the loss of secondary alteration product volatiles.

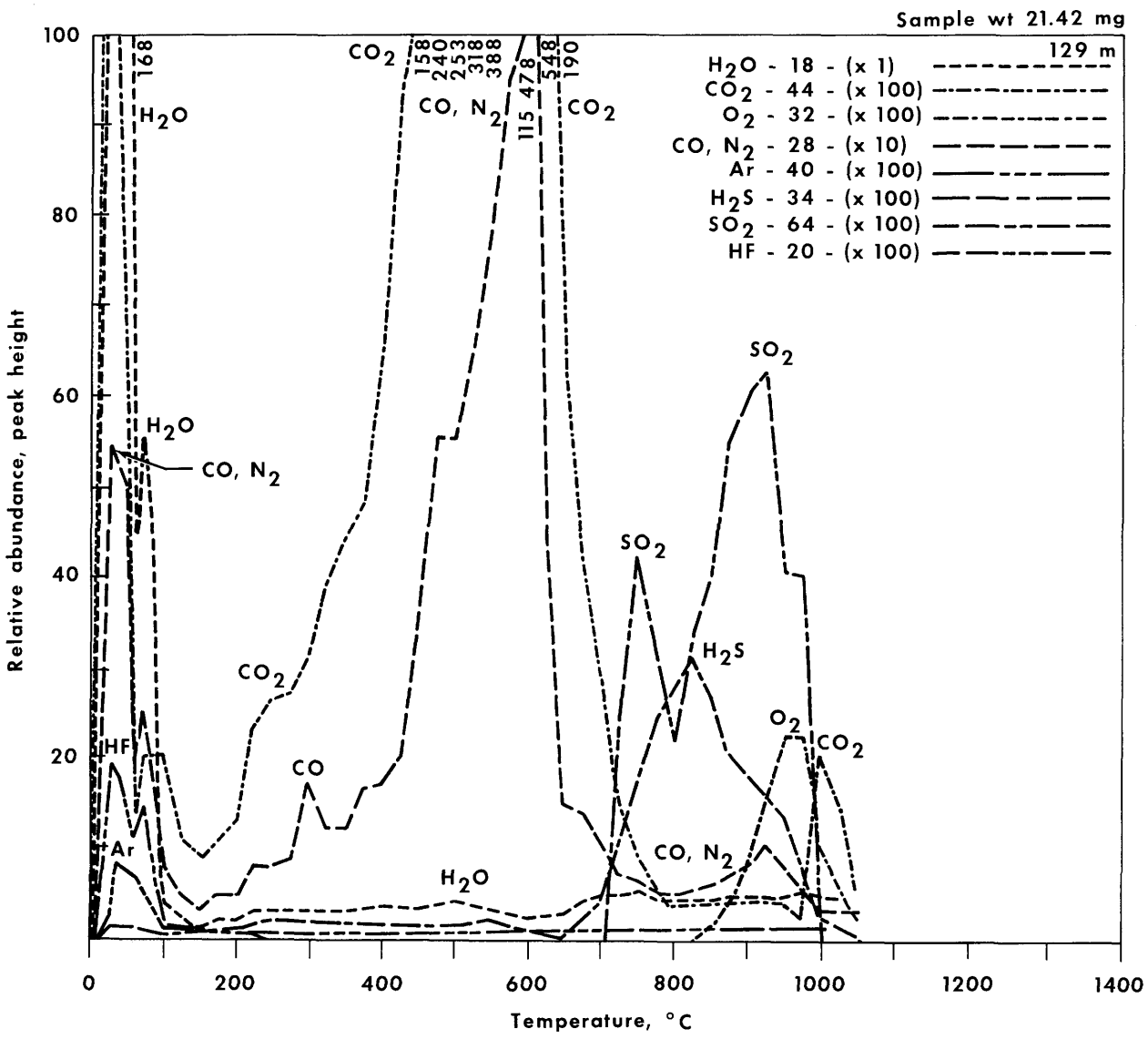

FIGURE 11.—Oldoinyo Lengai: Carbonatite. The Oldoinyo Lengai ash is one of the most volatile-rich ashes examined. The majority of the gases released are H_2O, CO_2, and SO_2, with minor amounts of HF, Ar, H_2S, O_2, CO, and N_2. The gas release pattern shows below 100°C the loosely adsorbed gases H_2O (major species), CO_2, CO/N_2, and HF. Between 300° and 700°C, decomposition of the carbonate phases Na_2CO_3, $CaCO_3$, etc., occurs. The carbon dioxide release in this temperature range accounts for almost 60 percent of the total volatiles released from the Oldoinyo Lengai ash. Decomposition of sulfur-bearing phases (e.g., $CaSO_4$, $MgSO_4$, etc.) or chemical reaction products of the sulfur-bearing phases with the silicates is evidenced by the release of SO_2 and H_2S between 700° and 1050°C, which accounts for almost 40 percent of the total weight loss for the ash sample. The volatile-rich ash sample lost 32.3 percent total weight during heating to 1050° C under vacuum.

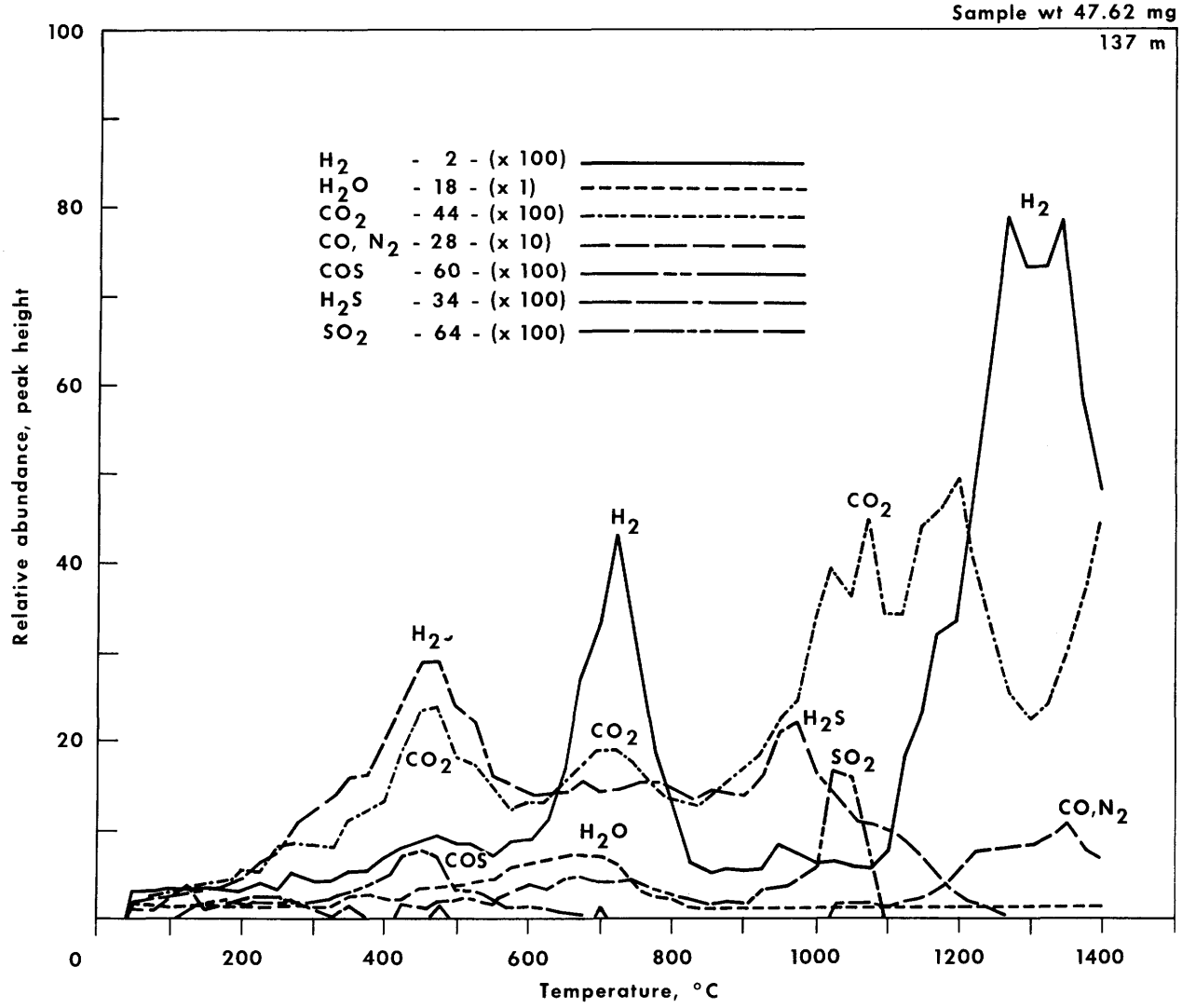

FIGURE 12.—Surtsey 1963 ash: Basaltic hyaloclastic. The Surtsey ash is depleted in its volatiles. The sample does not have any adsorbed gases which are typically released at temperatures below 200°C. Trace amounts of CO_2, H_2S, and COS are released between 300° and 600°C. Water is gradually evolved from the sample between 400° and 800°C. The gradual water release appears to result from a diffusional controlled type of release and not from the decomposition of hydrates. Hydrogen is released between 600° and 800°C. At temperatures above 1000°C, CO_2, CO, N_2, H_2, and SO_2 are evolved. These high temperature species are typical of reaction products of carbon, sulfur, oxygen, and hydrogen gases at the elevated temperature. During the heating of the Surtsey ash to 1000°C, only 0.84 weight percent was lost and only 4.01 weight percent after heating to 1400°C.

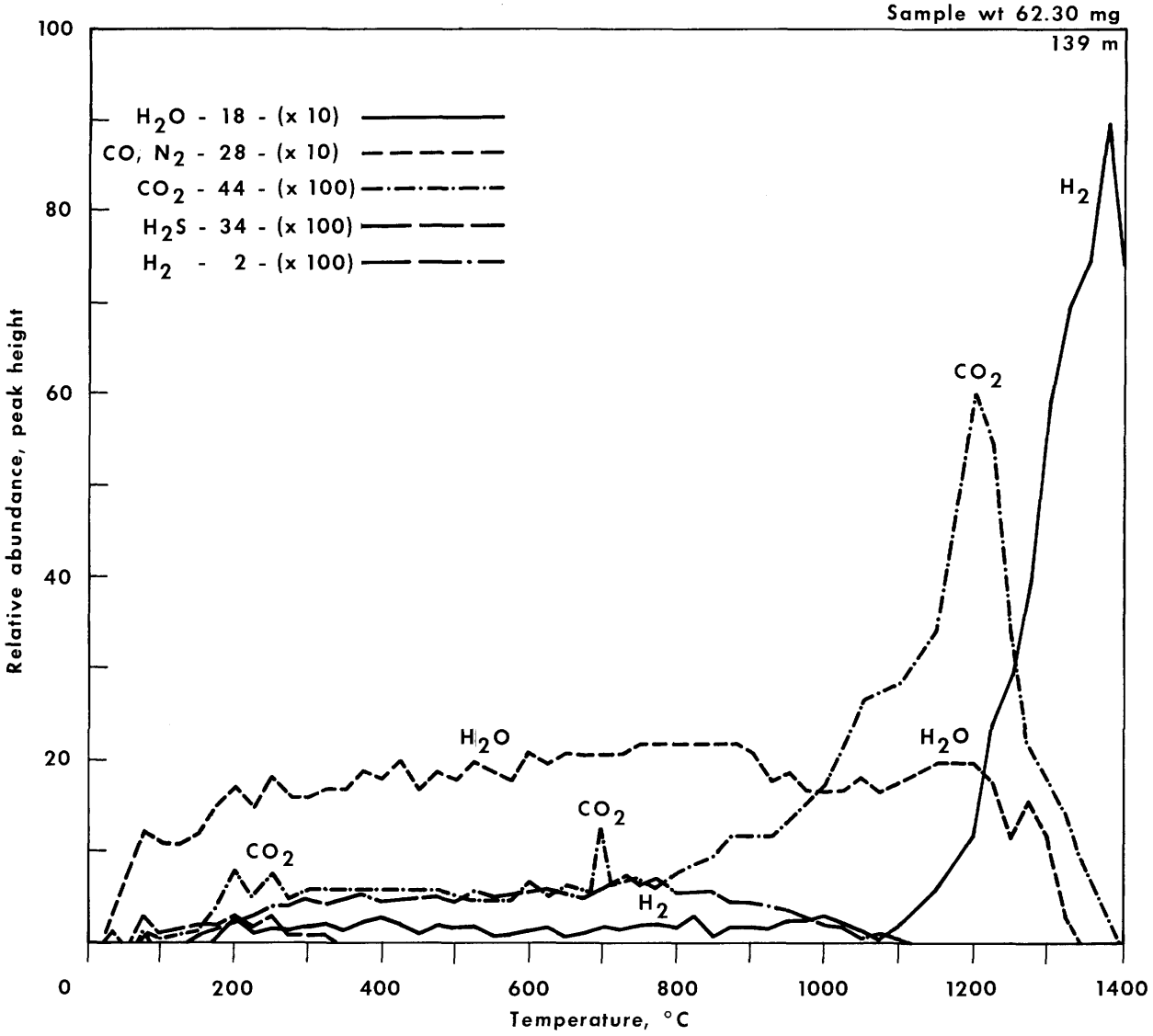

FIGURE 13.—Taal: Basaltic hyaloclastic. The basaltic ashes from the Taal 1968 eruption are depleted in volatiles. The ash sample did not evolve significant gases until above 1000°C. A sudden release of CO_2 at 700°C is characteristic of vesicular rupture. The CO_2 evolved above 1000°C is a reaction product of carbon-bearing phases with the silicate containing matrix. The sample has not been altered by secondary oxidation. Heating to 1200°C, the sample lost 0.51 weight percent and after 1400°C, 2.42 weight percent was lost from the ash sample. The depletion of volatile gases and absence of low temperature mineral phases from this basaltic ash is a direct result of the high temperatures associated with the phreatomagmatic eruption of the Taal volcano.

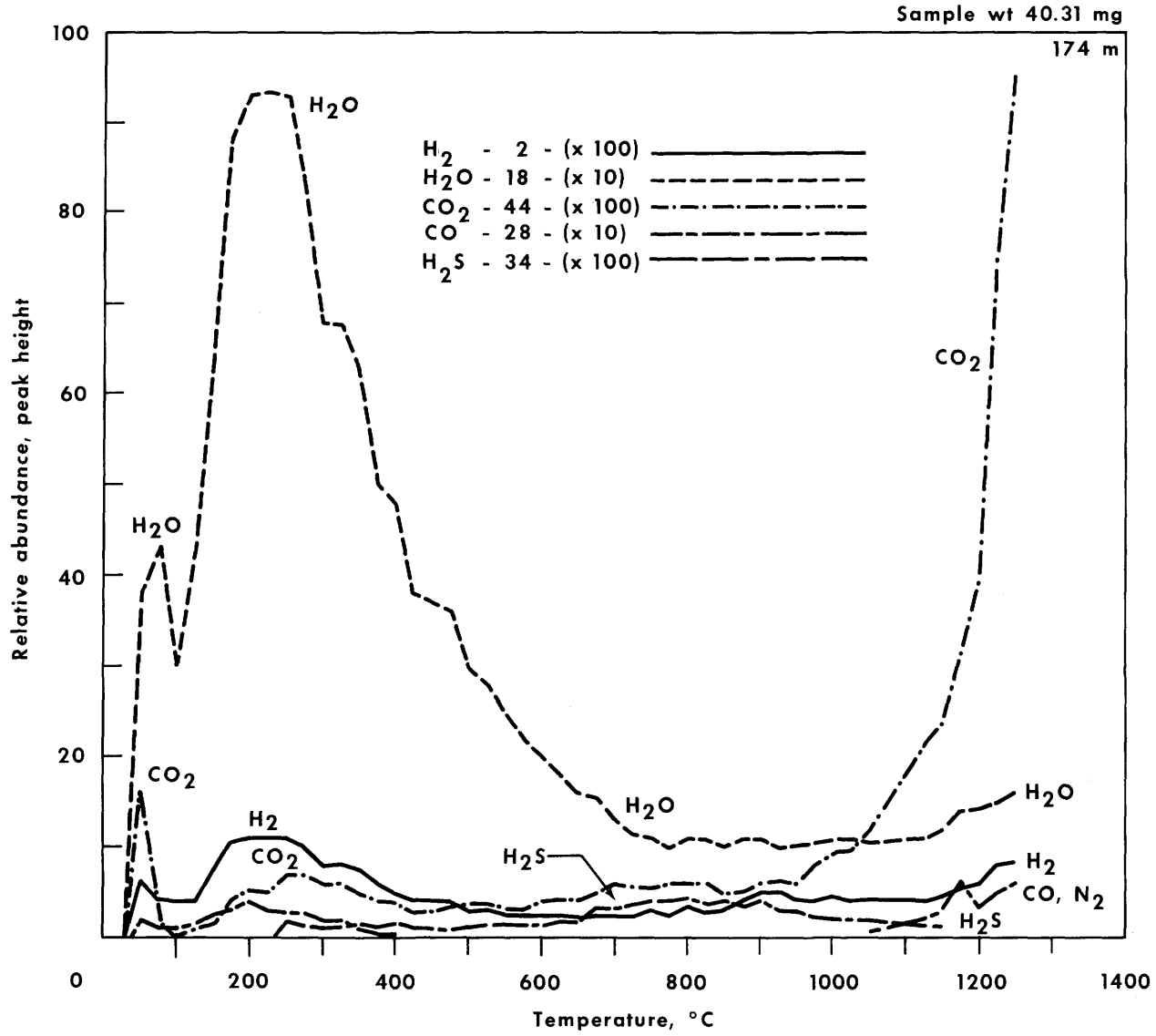

FIGURE 14.—Panum Crater, California: Rhyolitic hyaloclastic. The Panum crater rhyolitic ash has undergone extensive secondary alteration. The Pleistocene ash sample shows evidence of extensive weathering by ground water. Below 600°C, the sample lost large quantities of water, approximately 85 percent of the total gases released. Only trace quantities of H_2, CO_2, CO, and H_2S were released. Above 1000°C, the released CO_2 is noted. The CO_2 results from residual carbon reacting with the silicate mineral phases at elevated temperatures. The Panum Crater ash lost a total of 2.11 percent by weight during heating to 1250°C, with 1.71 percent of this weight loss occurring below 600°C.

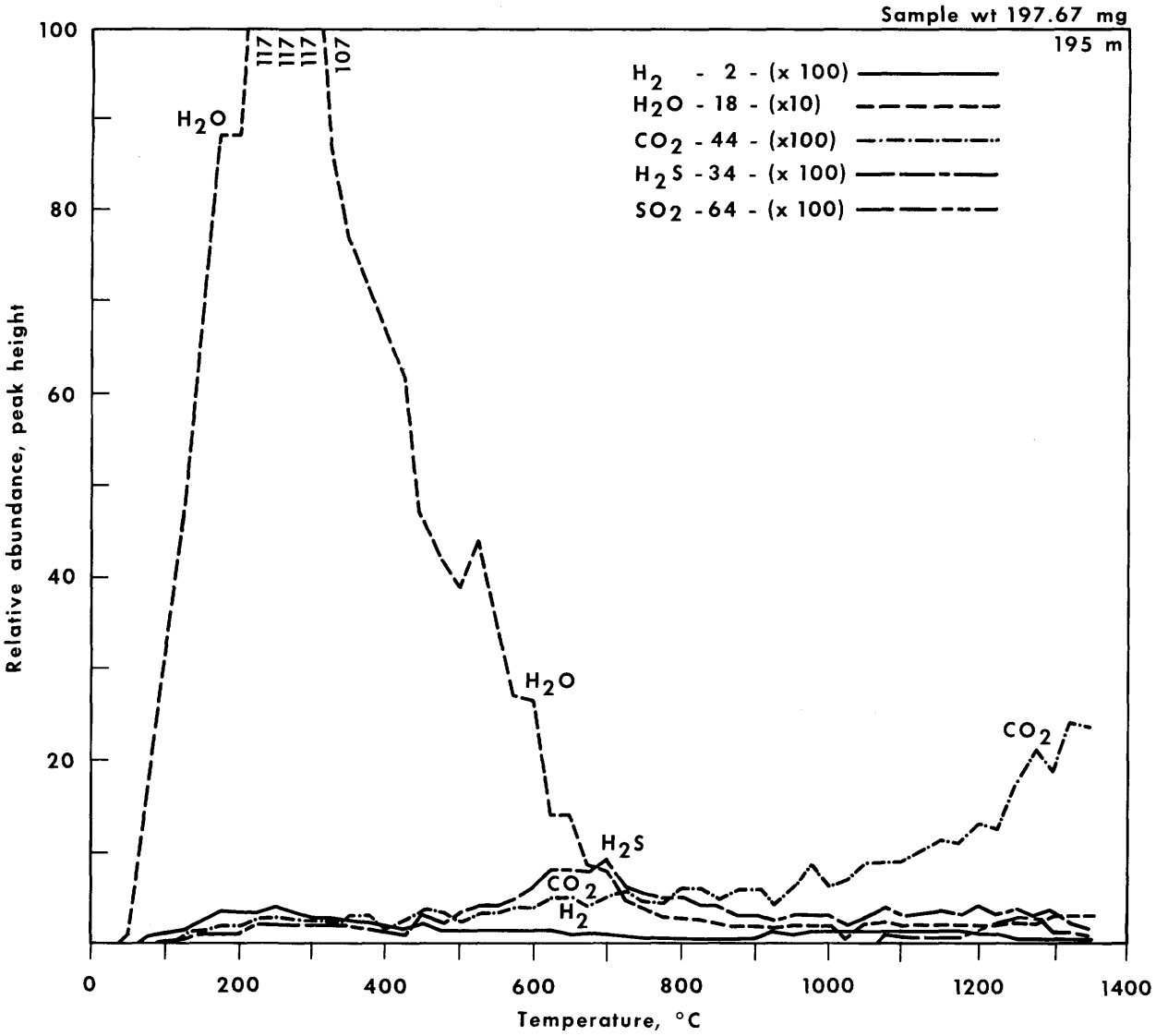

FIGURE 15.—Sugarloaf, Arizona: Rhyolitic hyaloclastic. The Sugarloaf hyaloclastic ash contains only water which is released below 600°–700°C. Only trace quantities of CO_2, H_2S, H_2, and SO_2 are released from the ash. The water released below 700°C accounts for 1.59 weight percent of total 1.99 percent weight loss which the ash sample underwent. The water which was evolved from the ash is undoubtedly derived from the secondary alteration of the sample before collection.

PLATES 1–33

Clast size	Clast name	Rock name (if majority of clasts in the size range)
>256	Coarse blocks	Pyroclastic breccia
64-256 mm	Fine blocks	
2-64 mm	Lapilli	Lapillistone
1/16-2 mm	Coarse ash	Tuff
<1/16 mm	Dust (or fine ash)	

A

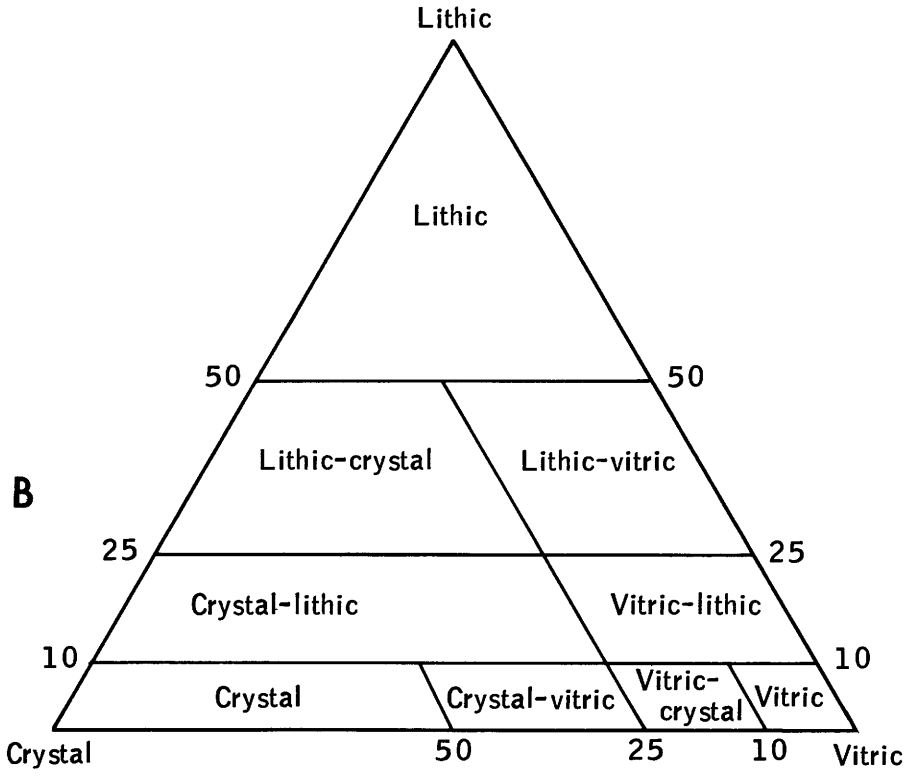

PLATE 1

Classification of volcaniclastic fragments. A, Size classification (Fisher, 1961). B, Compositional classification (Cook, 1965).

PLATE 2

Pacaya, Guatemala. A, SEM of basaltic vitric ash, consisting of light-brown sideromelane droplets and broken droplets. (Sideromelane refers to light- to medium-brown transparent glass [in thin section] of basaltic composition. Under a binocular microscope, sideromelane particles may appear to be black or very dark brown.) The grains in the center and upper left have fluidal shapes with smooth botryoidal surfaces. Round lumps on the grain surfaces were formed when expanding vesicles deformed the flexible outer skin. The 10– to 50–micron-thick flexible brown skin visible on many sideromelane droplets appears to have formed immediately on exposure to the atmosphere. In many droplets, this skin is broken by vertical joints a few microns apart and 10 to 50 microns high. In some cases, fluid from the droplet interior has forced its way through the cracks (Heiken and Lofgren, 1971). The dark-brown color of the skin is partly due to the closely spaced cracks and partly due to oxidation of the grain surface. Some vesicles broke open while the skin was still viscous, resulting in a smooth, curved lip around the cavity edge. The droplet in the center has a rough-ribbed appearance caused by the expansion of elongate pipe vesicles. The thin thread on the upper part of the grain is due to complete collapse of a vesicle while the droplet was still molten. (The scale is 100 microns.) B, Photomicrograph of sideromelane droplet twisted around its long axis during flight. The smooth fluidal surface has a thin, dark-brown skin that was formed immediately after extrusion. The large phenocrysts visible are of calcic plagioclase. (The scale is 100 microns.) C, SEM. All are broken droplets except the slightly rounded lithic fragment (aphanitic basalt) on the left. The fragment on the right has elongate, slightly flattened pipe vesicles, which were possibly shaped by flow before comminution. (The scale is 50 microns.) D, Photomicrograph of a broken sideromelane droplet. The outer skin is dark brown and can be seen on the round surfaces. Both broken ends are angular and lack the skin. The grain in the upper right corner is an olivine phenocryst. (The scale is 100 microns.) E, SEM of broken sideromelane droplets. The equant grain shape seems to be related to equant or slightly deformed vesicles. There is a crystal fragment (feldspar) in the foreground. (The scale is 100 microns.) F, Photomicrograph of the outer edge of a sideromelane grain; cross section of an elongate vesicle similar to those causing the ribbing of the grain in A. (The scale is 100 microns.)

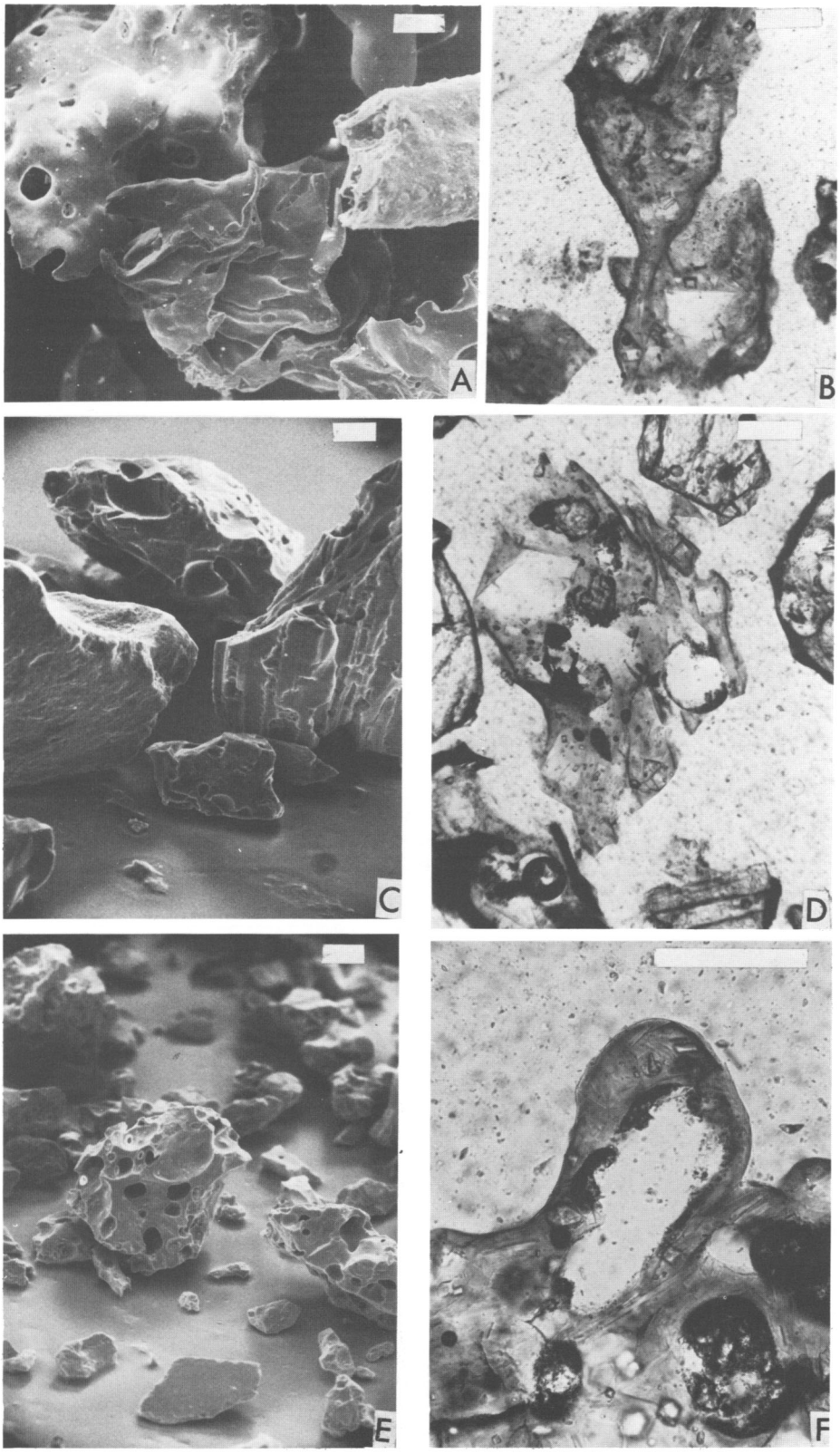
A
B
C
D
E
F

PLATE 3

Fuego, Guatemala. A, SEM of a broken sideromelane droplet. The smooth triangular patch is part of the droplet skin. The original smooth droplet surface is easy to distinguish from the irregular or conchoidal fracture surfaces of the broken sections. (The scale is 25 microns.) B, SEM of a broken vitric fragment with slightly deformed vesicles that are 20 to 125 microns in diameter. (The scale is 25 microns.) C, Photomicrograph of broken sideromelane and tachylite droplets characteristic of this ash. Nearly all the grains in this photo are a mixture of sideromelane and tachylite. (The scale is 100 microns.) D, SEM of a broken sideromelane droplet with very low vesicularity. The fracture along the long axis of the grain appears to correspond with a line of small vesicles. (The scale is 25 mircons.) E, SEM. The fragment in the foreground is a lithic fragment, probably aphanitic basalt. The fragment in the back is a broken droplet characterized by a smooth fluidal grain surface. (The scale is 50 microns.)

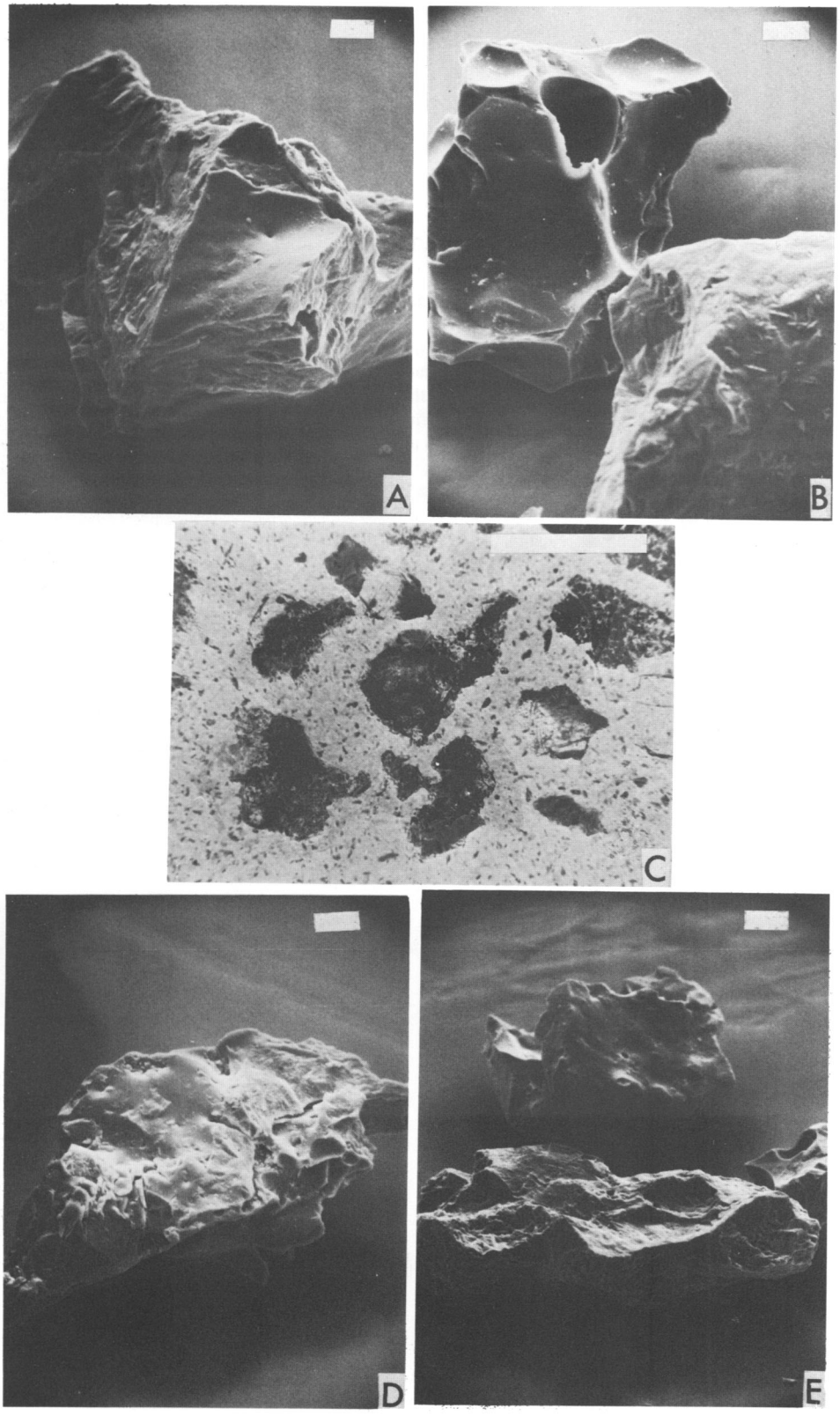
A
B
C
D
E

PLATE 4

Cerro Negro, Nicaragua. (All scales are 100 microns.) A, SEM of dark-brown sideromelane droplets. The smooth botryoidal outer surface or skin was deformed by expansion of the outermost vesicles. Vesicles open to the exterior were formed by (1) the bursting of gas bubbles (smooth cavity edge, rounded by surface tension), or (2) the breaking of the outer vesicle wall after the grain surface was rigid (sharp angular cavity edges). B, Photomicrograph of a sideromelane droplet (center) and tachylite fragments. There are abundant olivine and feldspar phenocrysts in the glass. C, SEM of an angular broken sideromelane droplet. D, Photomicrograph of an angular tachylite fragment (submicrocrystalline basalt). These fragments rarely have rounded fluidal edges.

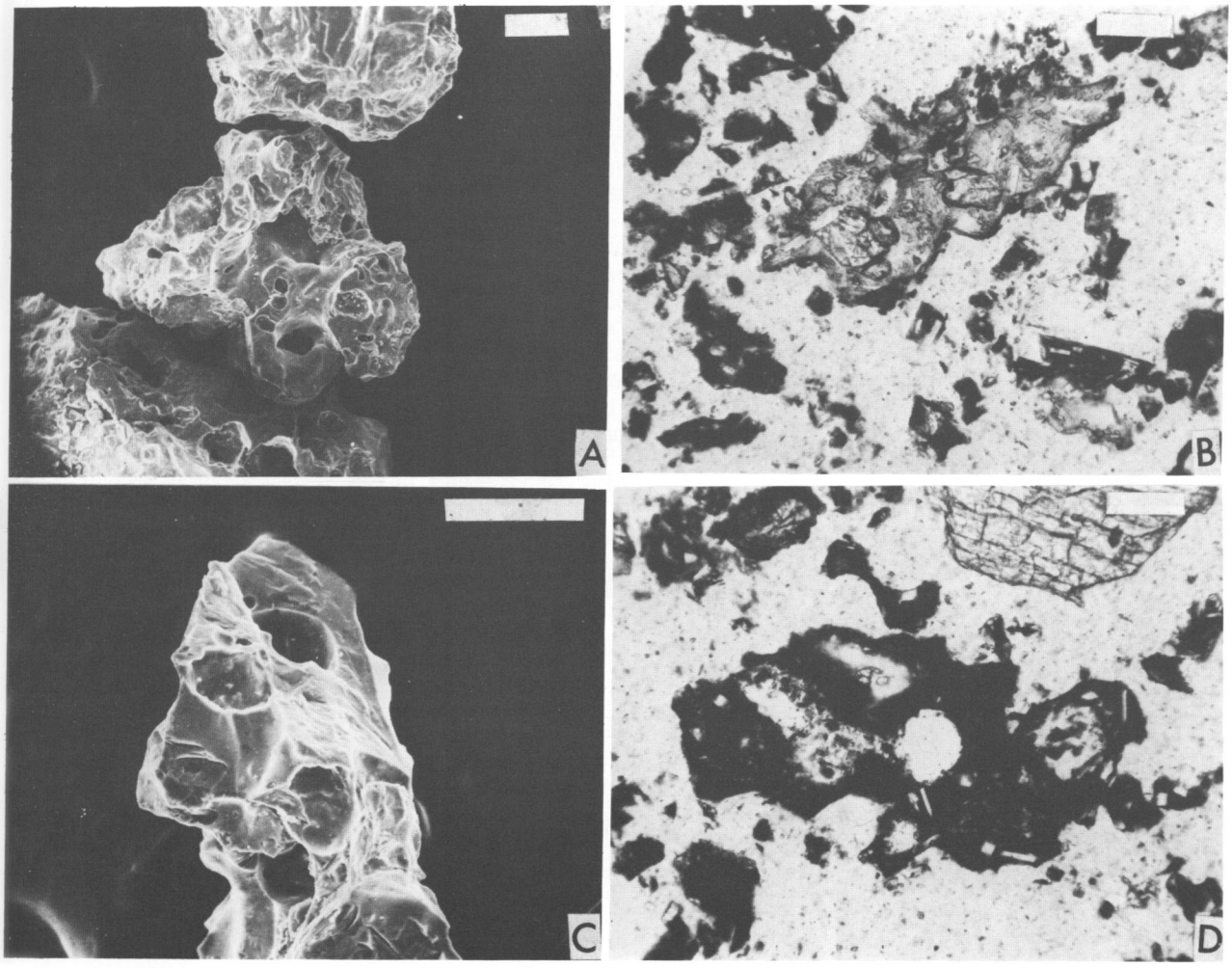
A
B
C
D

PLATE 5

Etna, Italy. A, SEM of a 116 × 52 micron agglutinate grain; glass-covered feldspar (?) laths are oriented parallel to the long grain axis. The grain is composed of several glassy grains welded together. (Scale is 13 microns.) B, SEM of a slightly elongate tachylite grain with an irregular, hackly surface. The hemispherical depression at the bottom of the grain is a broken vesicle. (Scale is 26 microns.) C, Closeup of B. Parts of the grain surface exhibit a diktytaxitic texture, consisting of an open framework of glass-coated feldspar crystals. The void space in these irregular areas is about 30 percent. (Scale is 3.3 microns.) D, SEM of a triangular, broken glass droplet. Vesicles exposed at the surface are 110 to 200 microns in diameter. Vesicle walls are coated with small droplets, which may be sulfur. Fracture surfaces are conchoidal. (Scale is 22 microns.) E, Photomicrograph of clear brown glass (sideromelane), tachylite grains, and a clinopyroxene grain. The sideromelane grains have low vesicularities and blocky shapes; this is unusual and normally characteristic of hyaloclastic ashes. These are broken droplets, however, as indicated by some grain edges which exhibit a "skin" characteristic of magmatic basaltic ash. The tachylite grains exhibit scalloped edges, which are across broken vesicles. (Scale is 61 mircons.) F, Photomicrograph of a partially oxidized brown glass droplet and several angular tachylite grains. (Scale is 61 microns.)

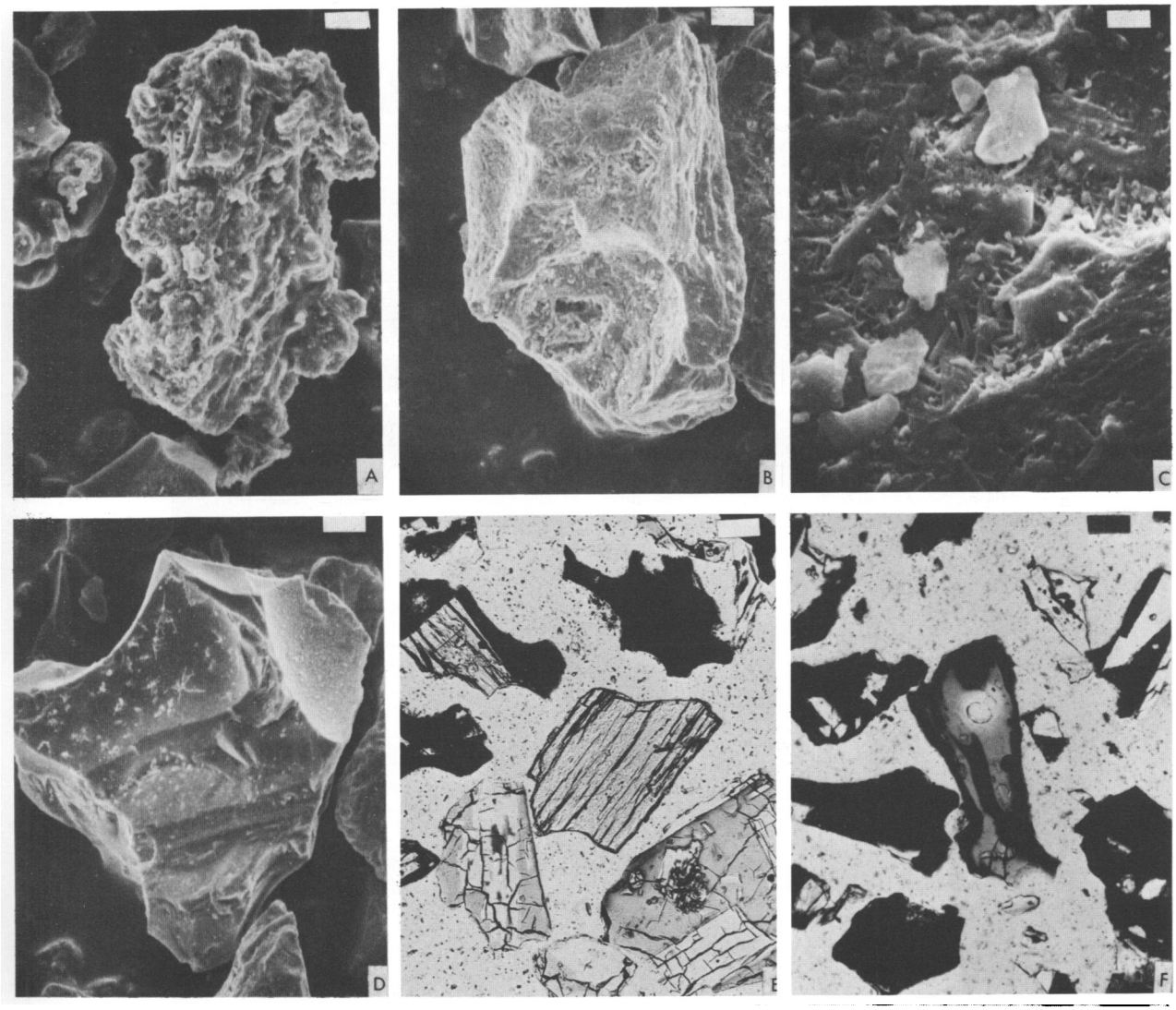
A
B
C
D
E
F

PLATE 6

Deception Island, Antarctica. A, Photomicrograph of very poorly sorted vitric ash, consisting of broken sideromelane droplets and ragged equant tachylite fragments. There are only a few olivine phenocrysts in addition to feldspar microlites visible in the sideromelane. (The scale is 100 microns.) B, SEM of a fine-grained basaltic ash. Most of the ash fragments have low vesicularity and are very angular. Rough fragment surfaces indicate chipping and grinding of ash particles during the eruption or by later reworking. (The latter idea is improbable.) (The scale is 100 microns.) C, SEM of a diktytaxitic glassy fragment. Feldspar microlites or very small phenocrysts with thin glass coatings form an open network where either (1) some of the fluid drained out from between the crystals, or (2) the vesicle shape was controlled by crystal shape and orientation. (The scale is 100 microns.) D, SEM; closeup of C. (The scale is 10 microns.) E, Photomicrograph of a broken sideromelane droplet exhibiting subparallel feldspar microlites oriented by flow. (The scale is 100 microns.) F, SEM of an elongate broken sideromelane droplet. Smooth round surfaces are of the outer skin. (The scale is 10 microns.)

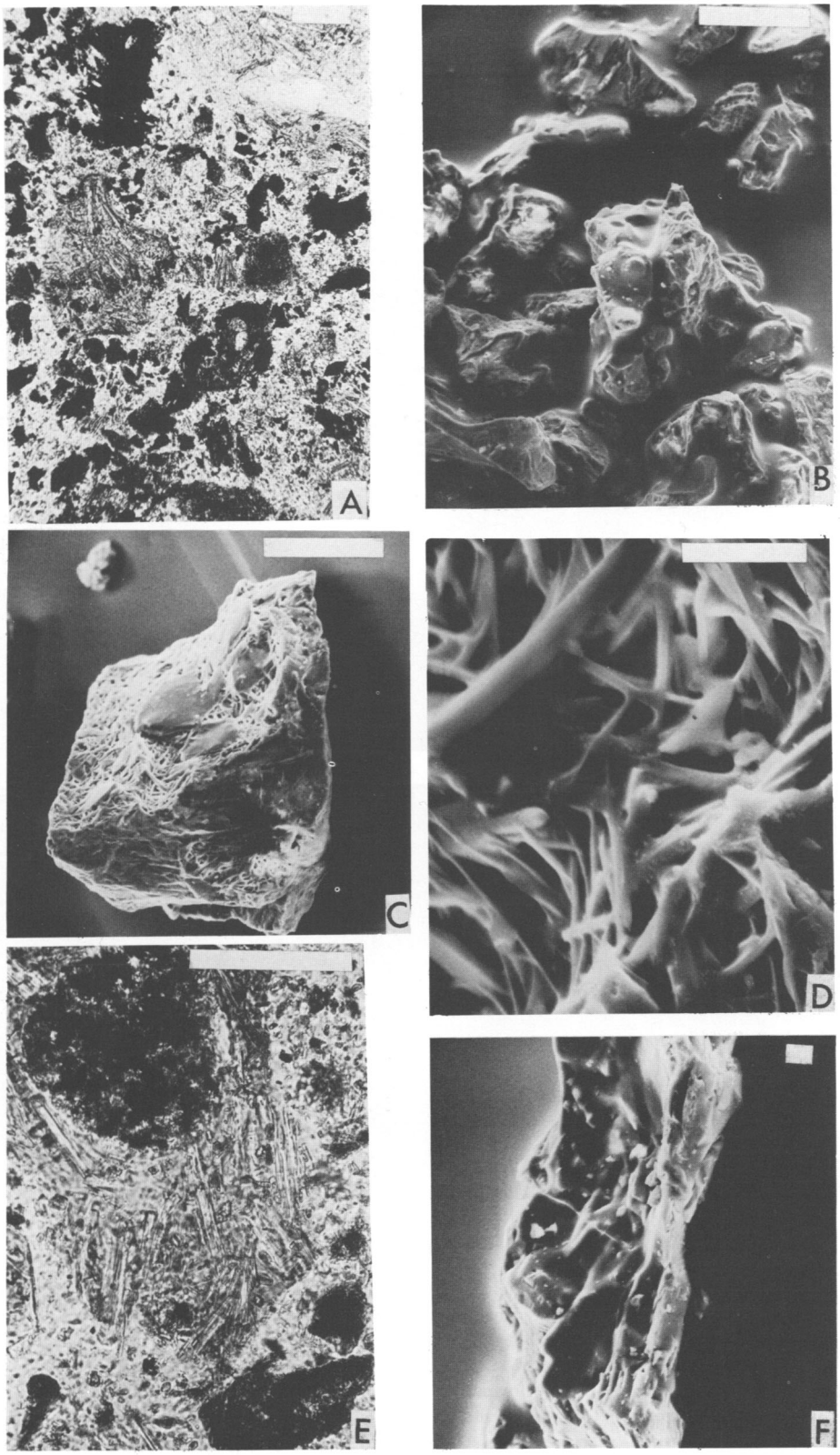
A
B
C
D
E
F

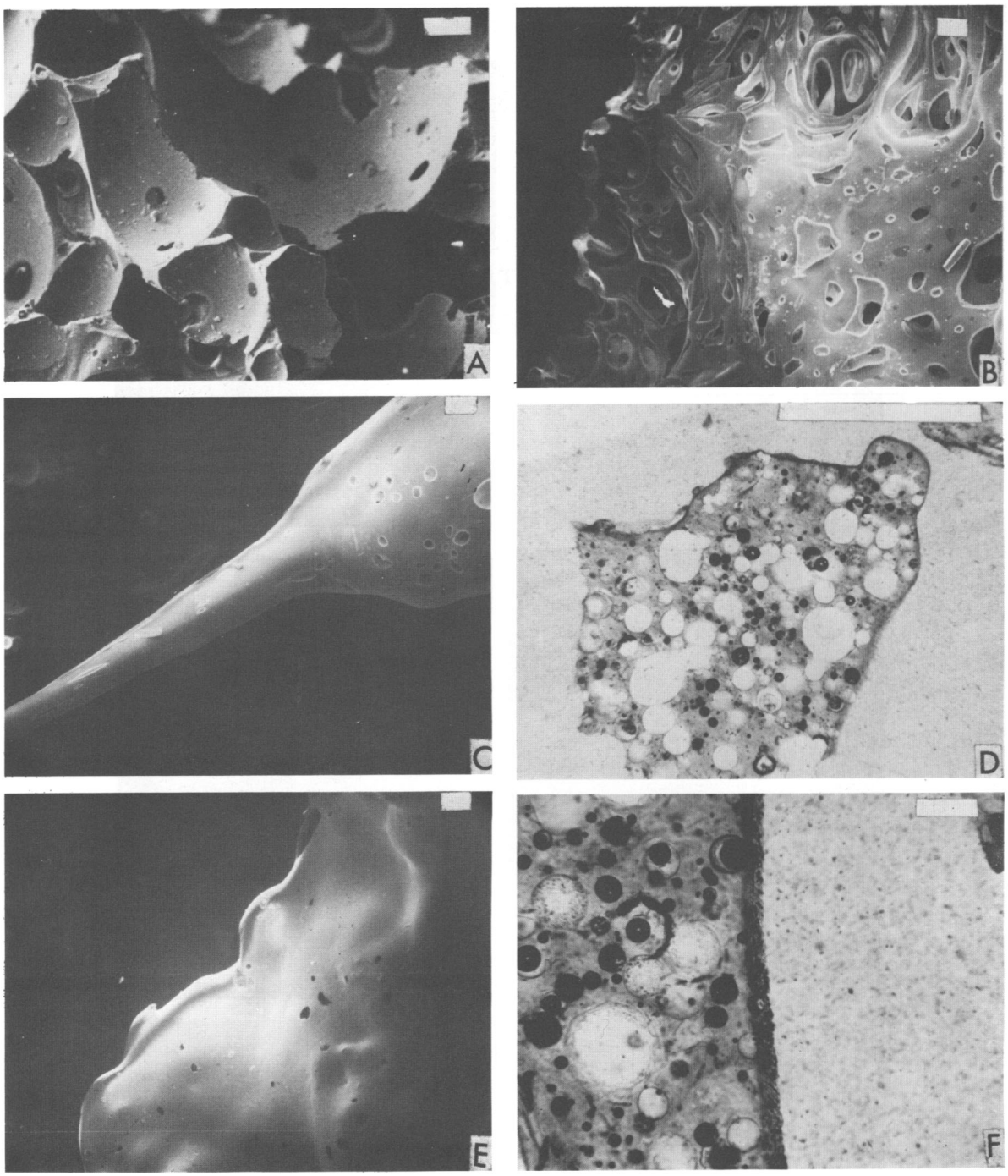

PLATE 7

Kilauea Iki, Hawaii. A, SEM of a scoriaceous sideromelane fragment, probably a broken droplet. Vesicle diameters range from 2 to 500 microns. Smaller vesicles adjacent to larger ones broke through the bubble walls instead of indenting them. (The scale is 100 microns.) B, SEM of a highly vesicular sideromelane droplet. Most of the vesicles are connected, forming an open network of spherical or ovoid chambers. The outer surface has a well-developed skin. (The scale is 100 microns.) C, SEM of the tail of a droplet formed during flight. If the elongation were completed, a Pele's hair would have been formed. (The scale is 100 microns.) D, Photomicrograph of a sideromelane droplet. The round edges on the top and right edges have a thin, dark-brown skin. The light-brown transparent glass is homogeneous. (The scale is 1 mm.) E, SEM of a sideromelane droplet with a flange around it that was possibly due to spinning. Holes in the surface are due to the breaking of outer vesicle walls after the hardening of the outer skin. (The scale is 100 microns.) F, Edge of a sideromelane droplet. The skin, with parallel contraction cracks, has been deformed by air drag. Dark circular areas are bubbles in the mounting medium. (The scale is 100 microns.) G, SEM of a 1.96–mm-diameter Pele's hair. The hair is ribbed, with ribs 20 to 300 microns across. The

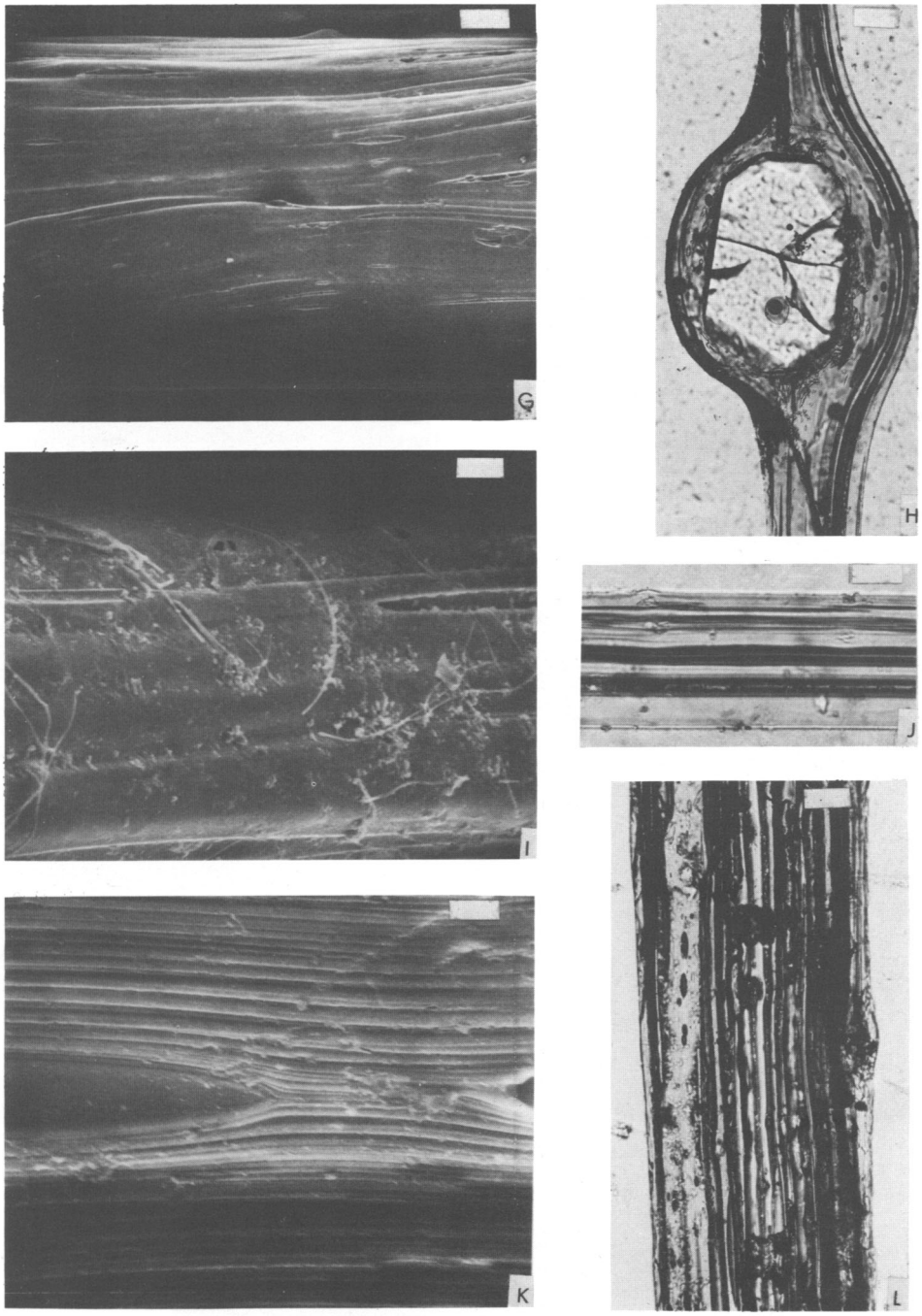

larger (300 micron) ribs are about 4.5 mm long and tapered at both ends. The ribs are slightly sinuous, possibly due to twisting about the long axis of the hair. (Scale is 280 microns.) H, Photomicrograph of a Pele's hair, with a bulge over an olivine phenocryst. The elongate vesicles are about 4 microns in diameter. (Scale is 61 microns.) I, SEM of a 253-micron-diameter Pele's hair, with a ribbed surface. Each rib is over an elongate vesicle. Adhering to the surface are 1- to 2-mircon-thick, curved Pelc's hairs. (Scale is 40 microns.) J, Photomicrograph of a 46-micron-diameter Pele's hair. The hair surface is smooth, broken only by small lumps over microphenocrysts of olivine and feldspar. The glass is pale brown (sideromelane). (Scale is 15.5 microns.) K, Detail of G. This is small-scale ribbing, consisting of square-edged ridges, 1 to 3 microns wide, separated by flat or slightly convex depressions, 2 to 5 microns wide. These may be cracks in the skin of the grain, where a vesicle erupted to the grain surface while the grain was still molten (left side of the photograph); the ribbing was spread and compressed around the vesicle. (Scale is 9 microns.) L, Photomicrograph of a 290-micron-diameter, vesicular Pele's hair. There appears to be a correlation between the degree of vesicularity and the number of ribs on a Pele's hair. The more vesicular grains have abundant ribs parallel to the long axis. (Scale is 61 microns.)

PLATE 8

Glass spheres from Kilauea Iki. A, SEM of a smooth brown sideromelane sphere. Holes in the surface are over outer vesicles. (The scale is 100 microns.) B, Photomicrograph of the edge of a sideromelane sphere similar to the one in A. Dark circles are vesicles filled with grinding compound. Phenocrysts are olivine and feldspar. (The scale is 500 microns.) C, Photomicrograph of the skin on a sphere edge, showing cooling joints deformed by air drag. (The scale is 100 microns.) D, SEM; closeup of a sideromelane sphere, showing smooth-walled depressions (collapse of outer vesicles before solidification) and depressions with ragged edges (outer skin broken after solidification). (The scale is 10 microns.) E, SEM of a dumbbell-shaped sideromelane droplet. The shape may be due to spinning that forced fluid to the extremities of the droplet. (The scale is 100 microns.)

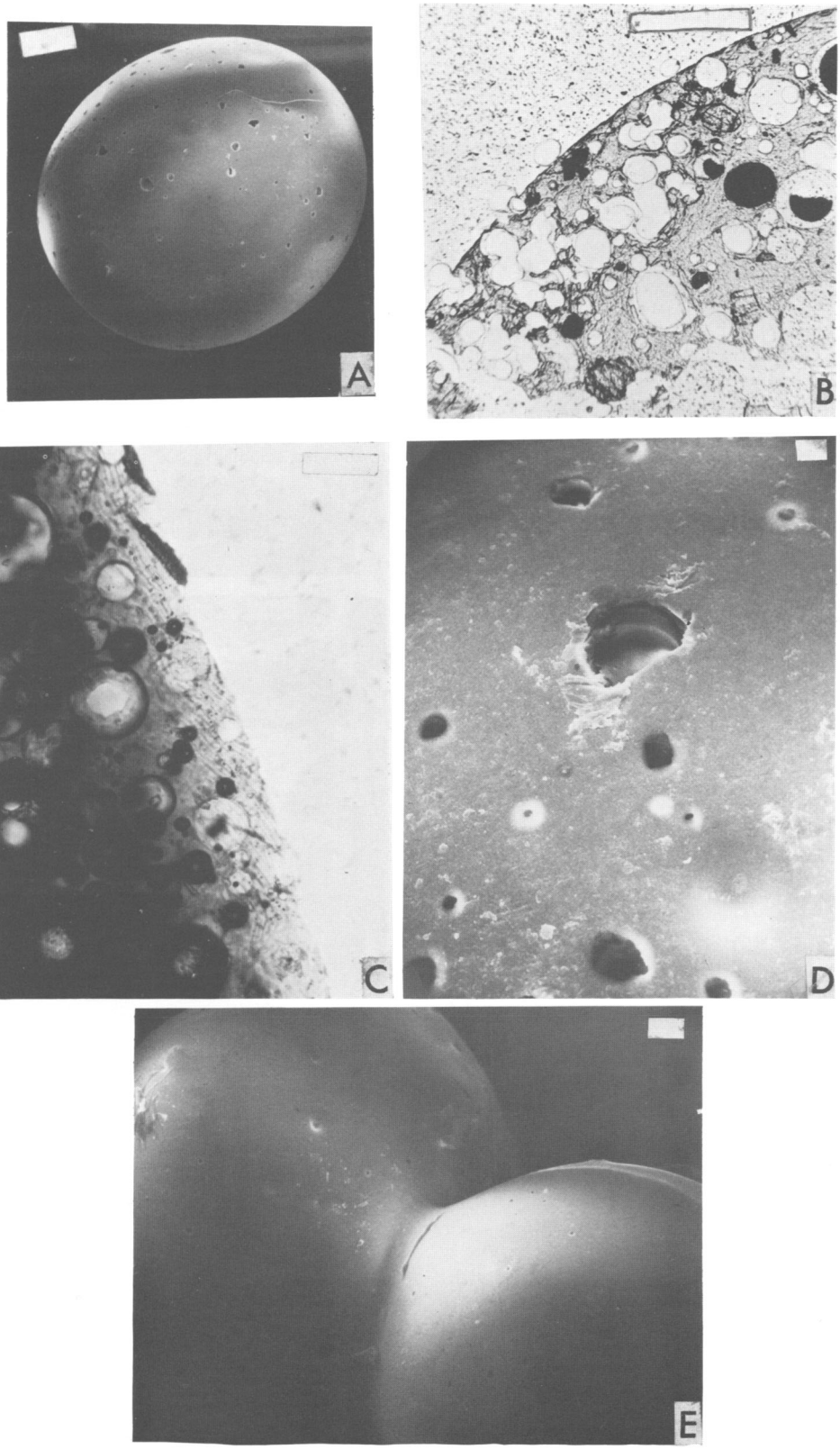
A
B
C
D
E

PLATE 9

Reticulite ash, Kilauea, Hawaii. A, SEM of lattice-like framework of triangular sideromelane rods, formed during extreme frothing of lava during lava fountaining. The triangular cross section is the line of contact between three expanding gas bubbles. (The scale is 100 microns.) B, Photomicrograph of a fragment similar to the one in A. There are no phenocrysts or microlites in the sideromelane. (The scale is 1 mm.) C, SEM. Surfaces of the reticulite lattice have been altered by weathering, and are cracked. (The scale is 100 microns.) D, Photomicrograph of reticulite. Details of triangular rods in cross section, showing smooth vesicle walls at the mutual contact between three bubbles. (The scale is 100 microns.)

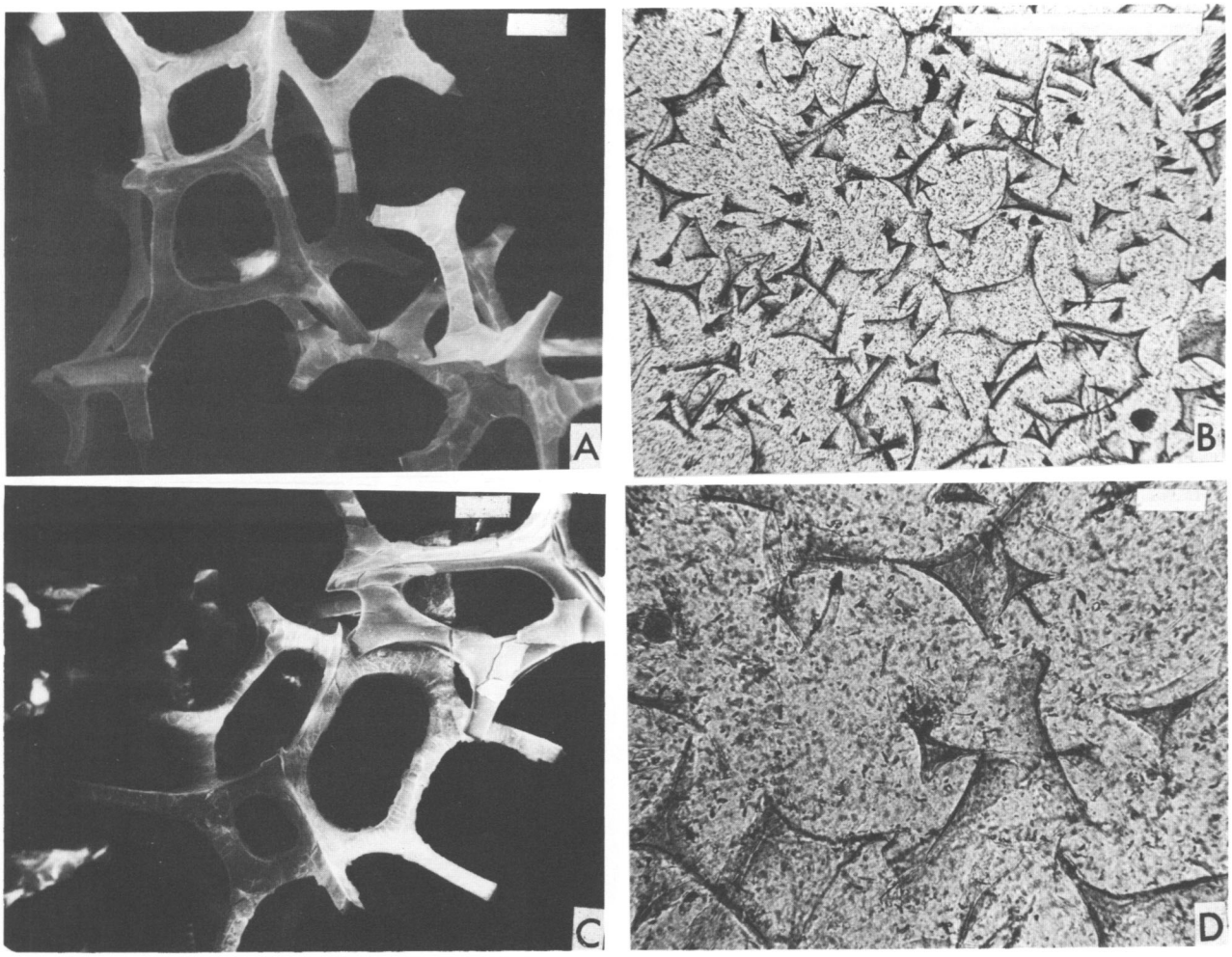
A
B
C
D

PLATE 10

Aloi-Alae vent, Hawaii (1969–1970 eruption). A, SEM of the edge of a broken, vesicular, sideromelane droplet. Compare the outer skin (right) with a slight texture or roughness to the smooth curved fractures across the grain (left). Note the 2- to 8-micron-thick skin exposed around the lip of a surface depression at the center bottom. (The scale is 100 microns.) B, SEM of a twisted, broken sideromelane rod that may have formed in the same manner as Pele's hair. (The scale is 100 microns.) C, SEM of part of a sideromelane sphere with a smooth surface. (The scale is 100 microns.) D, Photomicrograph of the interior of a clear sideromelane sphere, exhibiting spherulites of pyroxene (?) crystals. Spherulites are rare in glasses of basaltic composition. (The scale is 50 microns.)

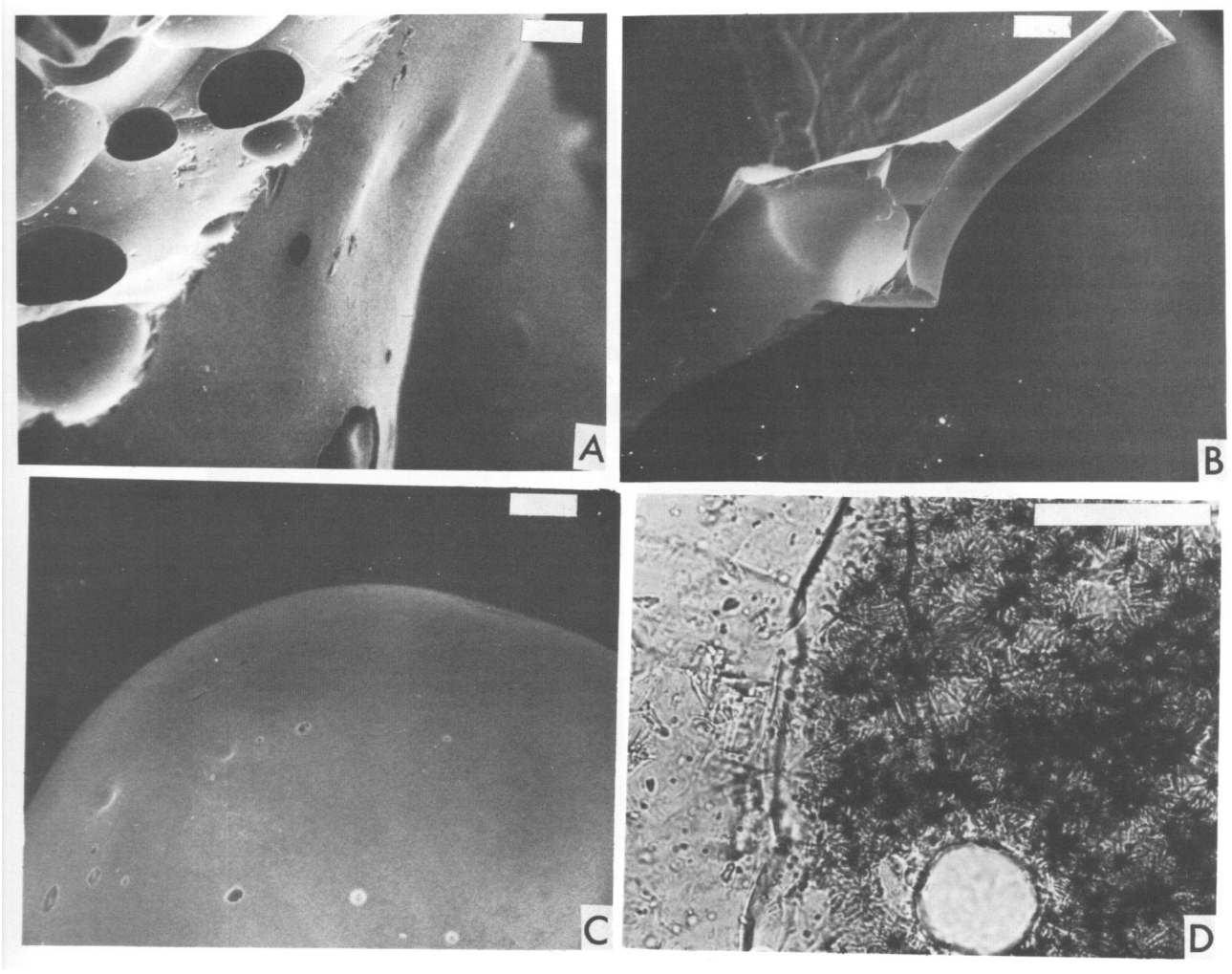
A
B
C
D

PLATE 11

Oshima, Japan. A, SEM of a broken sideromelane droplet partly immersed in the mounting medium. (The scale is 10 microns.) B, Photomicrograph of vitric-crystal ash, consisting of mainly sideromelane (medium-gray grain in center) and tachylite (black scoria) droplets. (The scale is 1 mm.) C, SEM. Blocky glass fragment on the right is probably part of a broken sideromelane droplet. The grain has low vesicularity, with only a few vesicles, 1 to 5 microns in diameter. Both particles are partly covered with sublimates. (The scale is 10 microns.) D, Photomicrograph of equant sideromelane and tachylite droplets. (The scale is 1 mm.) E, SEM of a scoriaceous sideromelane fragment that has been altered, probably by weathering. (The scale is 10 microns.) F, Photomicrograph of a vesicular sideromelane droplet welded to an angular tachylite fragment. Agglutinates similar to this one are common in this ash sample. (The scale is 100 microns.)

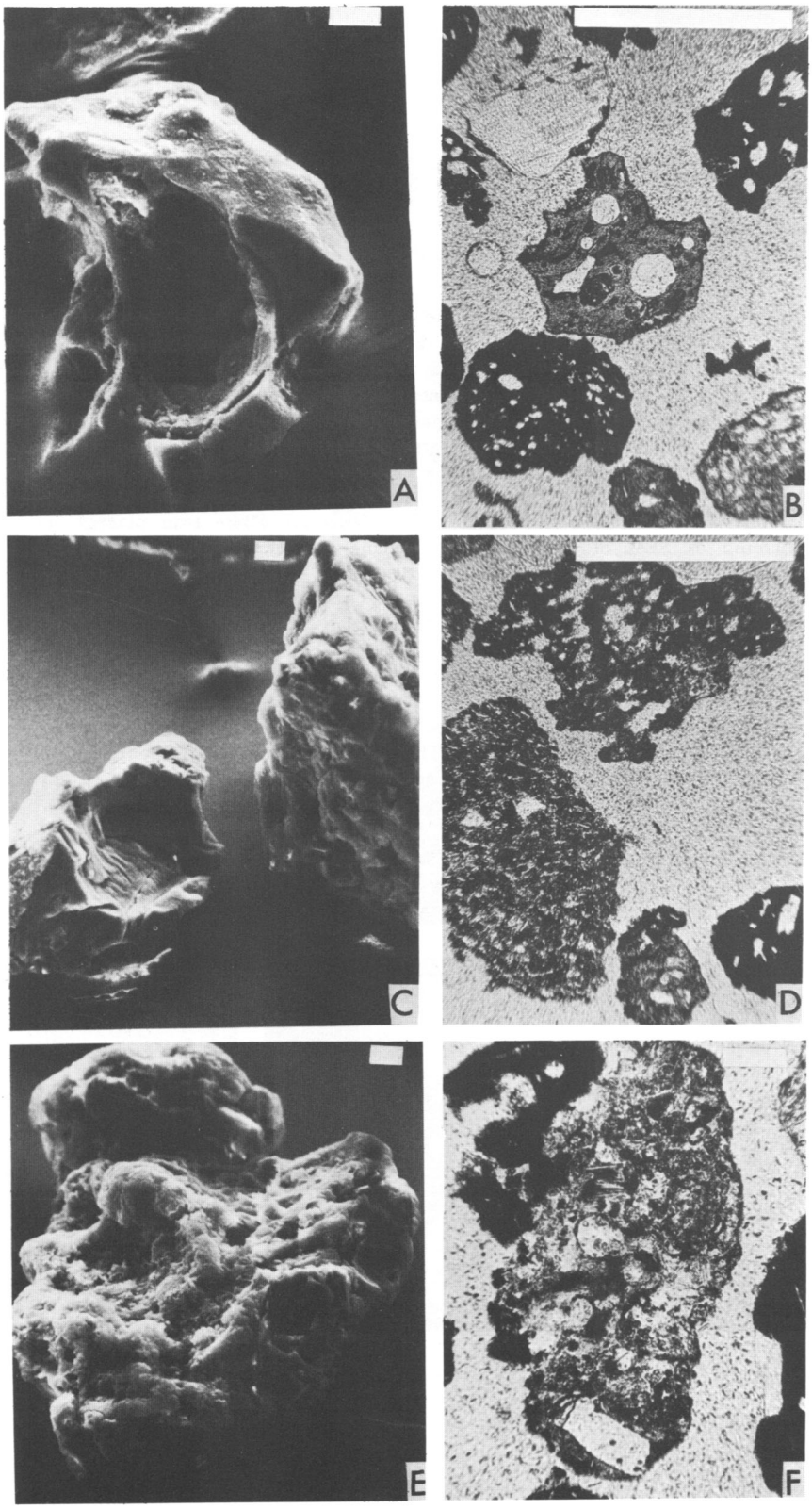
A
B
C
D
E
F

PLATE 12

Taal (ash from the cinder cone), 1958. A, Photomicrograph of a twisted sideromelane droplet (center), with a well-developed dark-brown skin. The tapered droplet tail was broken off. The glass contains 10 to 15 percent randomly oriented microlites of feldspar and pyroxene. The black grains are broken tachylite fragments. On the right and at the bottom of the photograph are sideromelane grains of hyaloclastic origin. (The scale is 100 microns.) B, SEM of a sideromelane droplet. The droplet appears to have twisted around the long axis during ejection from the vent. Surface bulges overlie vesicles or phenocrysts immediately below the droplet surface. (The scale is 10 microns.) C, SEM of a plagioclase crystal, with a thin glass coating welded to the surface. Horizontal parallel lines are albite twin planes. (The scale is 50 microns.) D, SEM of a broken sideromelane droplet. (The scale is 50 microns.) E, Photomicrograph of a broken sideromelane droplet. A dark-brown skin is well developed on the unbroken surfaces. Black grains are tachylite fragments. Other sideromelane fragments are blocky, do not have an outer skin, and are probably of hyaloclastic origin. (The scale is 100 microns.) F, SEM of a sideromelane droplet that has a smooth fluidal surface. White fragments are smaller glass fragments and crystals lying on the grain surface. (The scale is 100 microns.) G, SEM of a tachylite grain that lacks the smooth grain surfaces characteristic of unweathered sideromelane. (The scale is 50 microns.) H, SEM of a tachylite fragment with somewhat irregular rough-walled vesicles. (The scale is 100 microns.) I, SEM of a broken sideromelane fragment, similar to those in D and F. (The scale is 50 microns.)

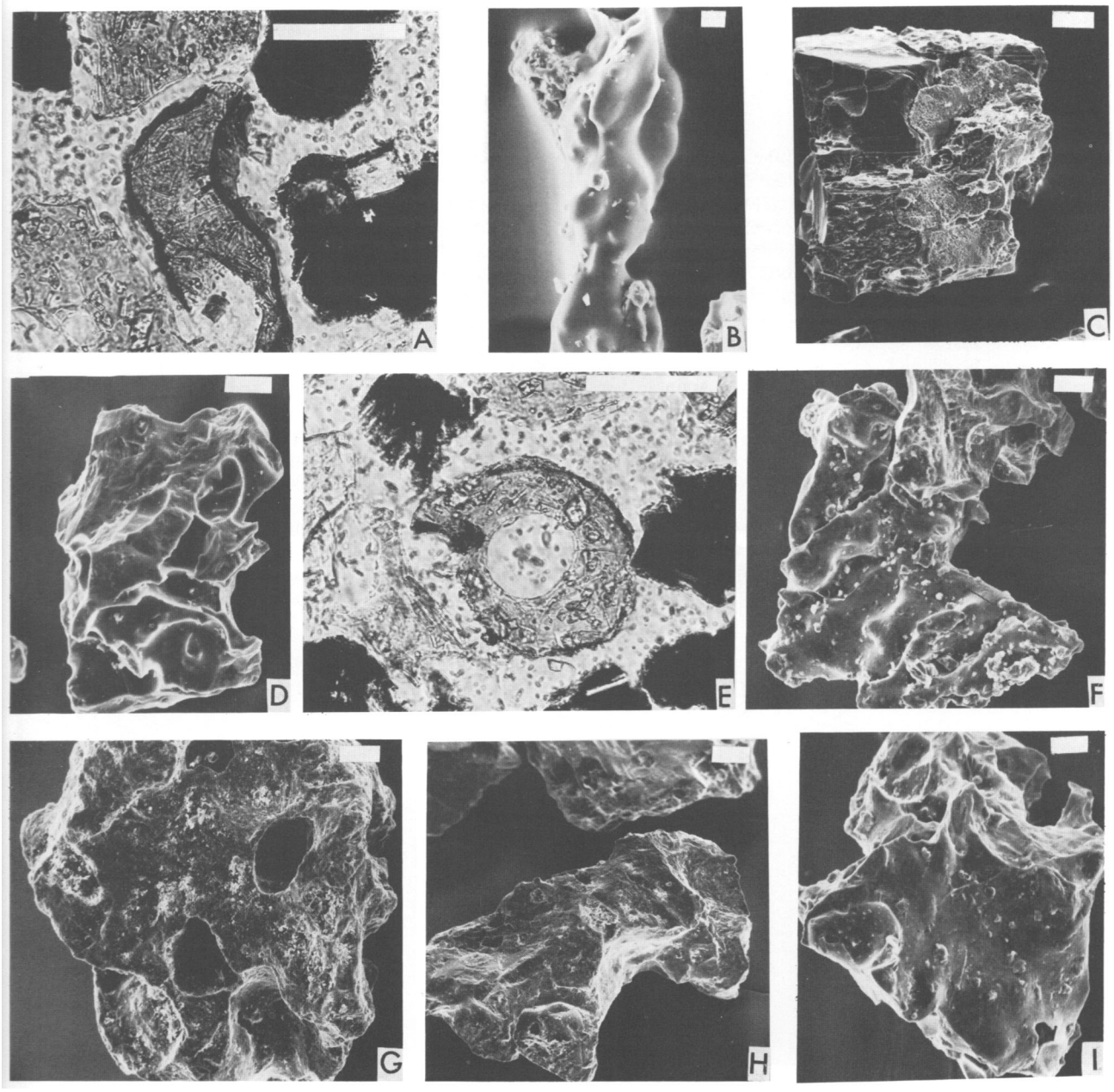
A
B
C
D
E
F
G
H
I

PLATE 13

Makaopuhi—Pele's hair. A, SEM of a smooth, cylindrical Pele's hair. The hair is broken at a bulge, exposing an ovoid, thin-walled vesicle (1–3 microns thick). The hair surface is perfectly smooth, with a few 1– to 2–micron-thick hairs stuck to the surface. (Scale is 100 microns.) B, SEM of same hair as in A. Several millimeters from the broken hair end, there is a change from a cylindrical to ribbed shape. In the lower part of the photo, the skin is broken over an elongate vesicle, resulting in a thin, dagger-shaped depression. (Scale is 210 microns.) C, SEM of a ribbed, 250–micron-diameter Pele's hair. There is one 165–micron-wide rib, flanked by 11– to 25–micron-wide ribs. The irregular lump is over a phenocryst beneath the grain surface. The grain surface is smooth, with the exception of patchy sublimate coatings. (Scale is 35 microns.) D, Photomicrograph of Pele's hair. These "hairs" are characterized by relatively low vesicularity. Vesicle walls and grain surfaces are deformed over clots of olivine and feldspar phenocrysts. The pale brown glass is homogeneous. (Scale is 154 microns.) E, Photomicrograph of a thin, nonvesicular hair, tapered to a point at one end. The hair is deformed over a clot of olivine phenocrysts; 18 percent of the hairs in this sample are nonvesicular. (Scale is 61 microns.) F, Photomicrograph of a vesicular Pele's hair. The extremely long, very thin vesicles in this hair are characteristic of Pele's hair from lava fountains. The bulge in the hair is over an olivine phenocryst. (Scale is 25 microns.) G, Photomicrograph of a Pele's hair, near a large bulge. The ovoid or spherical vesicles near the bulge are very unusual in a Pele's hair. Normally they are stretched out parallel to the long axis of the hair. The glass is pale brown and homogeneous; there are no patches of devitrifiied glass in this sample. (Scale is 154 microns.)

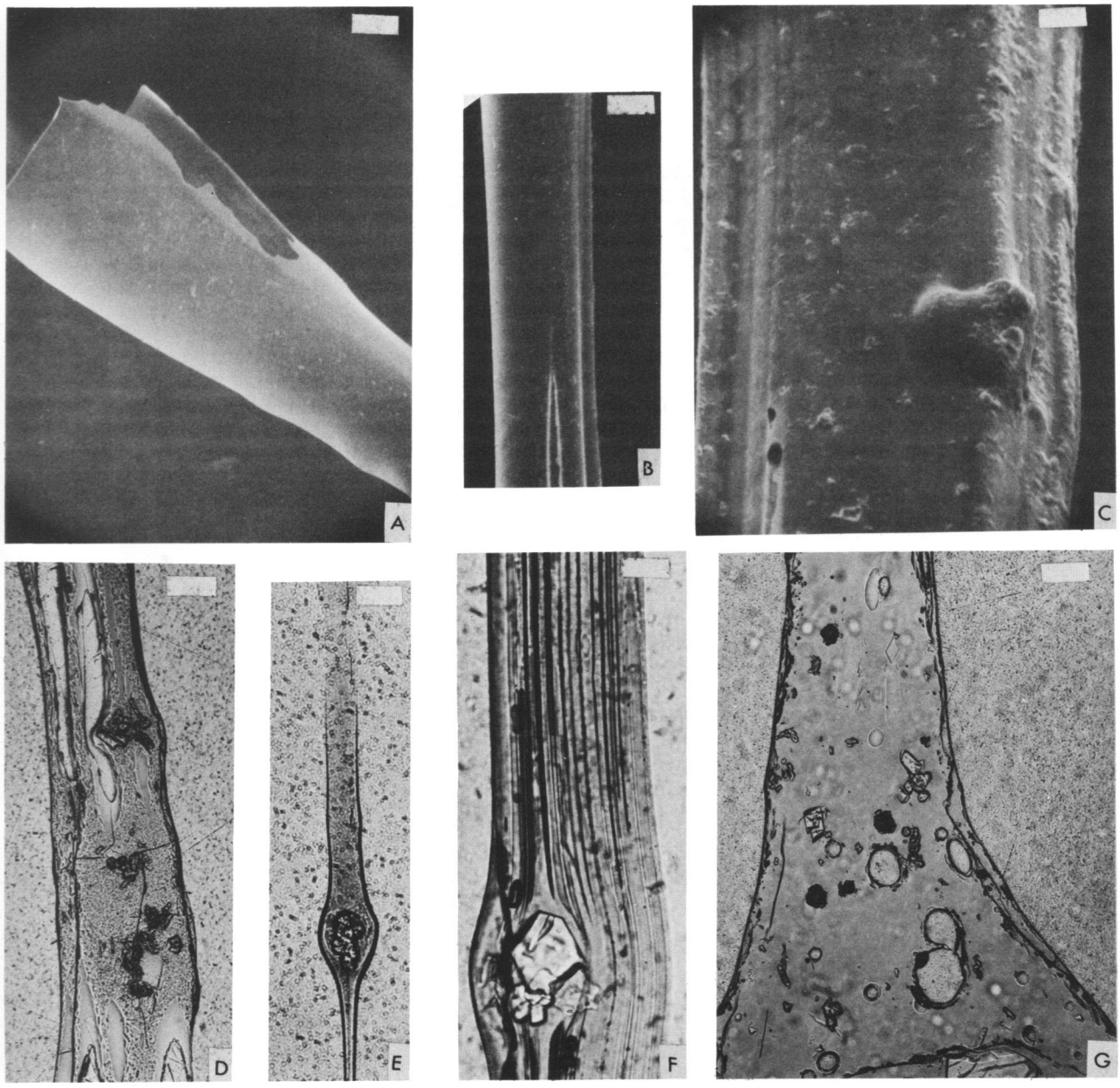
A
B
C
D
E
F
G

PLATE 14

Pahoehoe Flow Crust (crushed). A, SEM of a T-shaped brown glass fragment, consisting of a mutual wall between 3 large vesicles (5 mm to 1 cm diameter). Vesicle walls are curved and quite smooth except for some shallow depressions and lumps (over phenocrysts.) There are *no* smaller vesicles in the vesicle wall. In cross section, the I-shaped vesicle walls are as thin as 100 microns. Broken grain surfaces have a hackly to conchoidal fracture. (Scale is 830 microns.) B, Photomicrograph of the glass wall between three vesicles. It is pale brown, clear glass (sideromelane), with about 5 percent phenocrysts (feldspar and olivine) and 5 to 10 percent small patches of spherulites. (Scale is 154 microns.)

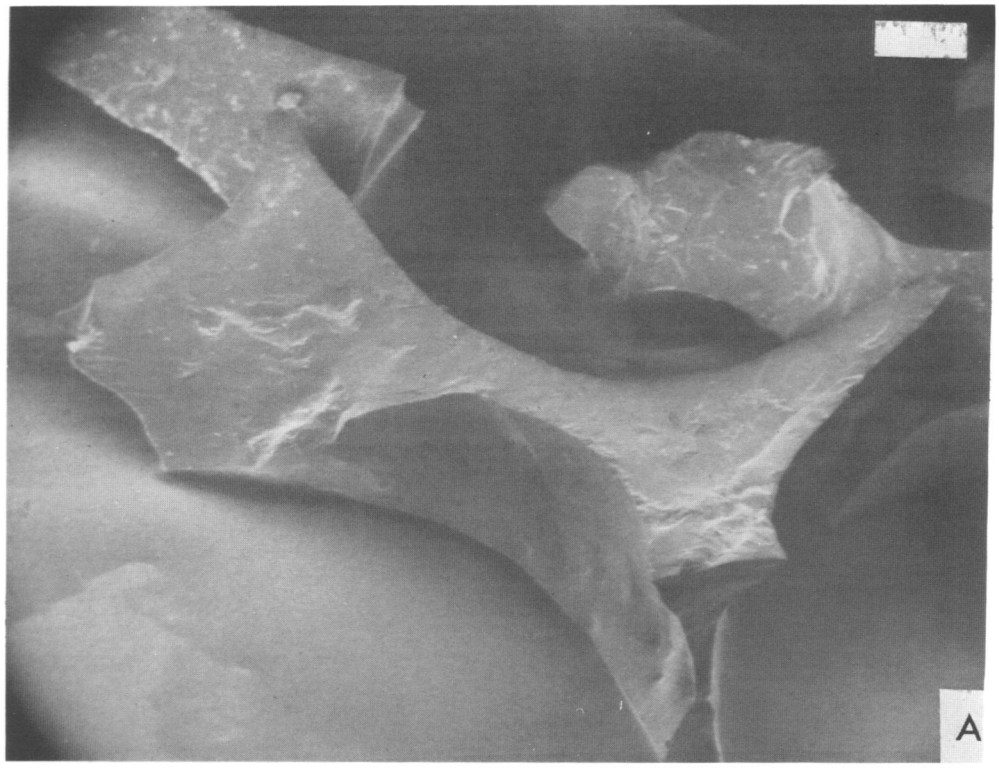
A

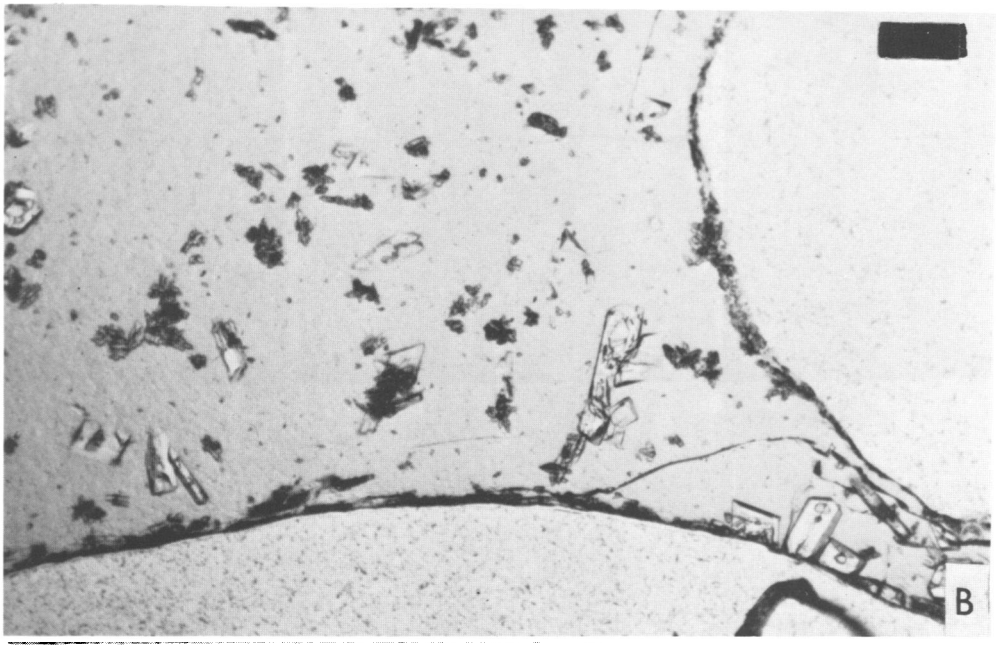
B

PLATE 15

Ruapehu, New Zealand. A, SEM of a broken light-brown glass droplet. The grain surface is partly covered with sublimates. (The scale is 10 microns.) B, Photomicrograph of a clear colorless pumice fragment, rounded either during the eruption or by later reworking. The outer edges were oxidized, resulting in a rim of a darker color glass. (The scale is 100 microns.) C, SEM. The center fragment is possibly a feldspar phenocryst, completely covered with sublimates. (The scale is 100 microns.) D, SEM of lithic-vitric ash. On the upper left is a feldspar phenocryst. Other fragments are andesite or colorless glass. All fragments are covered with a thin layer of sublimates. (The scale is 100 microns.) E, Photomicrograph of lithic-vitric ash, consisting of fragments of aphanitic andesite; mudstone; medium-crystalline pyroxene-hypersthene andesite; tachylite; feldspar-rich aphanitic andesite; crystals of andesine, hypersthene, and augite; and fine-grained glass shards and pumice. (The scale is 500 microns.) F, SEM of a vesicular equant glass fragment. Irregular fractures and pitting of grain surfaces indicate that the ash may have been reworked by water or wind. (The scale is 100 microns.)

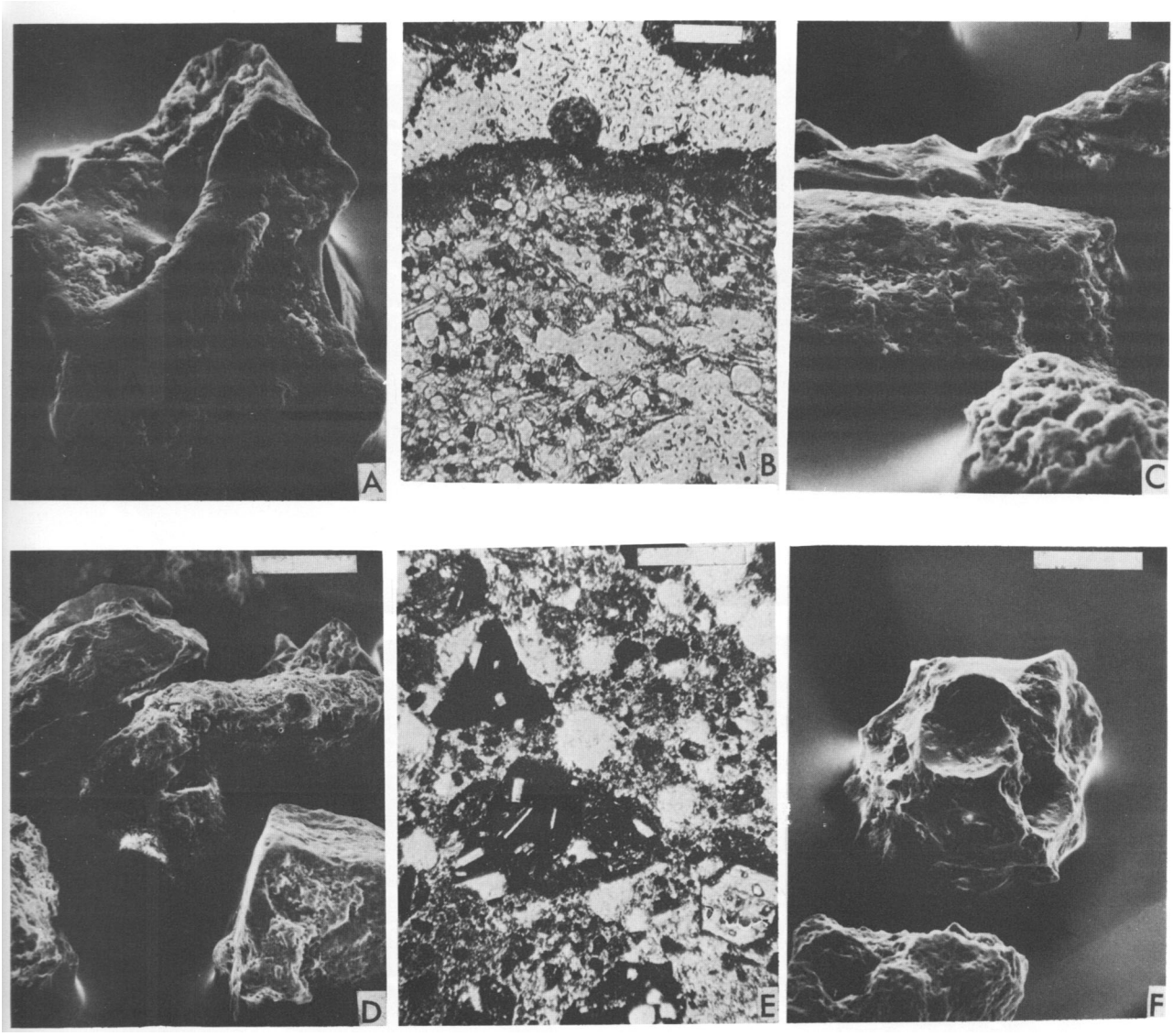
A
B
C
D
E
F

PLATE 16

Merapi, Indonesia. A, SEM of colorless glass shards that are partly covered by small (< 2 microns), loosely adhering glass fragments. The center shard has a single irregularly shaped vesicle. (The scale is 10 microns.) B, SEM. The large fragment in the center is a broken plagioclase crystal, exhibiting good albite twinning. (The scale is 10 microns.) C, SEM of mostly angular nonvesicular glass shards. The pointed fragments in the foreground are characteristic of this ash sample. (The scale is 10 microns.) D, Photomicrograph of a grain mount of this crystal-vitric ash, consisting of plagioclase, orthopyroxene, clinopyroxene, sharp angular and colorless glass shards, and opaque minerals. The ash is very fine grained and very well sorted. (The scale is 100 microns.)

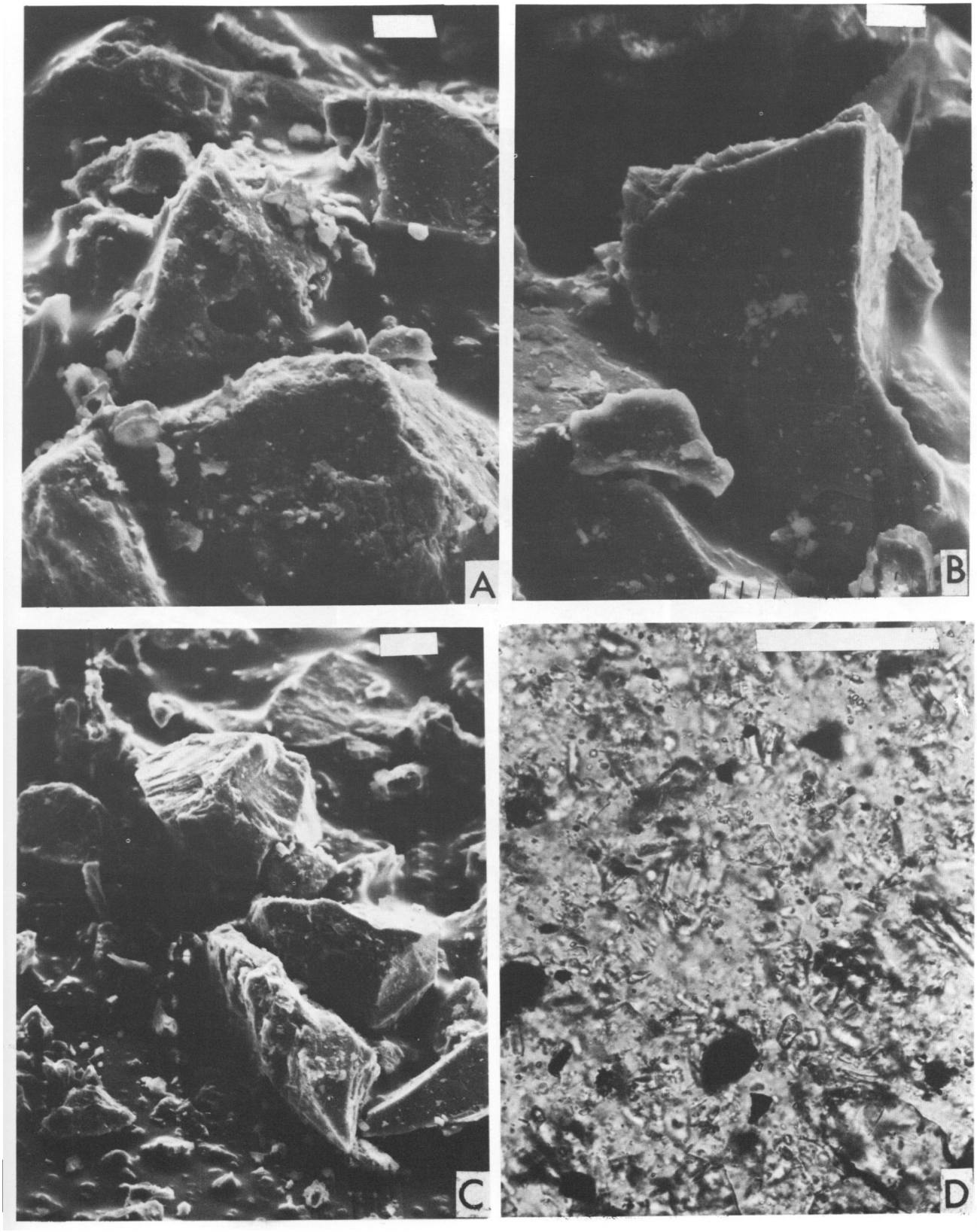
A
B
C
D

PLATE 17

Mayon, Philippines. A, SEM of colorless to gray/brown-colored vitric-crystal ash, consisting of mostly blocky or elongate shards and broken crystals, 5 to 20 microns long. (The scale is 100 microns.) B, Photomicrograph of vitric-crystal ash. In the center is a colorless vesicular glass fragment containing feldspar microlites. The edges of the fragment were oxidized to a dark reddish-brown color. The finer grained ash particles consist of broken crystals of augite, hypersthene, and plagioclase; colorless glass; and small, equant andesite fragments. (The scale is 100 microns.) C, SEM. At center right is a vesicular glass fragment. Most of the vesicles exposed at the grain surface were spherical. (The scale is 10 microns.) D, SEM of a vitric fragment containing ovoid or elongate vesicles up to 15 microns long. Angular fragments on the surface or in the center vesicle are loosely adhering fine-ash fragments. (The scale is 10 microns.) E, Photomicrograph of a scoria fragment consisting of colorless glass with oxidized zones around the edge and around some vesicles. (The scale is 100 microns.) F, SEM of an angular glass shard that is typical of the vitric portion of this ash sample. The smooth, slightly curved surface on the right is probably a vesicle wall remnant. (The scale is 10 microns.)

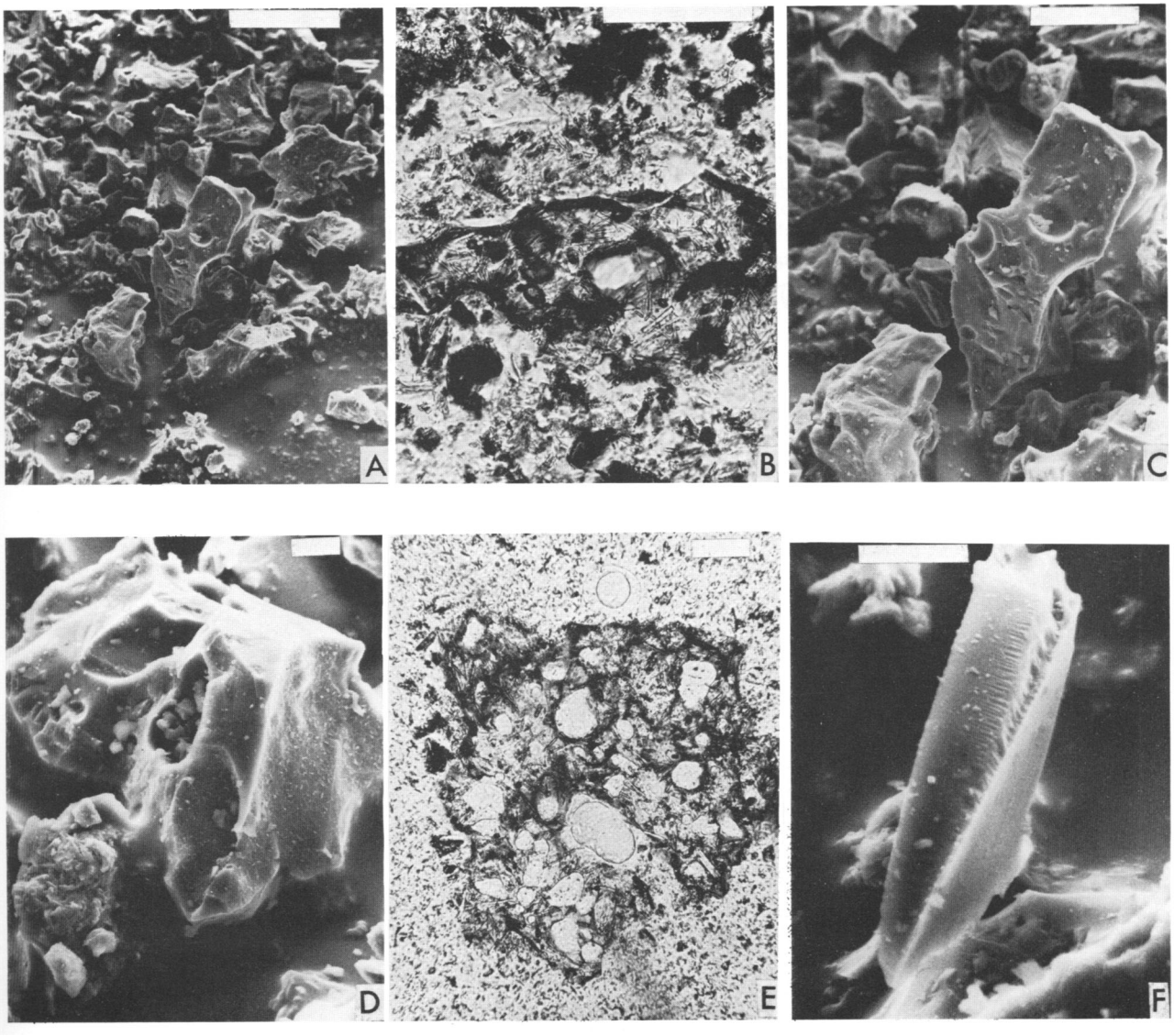
A
B
C
D
E
F

PLATE 18

Ash from Krakatau. Sketches copied from Plate IV of Judd (1888). (Scale is 100 microns.) A, Pumice dust (ash) which fell on board the *Arabella,* when about 1800 km from Krakatau. There is only a trace of phenocrysts at this distance. The sample consists of elongate U- or Y-shaped shards, which are broken vesicle wall fragments. B, Material similar to A, formed by crushing "common" Krakatau pumice in a mortar.

A B

PLATE 19

Santiaguito, Guatemala. A, SEM of a plagioclase crystal exhibiting albite twinning. Loose crystal fragments make up a substantial portion of this ash. (The scale is 50 microns.) B, Photomicrograph of a hyalocrystalline dacite fragment (lithic). Equant dacite fragments make up most of this ash. (The scale is 100 microns.) C, SEM of a broken vitric fragment. (The scale is 50 microns.) D, SEM of a broken vitric fragment partly coated with sublimates. The vesicles have irregular twisted shapes. (The scale is 50 microns.) E, Photomicrograph of an irregularly shaped hyalocrystalline fragment. The vesicle in the center has an odd irregular shape that is characteristic of the vesicles in this ash of dacite composition. (The scale is 50 microns.) F, SEM of a lithic ash consisting of equant dacite fragments and vesicular vitric fragments. (The scale is 100 microns.)

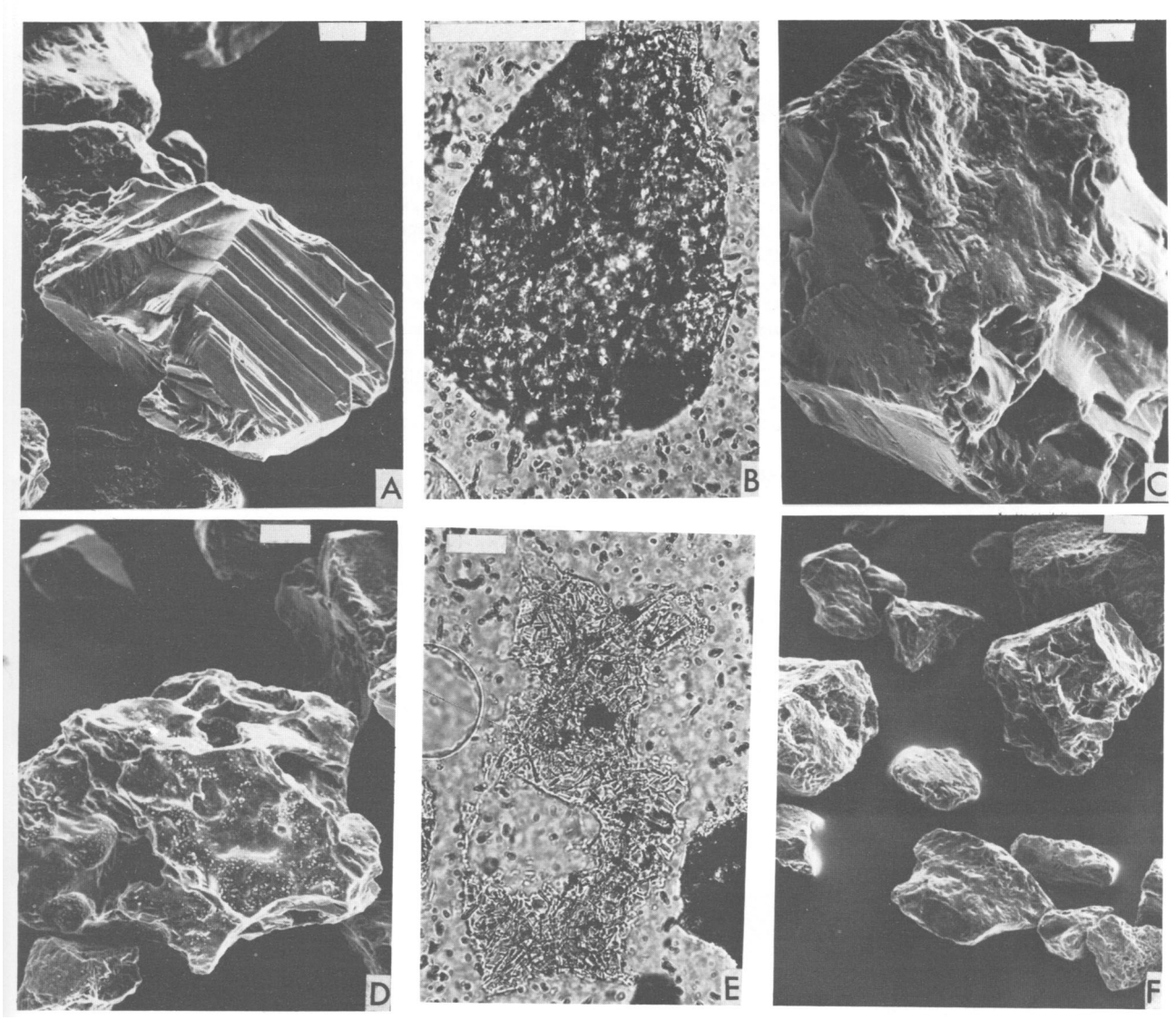
A
B
C
D
E
F

PLATE 20

Katmai, Alaska. A, SEM of a colorless pumice fragment, with pipe vesicles 5 to 50 microns in diameter. Vesicle walls are 0.5 to 2 microns thick. The overall grain shape is controlled by vesicle shape. (The scale is 100 microns.) B, SEM; closeup of A, showing in detail the vesicle shapes and thin vesicle walls. (The scale is 100 microns.) C, Photomicrograph of a pumice fragment similar to those in A and B. The vesicles are parallel with pipe or pod shapes. The glass is colorless. Dark spots are opaque minerals. (The scale is 100 microns.) D, SEM of pumice and shards, consisting of transparent colorless glass. All particles in the field of view are vitric fragments. (The scale is 100 microns.) E, SEM; closeup of the pumice fragment in D, illustrating different stages in the development of elongate pipelike vesicles. In the center is a nearly spherical vesicle. The pipe-shaped vesicles were formed by elongation and compression of spherical vesicles by flow in the extremely viscous magma near the ground surface. Small particles loosely adhering to the grain surface are small angular shards. (The scale is 100 microns.) F, Photomicrograph of a pumice fragment (center) and many shards that are triangular or needle-like in cross section. Most of the shards are broken vesicle walls. (The scale is 100 microns.) G, SEM of chains of spherical and podlike vesicles in different stages of being stretched out to form elongate pipe vesicles. Fragmental material in vesicles and on the surface are small shards loosely adhering to the surface of the pumice grains. (The scale is 20 microns.) H, SEM of a vitric fragment that is unique for this sample because the vesicles are not drawn out into pipe shapes. Most of the vesicles are flattened ovoids. Part of this fragment has no vesicles. (The scale is 10 microns.)

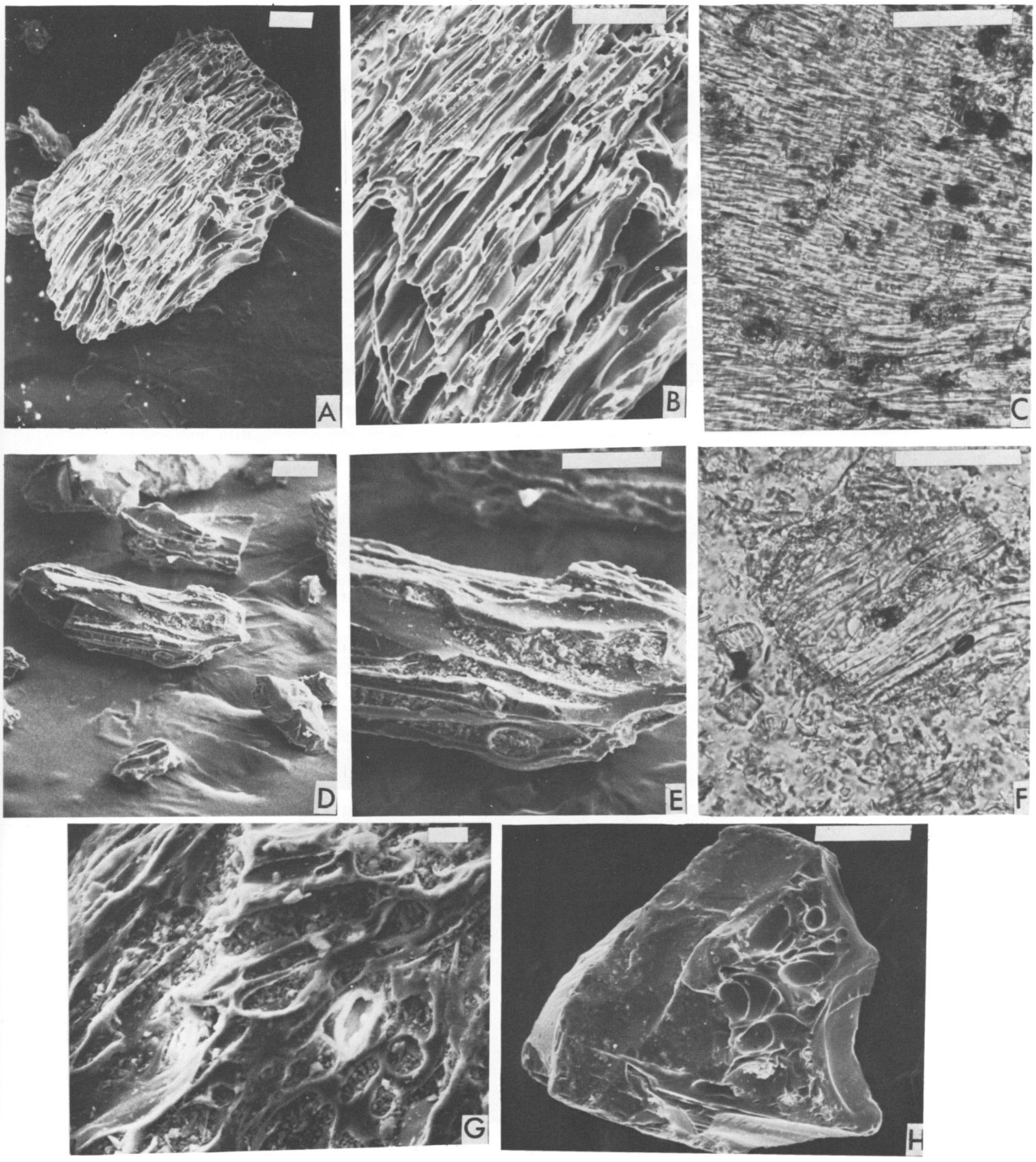
A
B
C
D
E
F
G
H

PLATE 21

Mazama ash. A, SEM of glass fragments ranging from 2.4 to 12 microns long. There are mostly elongate, furrowed, and curved platelike grains. Dust adhering to the grain surfaces is generally less than 1 micron in diameter The channeled fragments are thin walls of parallel, elongate vesicles, broken into short sections. (Scale is 7.3 microns.) B, SEM of a flattened, rectangular fragment with flattened, ovoid vesicles (ranging from 5 to 14 × 30 microns). Vesicle walls and surfaces are very smooth. (Scale is 10 microns.) C, SEM of a 100–micron-long pumice fragment. Pumice fragments of this size are rare in this sample. The vesicle walls are 1 to 3 microns thick. (Scale is 10 microns.) D, Photomicrograph of a pumice fragment and several angular shards. The glass is colorless, and contains very few microlites. Compare the cross section of the pumice grain to the SEM photograph of a similar grain in C. (Scale is 15.5 microns.) Photomicrograph of a group of shards which are typical of this sample. Angular, curved, or Y-shapes are common. The grain on the right is a very small pumice fragment, with one intact vesicle. (Scale is 6.5 microns.)

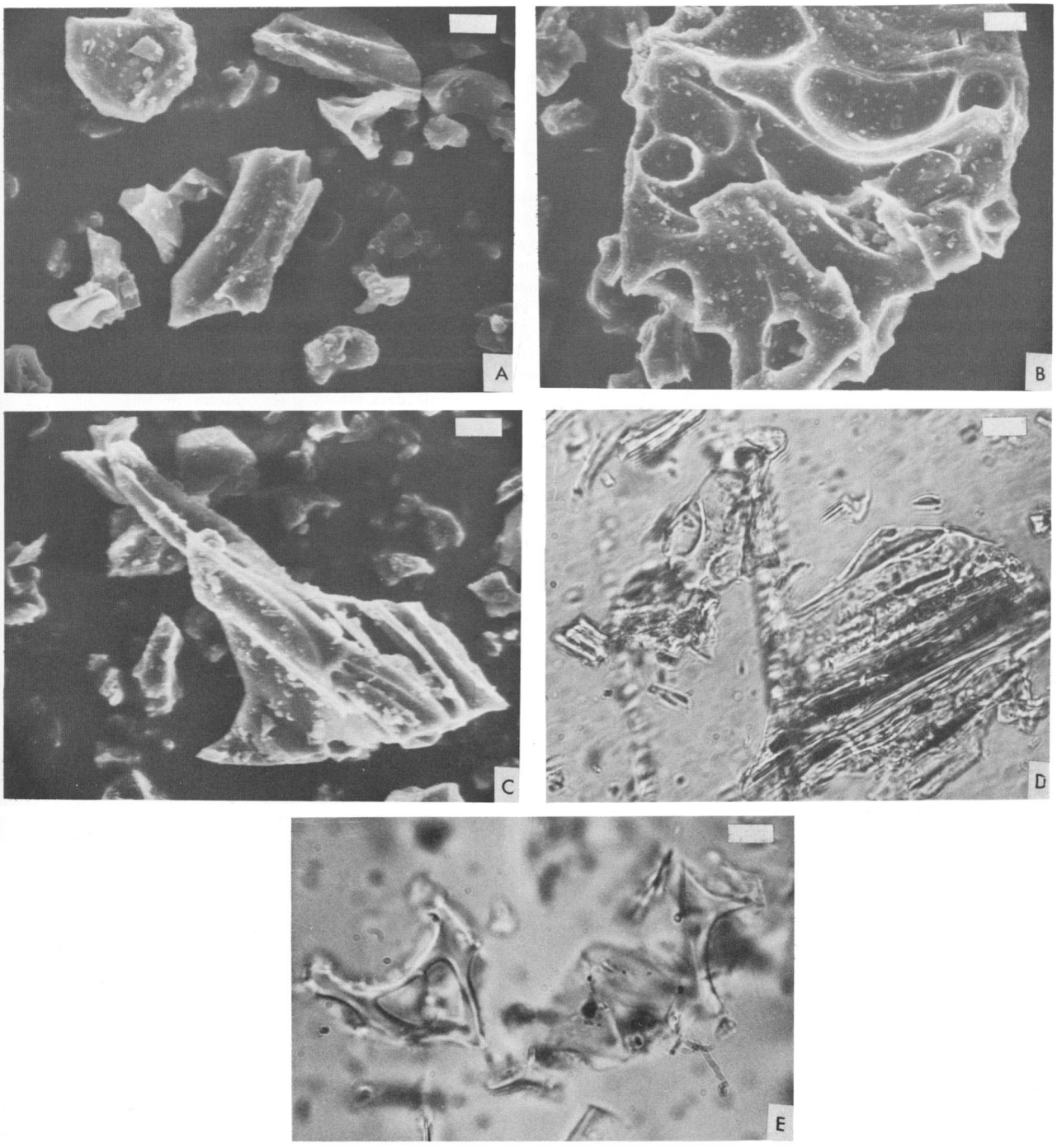
A
B
C
D
E

PLATE 22

Oldoinyo Lengai, Tanzania. A, SEM of a carbonatite ash. Several excellent hexagonal nepheline crystals are visible in this sample. Other crystals are completely coated with trona. (The scale is 100 microns.) B, SEM; closeup of the surface of a nepheline crystal, showing clumps of trona crystals. These may have formed by solution and precipitation on grain surfaces by rainwater. (The scale is 10 microns.) C, SEM of ash fragment (nepheline crystal?) partly covered with trona crystals. (The scale is 100 microns.) D, SEM; closeup of the surface of the grain in C. Delicate intergrown bladelike crystals of trona fill most of the depressions in the grain surface. (The scale is 10 microns.) E, Photomicrograph of carbonatite ash. The clear crystals are nepheline coated with trona. The opaque clots are aggregates of trona and small crystals of apatite, pyroxene, and wollastonite. There are some small dark-brown glass spheres in this sample. (The scale is 1 mm.) F, Photomicrograph of a euhedral nepheline crystal in the ash. It is zoned with crystals of apatite growing parallel to the outer rims of the grain. (The scale is 100 microns.)

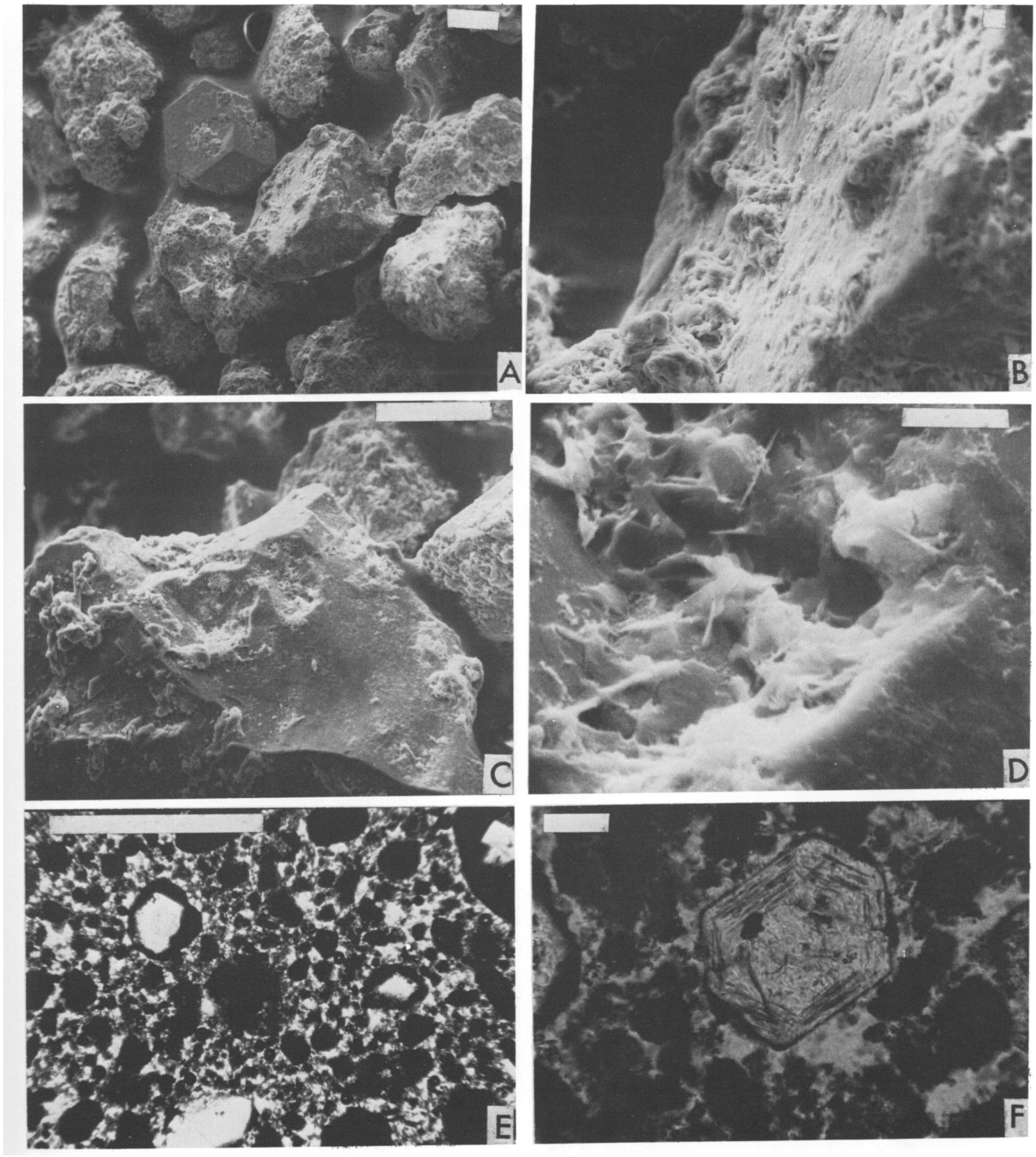
A
B
C
D
E
F

PLATE 23

Capelinhos, Azore Islands. (All scales are 100 microns.) A, SEM of equant blocky sideromelane fragments. The low vesicularity and smooth fracture surfaces are characteristic of hyaloclastic ash. Vesicle diameters range from 5 to 70 microns. B, Photomicrograph of sideromelane fragments, illustrating the rectangular or polygonal shapes observed in thin section. Low vesicularity and few microlites are also characteristic of hyaloclastic ash. Dark circles are bubbles in the mounting medium. C, SEM of sideromelane fragment with surfaces exhibiting conchoidal fractures. The fragment may have been chipped during or after ejection from the vent. D, Photomicrograph of sideromelane fragments. The large fragment in the center contains several feldspar phenocrysts. Dark circular spots are bubbles in the mounting medium.

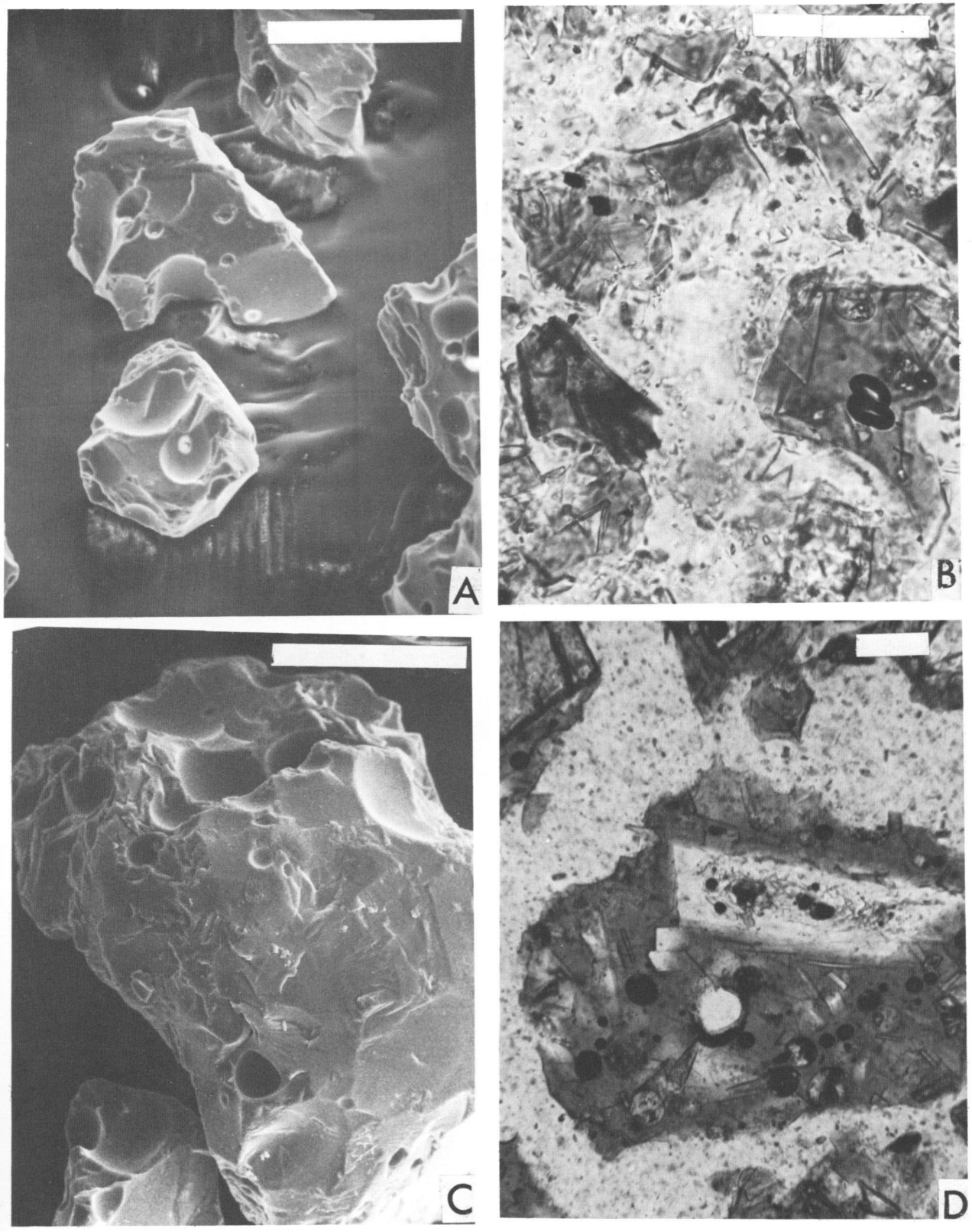
A
B
C
D

PLATE 24

Surtsey, Vestmann Islands, Iceland. (All scales are 100 microns.) A, SEM of blocky sideromelane fragments with smooth fracture surfaces characteristic of hyaloclastic ash. There is a wide range of vesicle diameters. B, Photomicrograph of sideromelane fragments exhibiting rectangular or polygonal shapes. The glass is homogeneous and has no skin similar to the skin on sideromelane droplets from magmatic eruptions. C, SEM of a blocky sideromelane fragment. The vesicles are randomly spaced and are generally far apart. D, SEM of sideromelane fragments with a wide range of vesicularities. The fragment on the right is atypical of the fragments in this ash sample.

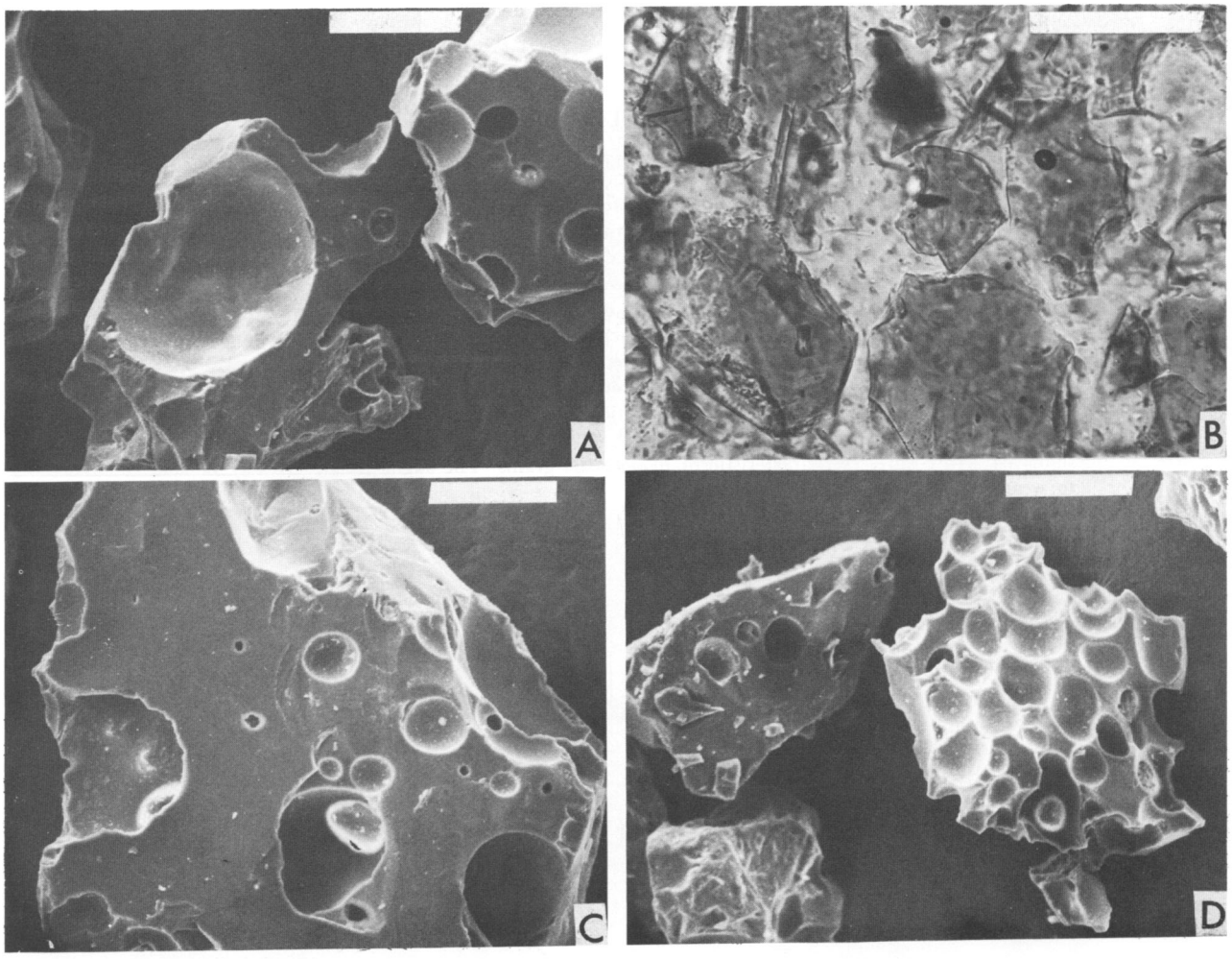
A
B
C
D

PLATE 25

Taal, Philippines. A, SEM of blocky, nonvesicular sideromelane fragments. (The scale is 25 microns.) B, Photomicrograph of moderately well-sorted ash consisting of (1) equant sideromelane fragments, (2) equant tachylite fragments, (3) clinopyroxene crystals, and (4) feldspar crystals ($\simeq An_{45}$). (The scale is 500 microns.) C, SEM of a feldspar phenocryst coated with moderately vesicular sideromelane. Parallel grooves and ridges in the crystal fragment are due to twinning. (The scale is 50 microns.) D, SEM of blocky sideromelane and tachylite fragments. The two fragments in the foreground may be tachylite. Lath-shaped, twinned feldspar microlites, with lengths ranging from 5 to 25 microns, are visible on the grain surfaces. (The scale is 50 microns.) E, Photomicrograph of blocky sideromelane fragments probably of hyaloclastic origin. In contrast with droplets from magmatic eruptions of basaltic liquid, there is no skin on the ash fragments. (The scale is 100 microns.) F, SEM of blocky sideromelane fragments with smooth fracture surfaces characteristic of hyaloclastic grains. The slight roughness may be due to weathering. (The scale is 25 microns.)

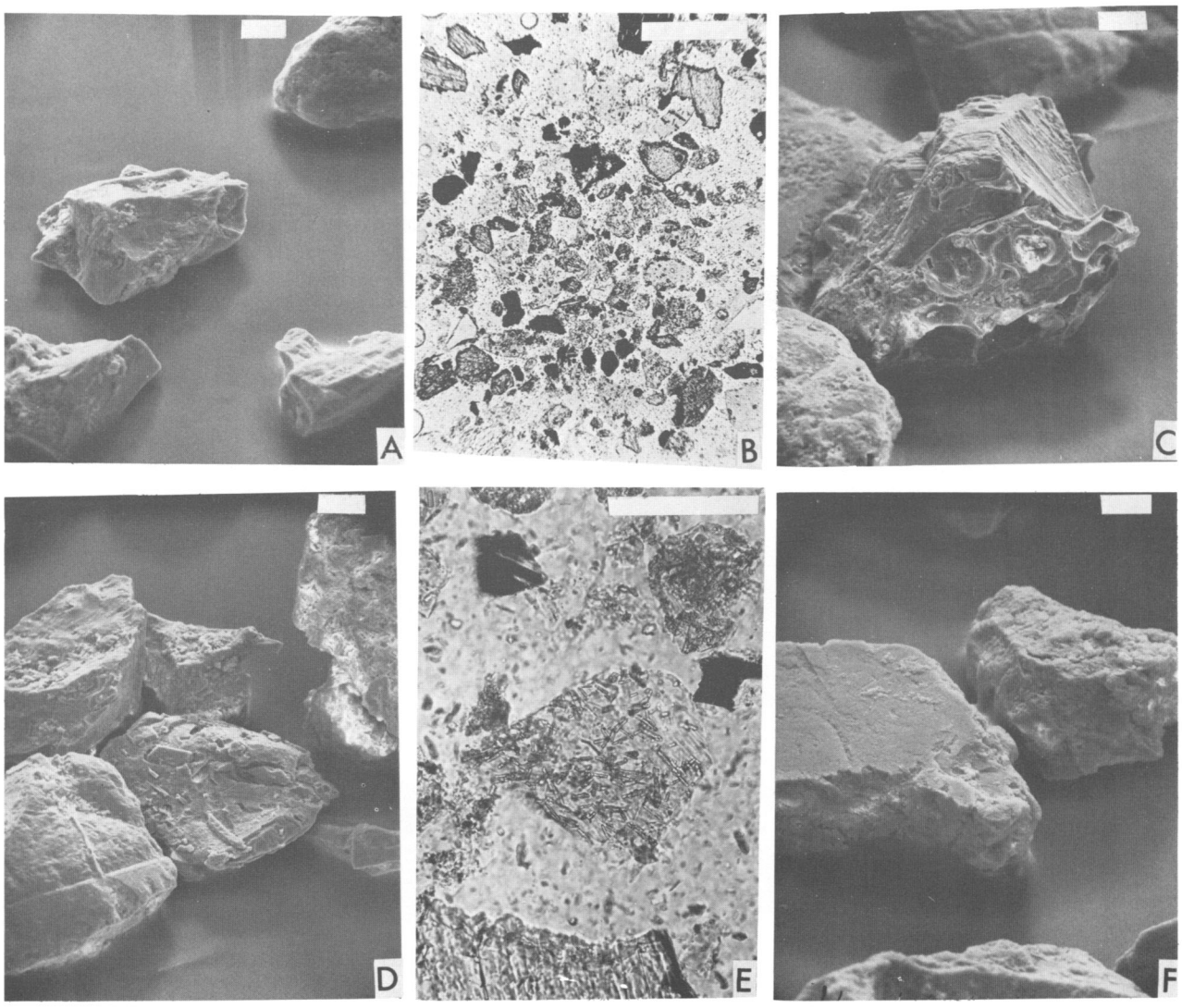
A
B
C
D
E
F

PLATE 26

Table Rock Tuff-Ring Complex, Oregon. A, SEM of blocky sideromelane fragments. The freshest fragment in the upper right center has a very low vesicularity. The grain surface has been etched by weathering. The other fragments have been altered to palagonite, a mixture of clays, zeolites, and iron oxides. The older ash (Pleistocene age) is included for comparison with fresh hyaloclastic ash from Capelinhos and Surtsey (Figures 20 and 21). (The scale is 100 microns.) B, Photomicrograph of angular sideromelane fragments. The dark rims on each fragment consist of palagonite and are not chilled skins. (The scale is 100 microns.) C, SEM; closeup of the etched sideromelane grain in A. Vesicle diameters range from 1 to 10 microns. (The scale is 10 microns.) D, Photomicrograph of blocky sideromelane fragment. (The scale is 100 microns.)

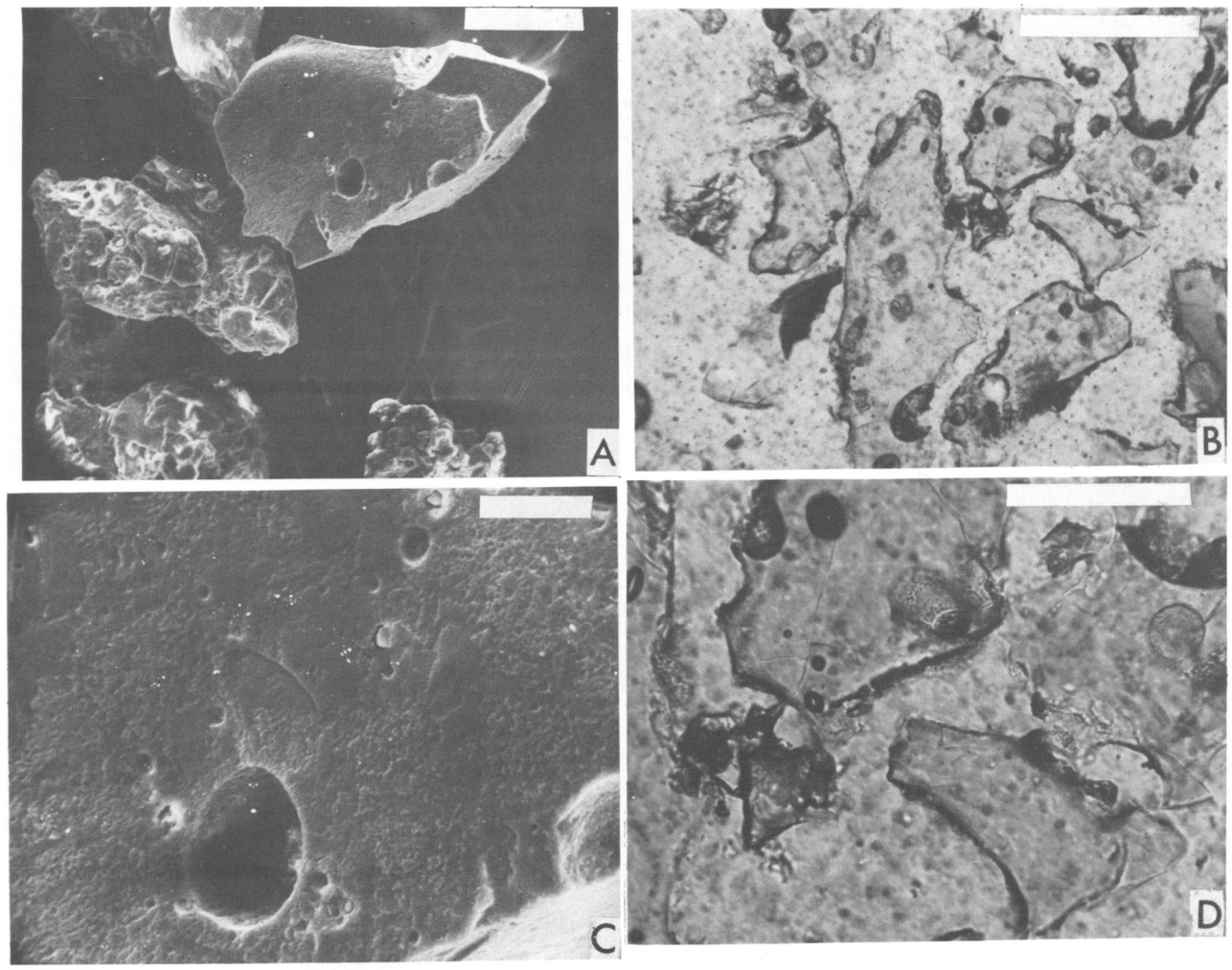
A
B
C
D

PLATE 27

Kilauea, Hawaii (1924 phreatic eruption). (All scales are 100 microns.) A, SEM. The ash is composed of mostly equant blocky basalt fragments. Some have been weathered. B, Photomicrograph of the lithic-crystal ash that consists of (1) holocrystalline basalt, (2) altered hyalocrystalline basalt fragments, (3) olivine-rich basalt, (4) tachylite, (5) equant olivine crystals, (6) opaque minerals, (7) an orthopyroxene, (8) tabular, slightly rounded sideromelane fragments with abundant feldspar microlites, and (9) blocky nonvesicular sideromelane fragments with no vesicles, partly altered to palagonite. C, SEM of vesicular basalt fragment (center). Clump of small angular sideromelane and tachylite fragments (left side).

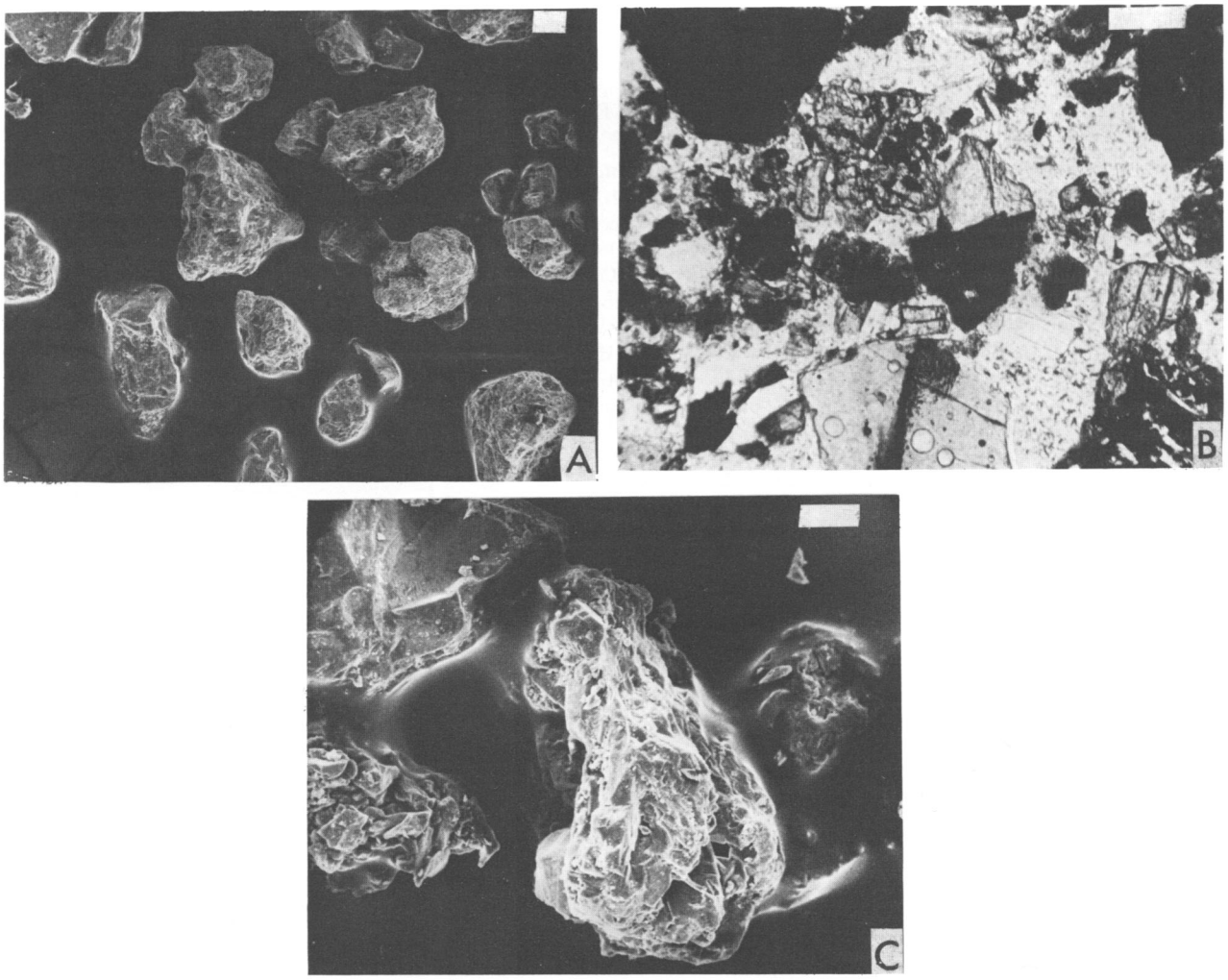
A
B
C

PLATE 28

Panum Crater, California. A, SEM of a broken pumice fragment containing flattened pipe vesicles. There are both smooth and conchoidal fracture surfaces. (The scale is 10 microns.) B, Photomicrograph of shards in the colorless crystal ash. The two largest fragments (upper left and lower right) are pumiceous, with vesicles 0.5 to 20 microns across (in cross section). Smaller shards are square or crescent shaped. (The scale is 100 microns.) C, SEM. The largest fragment is pumice, with subparallel, somewhat curved pipe vesicles. It has been pitted, probably by weathering. (The scale is 10 microns.) D, SEM of a pumice fragment, with flattened pipe vesicles similar to the fragment in A. The main difference is the smooth outer surface (on the upper right), which may be an outer skin. (The scale is 10 microns.) E, Photomicrograph of well-sorted, colorless shards and pumice fragments. (The scale is 100 microns.) F, SEM of a colorless ash consisting of sharp, angular, elongated shards. The shards are possibly fragments of vesicle walls from broken pumice fragments. (The scale is 10 microns.)

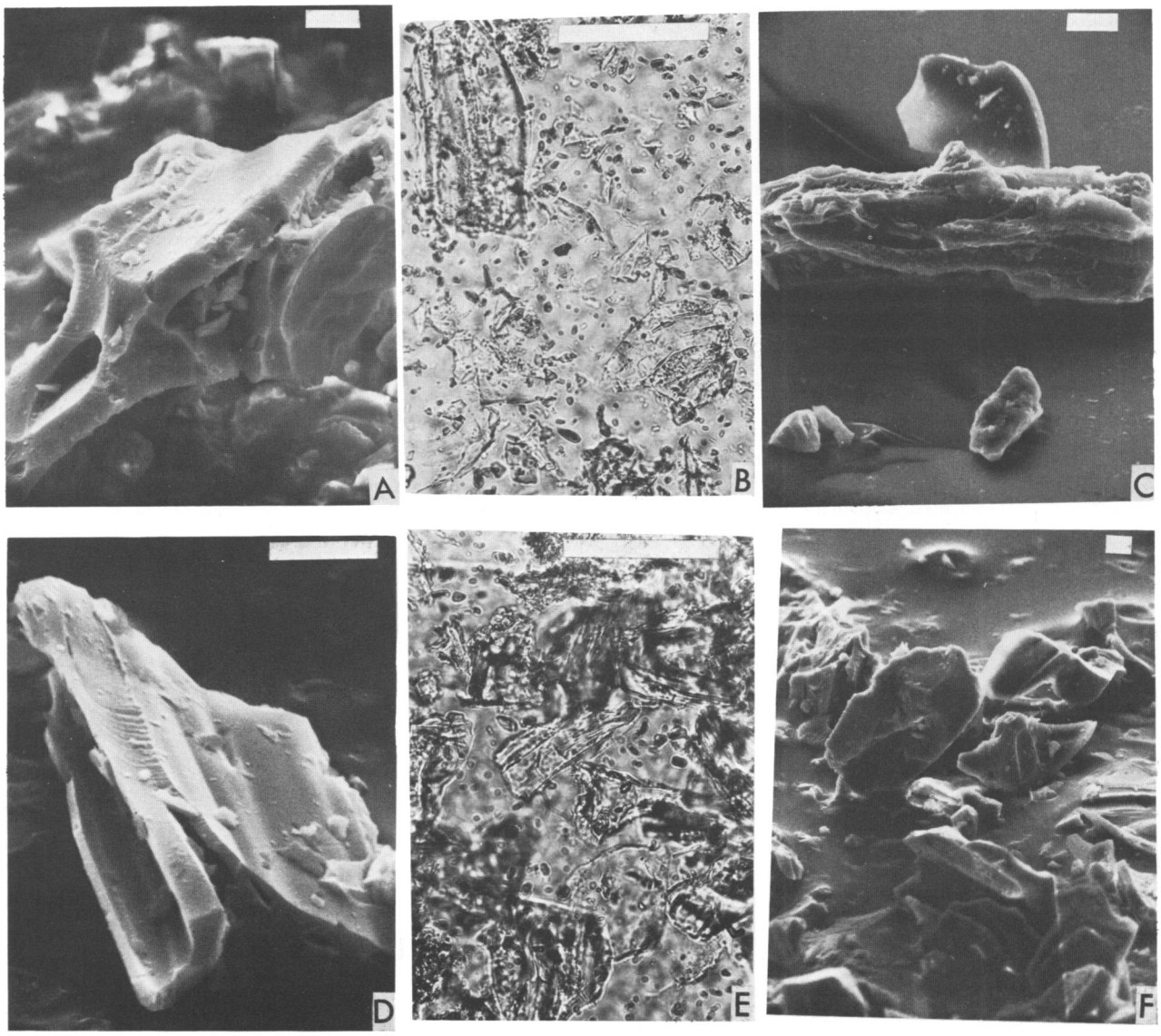
A
B
C
D
E
F

PLATE 29

Sugarloaf Ash, San Francisco Mountains, Arizona. A, SEM. The fragment in the foreground is a lithic fragment consisting of rhyolite. The two angular fragments in the back are colorless glass. There are very few vesicles visible in the vitric fragments. (The scale is 50 microns.) B, SEM of an angular, blocky vitric fragment; most of the grain surfaces are smooth or conchoidal. (The scale is 20 microns.) C, SEM. Lithic fragments (rhyolite) with rough, irregular grain surfaces are visible in the foreground. The angular, blocky fragments in the back, which have smooth grain surfaces, are colorless glass. (The scale is 50 microns.) D, Photomicrograph of colorless angular shards and pumice in a matrix of fine-grained glass fragments. Most of the fragments are not vesicular. Those that are vesicular have very low vesicularity. (The scale is 100 microns.) E, Photomicrograph of a vitric-lithic ash. Most of the colorless fragments are nonvesicular rhyolitic glass, as in the fine-grained matrix. The large rounded fragment in the lower center is hyalocrystalline rhyolite. The large colorless fragment at the right is pumice of moderate vesicularity, with an accretionary rim of fine-grained glass fragments. (The scale is 500 microns.) F, Photomicrograph of a blocky angular glass fragment similar to the one in C. It is a matrix of smaller glass fragments. (The scale is 100 microns.)

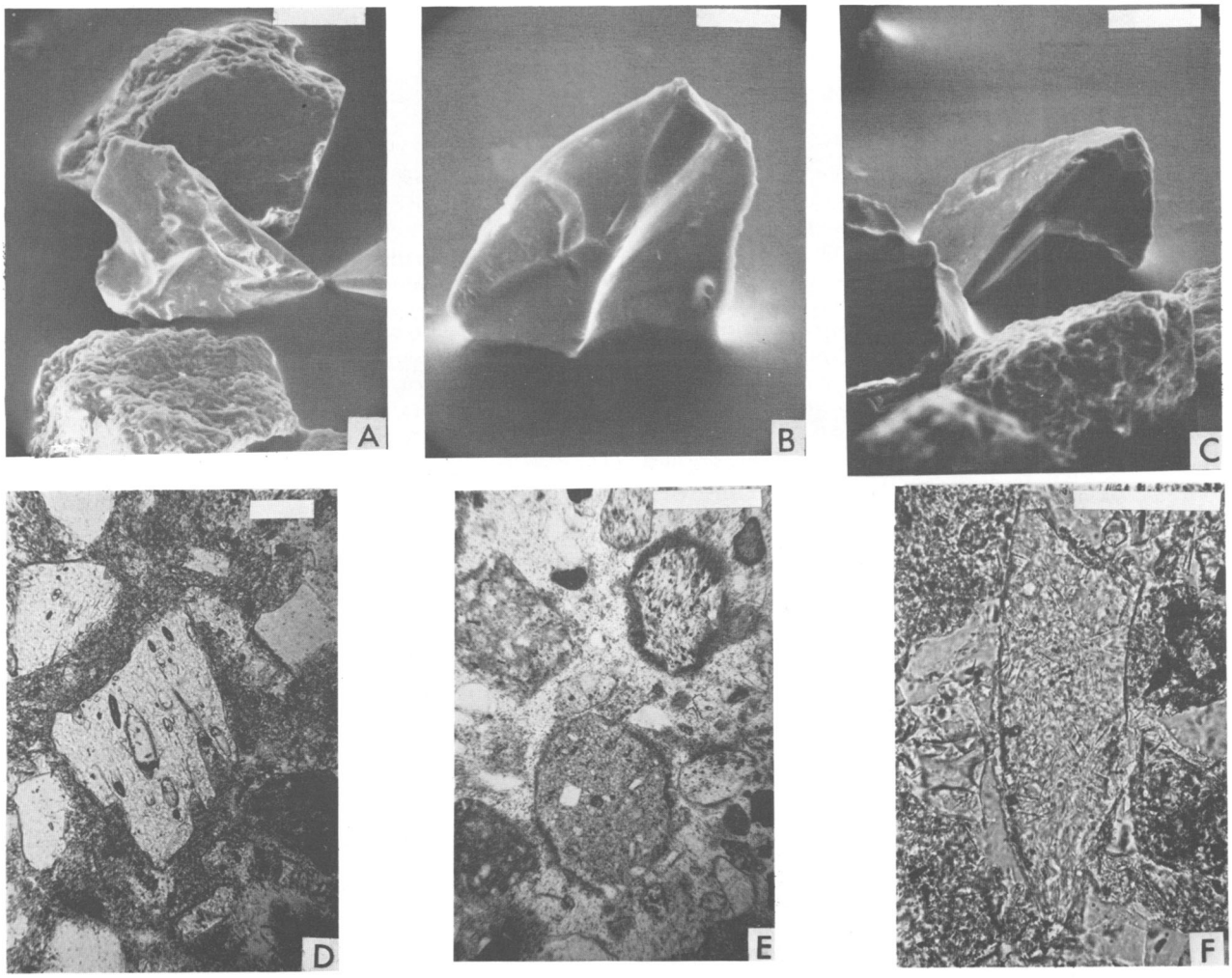
A
B
C
D
E
F

PLATE 30

Puu Hou littoral cones. A, SEM of vitric ash consisting of (1) angular blocky glass fragments formed by rapid chilling of the lava and subsequent contraction and shattering (good example in upper left center) and (2) broken droplets with fluidal surfaces. Most of the ash exhibits low vesicularity. (The scale is 100 microns.) B, Photomicrograph of vitric ash. The ash consists of mostly sideromelane fragments, with a few tachylite grains (black grains in photograph). The blocky sideromelane fragments contain 2 to 8 percent olivine phenocrysts and up to 20 percent feldspar and pyroxene microlites. (The scale is 500 microns.) C, SEM. The highly angular sideromelane fragments appear to have been broken from an area between large vesicles. The smooth fracture surfaces of glass between vesicles is characteristic of hyaloclastic ash. (The scale is 100 microns.) D, Photomicrograph of vitric ash. In the center is an angular sideromelane fragment of hyaloclastic origin, with an olivine phenocryst attached to one side. Microlites in the glass are randomly oriented. (The scale is 500 microns.) E, SEM of a broken sideromelane droplet. The smooth curved surface is part of the original droplet surface. (The scale is 100 microns.) F, Photomicrograph of twisted sideromelane droplets with 2- to 5-micron-thick skins. (The scale is 100 microns.) G, SEM of hyaloclastic fragment, with vesicles several hundred microns long. (The scale is 100 microns.) H, SEM of a broken sideromelane droplet (lower center) surrounded by hyaloclastic fragments. (The scale is 100 microns.)

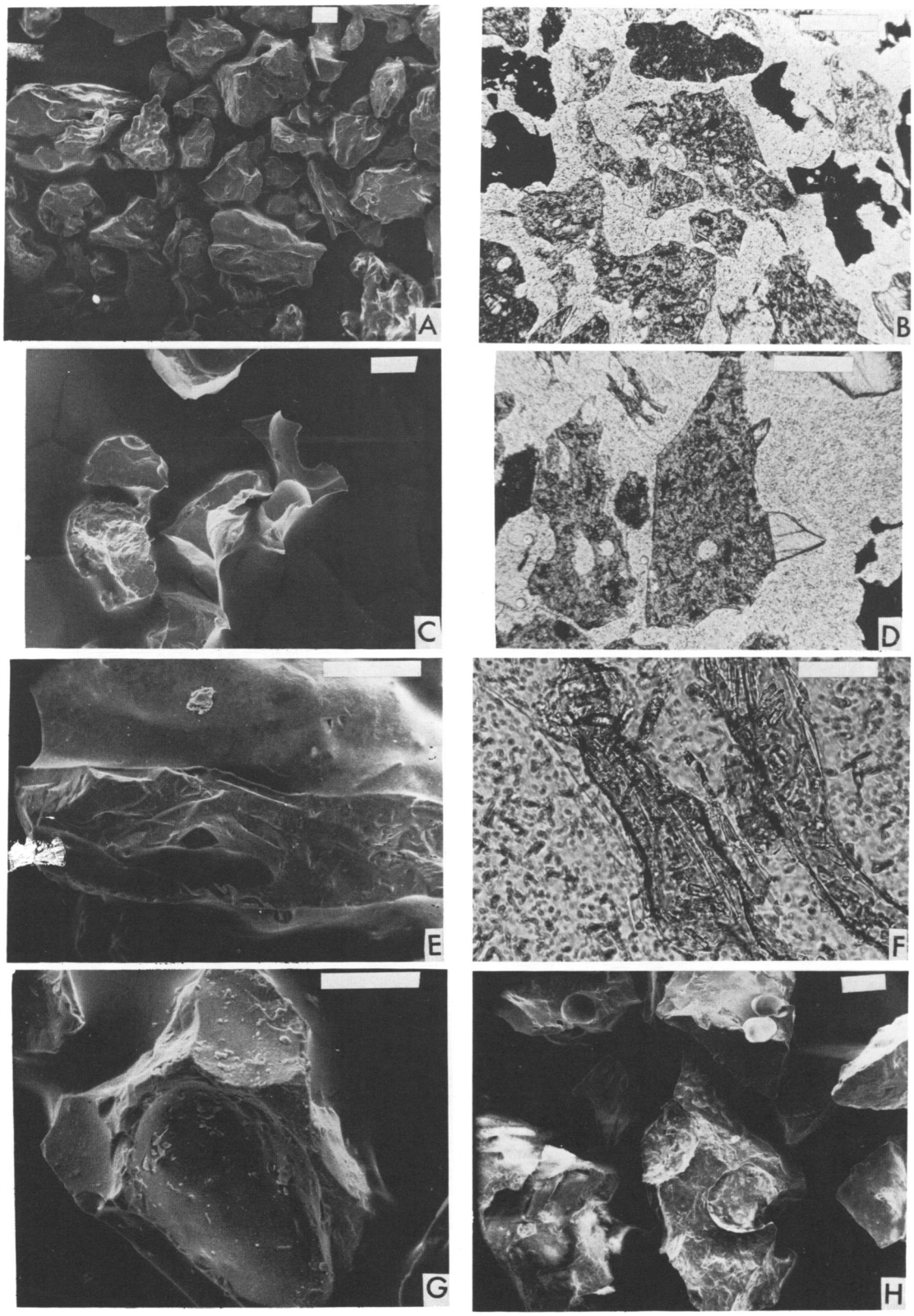
A
B
C
D
E
F
G
H

PLATE 31

Sand Hills littoral cones. A, SEM of a sideromelane ash consisting of (1) angular pyramidal and crescent-shaped grains with very low vesicularities, (2) equant blocky grains with low or moderate vesicularity, and (3) droplets or broken droplets with moderate vesicularity. (The scale is 100 microns.) B, SEM of a broken glass droplet. The original outer surface with a small skin is visible in the upper central part of the fragment. Lumps in the skin are over vesicles located just below the surface. Fracture surfaces are irregular and, in some places, conchoidal. (The scale is 100 microns.) C, Photomicrograph of sideromelane ash fragments. On the bottom is an elongate sideromelane droplet with elongate vesicles. The angular fragments above the droplet are of hyaloclastic origin. (The scale is 500 microns.) D, Photomicrograph of the edge of a sideromelane droplet with a thin dark skin. (The scale is 100 microns.) E, SEM of a pyramidal angular sideromelane fragment of hyaloclastic origin. The smooth fracture surfaces formed by chilling of the lava and contraction of the cooling glass are unlike the conchoidal fractures formed by crushing. (The scale is 100 microns.) F, SEM of a broken droplet (center) with moderate vesicularity. (The scale is 100 microns.)

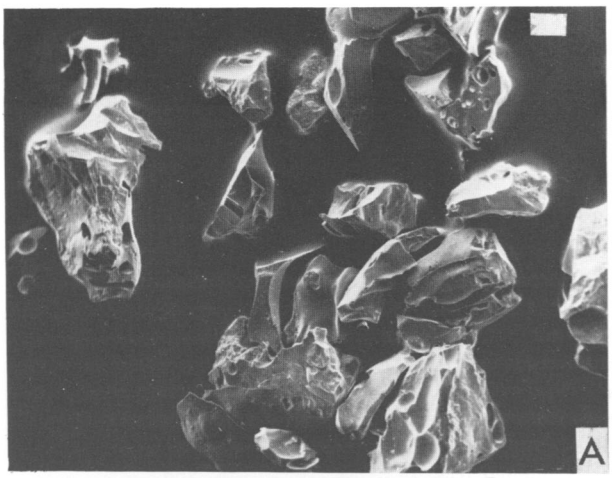
A

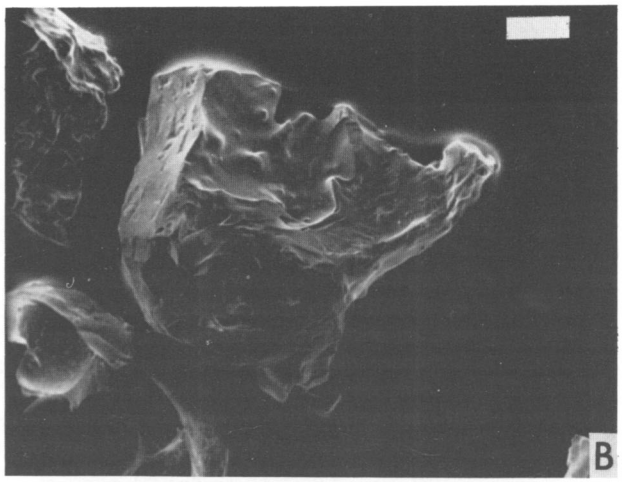
B

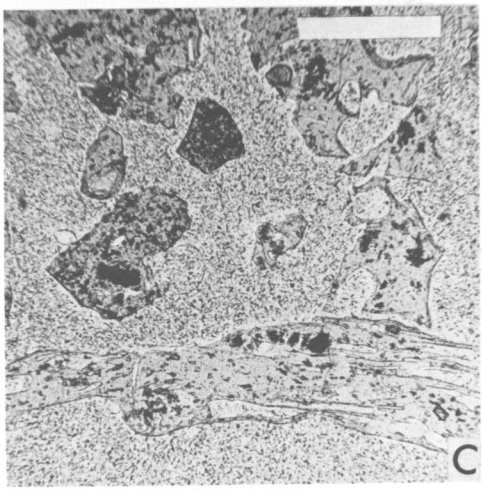
C


D

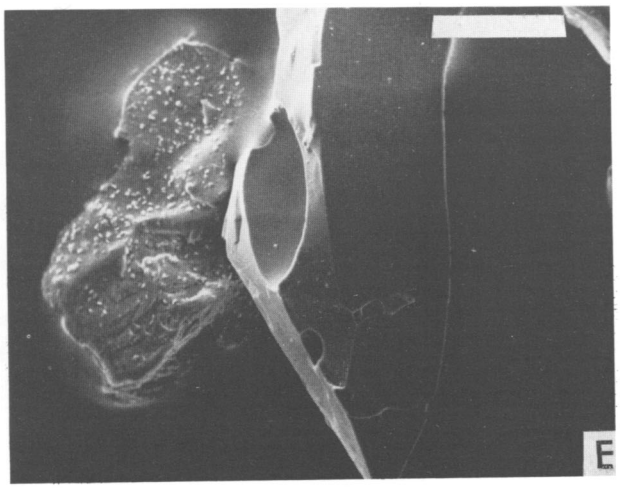
E

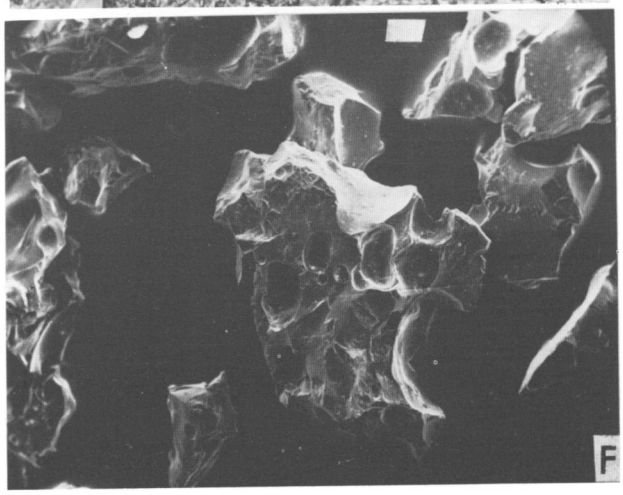
F

PLATE 32

Glass from the Ries Basin, Germany. A, SEM of a colorless glass fragment from the matrix of a suevite breccia. The fragment is weathered, masking the original grain shape. The broken outer edge exposes subparallel pipe vesicles. Half of this fragment is nonvesicular. (The scale is 100 microns.) B, Photomicrograph of K-Na feldspar glass, showing vesicles, schlieren, and an inclusion of quartz glass (Q). Ötting quarry (from von Engelhardt and Stöffler, 1968). (The scale is 100 microns.) C, SEM; closeup of the vitric fragment in A, showing elongate vesicles with diameters of 2 to 8 microns. (The scale is 10 microns.) D, Photomicrograph of a thin section of inhomogeneous Ries glass, showing partly melted crystals, rock fragments, and well-defined schlieren (Hörz, 1965). E, Silhouettes of bombs from the Ries Crater, included for comparison with the fine-grained fragments (Hörz, 1965). The fluidal shapes are similar to many droplets from basaltic eruptions. (The scale is 20 cm.) F, Photomicrograph of unrecrystallized banded glass from the Ries Basin. Bands are of slightly different compositions. The inhomogeneity of these glasses is characteristic of glassy ejecta from impact craters (von Engelhardt and Stöffler, 1968). (The scale is 100 microns.)

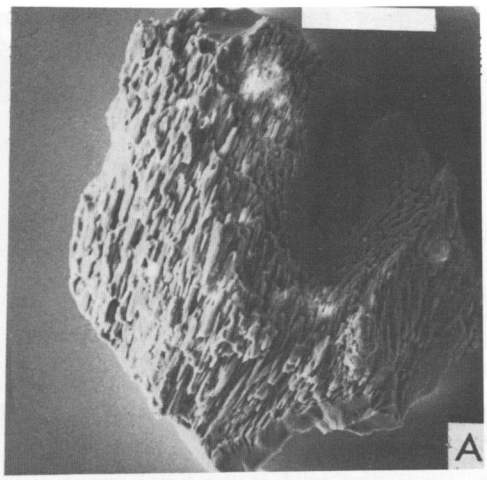
A

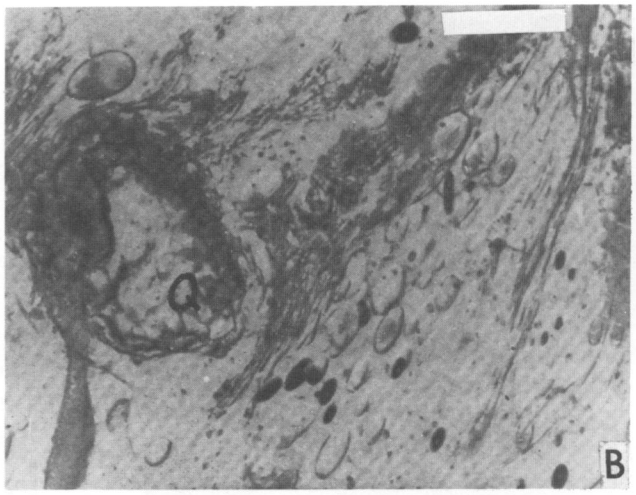
B

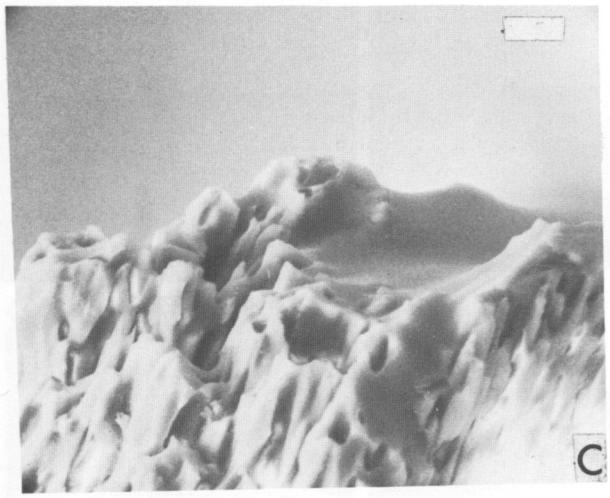
C

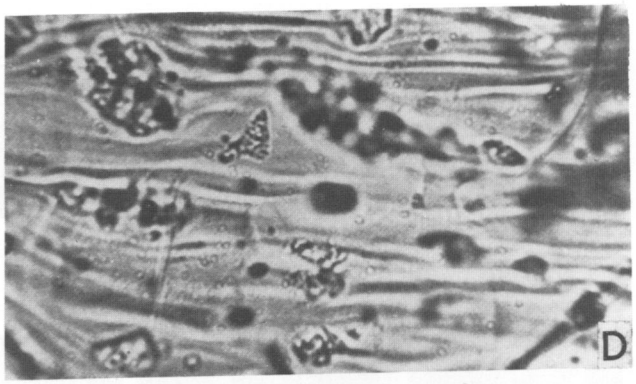
D

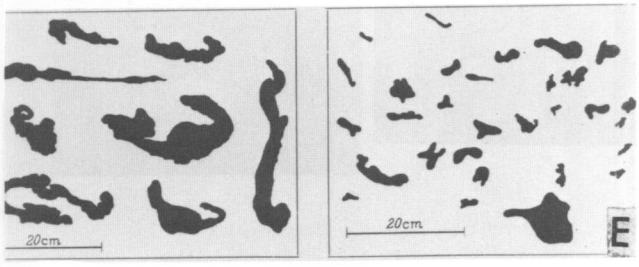
20cm
20cm
E

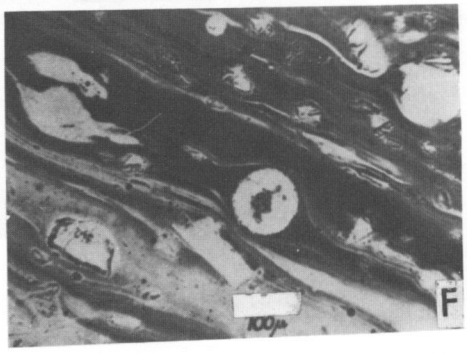
100μ
F

PLATE 33

Dial-Pack explosion. A, SEM of the surface of a glass sphere studded with smaller spheres and droplets. (The scale is 100 microns.) B, Photomicrograph of a thin section through a hollow glass sphere similar to the one in A. The space on the right is the hollow center; on the left, the sphere surface. The 400–micron-thick walls consist of moderately vesicular inhomogeneous glass spheres. (The scale is 500 microns.) C, SEM of glass spheres welded to the surface of a larger sphere. Nearly all the sphere sizes present in the sample are visible in this photograph. (The scale is 100 microns.) D, Photomicrograph of a thin section through an oblate glass spheroid welded to the surface of a larger sphere, similar to that in C. Both spheres are vesicular. (The scale is 100 microns.) E, SEM of the surface of a large sphere with abundant smaller spheres imbedded in it. The smaller spheres, which quenched faster, were solid at the time of collision with the larger sphere. (The scale is 10 microns.) F, Photomicrograph of a thin section through the edge of a glass sphere, with a smaller sphere imbedded in the surface. (The scale is 100 microns.) G, SEM of a glass sphere that is unique because of the relatively smooth surface which is free of smaller particles imbedded in it. (The scale is 100 microns.) H, SEM of a deformed glass droplet on the surface of a larger glass sphere. The smaller droplet was still molten when it collided with the larger sphere, spreading over the surface. (The scale is 10 microns.) I, Photomicrograph of a thin section through a droplet similar to the one in H, which collided with the larger sphere while it was still molten. (The scale is 100 microns.) J, Photomicrograph of a thin section through a glass sphere, showing the inhomogeneity of the glass. Schlieren consist of dark-brown and colorless wisps and bands. There are some vesicles (light circles) and bubbles in the thin-section mounting media (dark circles). (The scale is 100 microns.)

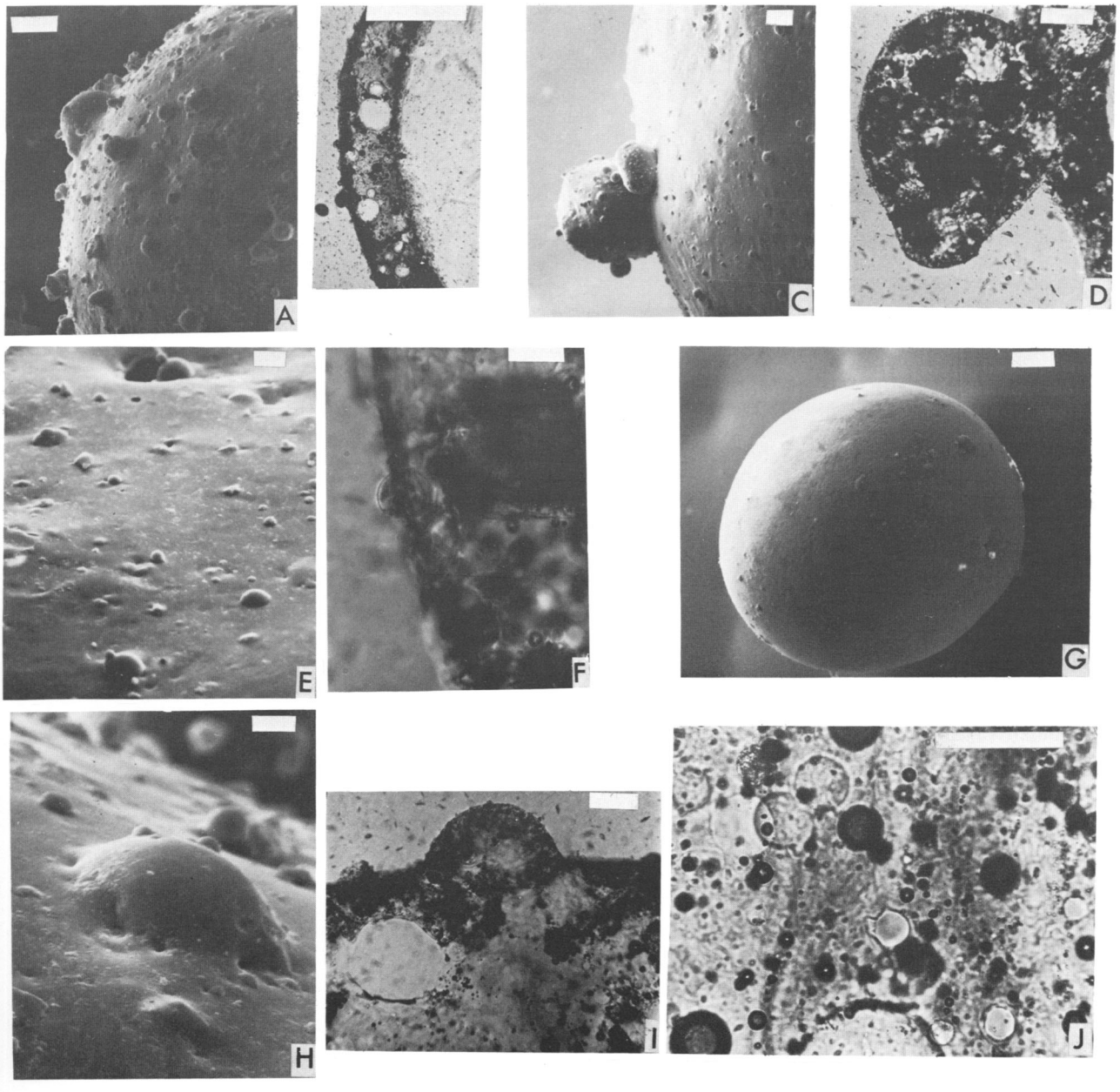

☆ U.S. GOVERNMENT PRINTING OFFICE: 1973—546-357/5